ret in 3-17

NASA CR-132570

AN INVESTIGATION OF ROOFTOP STOLPORT AERODYNAMICS

By Jeffrey N. Blanton and Hermon M. Parker

ABSTRACT

An investigation into aerodynamic problems associated with large building rooftop STOLports has been performed. Initially, a qualitative flow visualization study indicated two essential problems: (1) the establishment of smooth, steady, attached flow over the rooftop, and (2) the generation of acceptable crosswind profile once (1) has been achieved. This study indicated that (1) could be achieved by attaching circular-arc rounded edge extensions to the upper edges of the building and that crosswind profiles could be modified by the addition of porous vertical fences to the lateral edges of the rooftop. Important fence parameters associated with crosswind alteration were found to be solidity, fence element number and spacing. Large scale building induced velocity fluctuations were discovered for most configurations tested and a possible explanation for their occurrence was postulated. Finally, a simple equation relating fence solidity to the resulting velocity profile was developed and tested for non-uniform single element fences with 30 percent maximum solidity.

AN INVESTIGATION OF ROOFTOP STOLPORT AERODYNAMICS

Jeffery N. Blanton and Hermon M. Parker
University of Virginia

SUMMARY

An investigation into aerodynamic problems associated with large building rooftop STOLports has been performed. A qualitative flow visualization program carried out at the Langley Research Center indicated two essential problems: (1) the establishment of smooth, steady, attach< flow over the rooftop; and, (2) the generation of an acceptable crosswind profile once (1) has been achieved. It was found that the configuration of the building itself determines the gross nature of the flow over the rooftop and that relatively smooth attached flow could be achieved by the addition of circular-arc rounded edge extensions to the upper edges of the building. It was further determined that crosswind profiles could be altered by the addition of vertical fences along the lateral edges of the building rooftop.

A more quantitative program was undertaken at the University of Virginia. Effects of various fence parameters such as screen wire and mesh size, number of elements, etc., were investigated. Also a brief study of building induced turbulence was carried out and a qualitative description of the generation of the turbulence was hypothesized.

In an effort to isolate fence effects from building effects, a study of simple one element fences in the absence of a building model showed that downstream flow velocity was reduced over a height equal to that of the fence. In contrast to this, a fence installed on a building model affects the downstream flow up to approximately two fence heights. Finally, a simple equation relating the velocity at any height behind a one element fence to the fence solidity (ratio of projected wire area to projected total area) was derived and validated for low solidity fences (up to 0.30 area blockage).

INTRODUCTION

During recent years, the rapid increase in the number of air passenger miles traveled has imposed considerable hardships on contemporary air transportation systems. Both airports and airspace are congested to the extent that some immediate relief is needed. This is particularly true of short-haul operations where times required for ground transportation to and from the terminal areas often compare in magnitude to flight time. With the development of STOL aircraft has come the possibility of supplying some needed relief. Many variations of possible STOL transportation systems have been proposed, and many points of view have been expressed concerning the advantages and disadvantages of various components of these systems. One of the few issues upon which there is agreement is that the STOL passenger would definitely be subjected to conditions quite different from those to which he has been accustomed in traveling between major cities. The uncertainty concerning the acceptability

of these factors to the traveling public has undoubtedly been an important factor contributing to the hesitation which has been evident in making a commitment to implement a STOL system.

In order to help alleviate some of these uncertainties, a program was initiated at the University of Virginia, through its Center for the Application of Science and Engineering to Public Affairs, to develop modeling techniques to predict human acceptance of proposed STOL systems and to develop acceptability criteria for the many variables and their trade-off possibilities. This requires a thorough understanding of the nature of the variables and a quantitative formulation of response to them.

The work reported herein represents one facet of this overall program which arose from the following considerations. STOLcraft can be accommodated in relatively small terminal areas; it is, therefore, possible that STOLports can be placed nearer the population centers of cities. Such an arrangement would have two major advantages. First, it would improve short-haul air transportation directly by decreasing ground travel time and consequent total trip time. Second, it would aid long-haul air transportation by relieving congestion at conventional airports currently caused by short-haul operations.

One means of placing STOLports near city centers is to utilize the roofs of very large downtown buildings as landing and takeoff areas. This would minimize disruption of normal downtown economic activities since the building itself could be used for varied revenue producing activities, as well as for the STOL terminal. An artist's conception of such a STOLport is shown in figure 1. There are, however, many types of problems associated with the development of such an unconventional airport, and the present work is directed toward those related to the quality of the airflow over such a structure. There are two important issues involved. One is the nature of the local flow near the landing surface induced by the design of the structure. This will have a direct influence on the motion experienced by the aircraft (and its passengers) in the landing and takeoff maneuvers - as well as in the safety of these activities. The other arises from the fact that the need to restrict the STOLport to a single runway will generally give rise to crosswind problems which could effect the quality and safety of the landings and takeoffs and the reliability of the system operation. Thus, the possibility of alleviating crosswind problems and generally improving flow quality through the use of wind screens and proper building design was deemed worthy of study.

SYMBOLS

a	arc length of rounded edge extensions, cm (in.)
b	building model width, cm (in.)
C_D	screen drag coefficient based on average interstitial velocity and blocked area (see eq. A-4)
h_b	building model height, cm (in.)
h_f	fence height, cm (in.)
h_r	height of measurement above model, cm (in.)
K	local drag coefficient of a variable solidity screen
$p_1 - p_2$	total pressure drop across screen or total pressure drop from far upstream to far downstream, N/m^2 (lb/ft^2)
p_{∞_1}	static pressure far upstream of a screen, N/m^2 (lb/ft^2)
p_{∞_2}	static pressure far downstream of a screen, N/m^2 (lb/ft^2)
q	dynamic pressure, N/m^2 (lb/ft^2)
Re	Reynolds number, $\dfrac{\rho V_{cw} b}{\mu}$
S	distance between upstream and downstream fences, cm (in.)
u(y)	local velocity in flow field, m/sec (ft/sec)
U_∞	free-stream velocity, m/sec (ft/sec)
V_a	aircraft air speed, kts

2(a)

V_{cw} crosswind velocity, m/sec/kts (ft/sec)

V_{cw_ℓ} local crosswind velocity, m/sec (ft/sec)

$V_{cw_{max}}$ maximum crosswind velocity, m/sec (ft/sec)

V_g aircraft ground speed, kts

x horizontal distance measured from fence, cm (in.)

y vertical distance measured from bottom of screen, cm (in.)

y_0 vertical distance measured on the screen, cm (in.)

ρ density of air, gm/cm^3 ($slugs/ft^3$)

μ viscosity of air, $Nsec/m^2$ (slug/ft-sec)

σ_ℓ local turbulence, $\dfrac{\text{rms-velocity fluctuation}}{\text{mean velocity}}$

ξ local solidity of screen = projected blocked area/projected total area

QUALITATIVE INVESTIGATION

The initial study into the feasibility of utilizing large building roof-tops as elevated STOLports was begun in November 1969, in a joint effort by the University of Virginia, Department of Aerospace Engineering and Engineering Physics, and the Langley Research Center, Low Speed Vehicles Branch. Initial studies were of a qualitative nature and were performed in the 17-foot test section of the 300-mph 7-by 10-foot wind tunnel at the Langley Research Center. The purpose of this program was the qualitative observation of the overall flow field associated with a rooftop STOLport and the influence of the building configuration changes on that flow.

Test Set Up

The primary experimental technique utilized in this initial investigation was flow visualization achieved by the use of smoke and tufts. Figure 2 is a photograph of one of the configurations tested, and figure 3 shows cross sections of six of the configurations tested. The first configuration in figure 3 is the solid rectangular parallelepiped building itself. Next is a series of four configurations, each having an elevated rooftop (or raised deck). The first in this series is the basic raised deck. The second has side ramps, which were tried because they offered a method of lateral containment for landing STOLcraft. A circular arc side overhang was also tried. (See third configuration in the series.) Finally, porous side fences were added to the raised deck with curved overhang in an attempt to modify the crosswind velocity profiles; each side fence was constructed of three rather closely-spaced pieces of stainless steel screening of different heights. Figure 2 is a photograph of this fourth elevated-rooftop configuration with its curved overhang and porous side fences. The last configuration in figure 3 differs from the preceding one in that the space under the raised deck is closed in order to determine whether the raised deck is essential in achieving the desired flow patterns.

The building models are 1.2 meters by 2.4 meters (4 ft by 8 ft) by either 41 cm or 51 cm (16 in or 20 in) high, depending on the configuration. If the full-scale building is 152 meters (500 ft) wide, then the 15 cm (6 in) height of the model fences corresponds to an actual fence height of 19 meters (62.5 ft) and the full-scale building would be 51 or 63 meters high (167 or 208 ft high). The building model was mounted so that it could be placed at any yaw angle to the tunnel flow; in figure 2, the tunnel flow is parallel to the model runway.

Qualitative Test Results

A motion-picture film supplement showing smoke flow over the various building models has been prepared.* Six frames from this film are presented as figures 4 through 9. Figures 4 through 7 show the flow over the four configurations in the elevated-rooftop series. Figure 8 shows the flow over the solid rectangular parallelepiped building alone, and figure 9 is of the solid building with rounded edges but not fences. In each case, the flow is from left to right and the tunnel flow is at 90° to the runway (pure crosswind).

Figure 4 shows the flow over the model with the basic deck. (See the first schematic in the elevated-rooftop series in figure 3.) The flow is not good. It is separated at the leading edge, and reattachment does not occur. Over the entire rooftop, the flow is highly turbulent and unsteady.

---

*This film supplement (16 mm, 23 min, color, narrated) may be obtained on loan by requesting film serial number L-1114 entitled "Roof-Top STOL/Port Flow Visualization" from NASA Langley Research Center, Attn: Photographic Branch, Mail Stop 171, Hampton, Virginia 23665.

Flow over the second configuration in the elevated-rooftop series is shown in figure 5. The addition of side ramps to the basic raised deck is seen to be detrimental. The separation angle is larger. In the center region, the flow is even more turbulent and unsteady than that over the basic rai_ed deck. The unsteady flow region extends very high above the model. This configuration has the worst flcw of any of those tested.

Figure 6 shows the flow over the third configuration in the elevated-rooftop series. The effect of adding rounded edges to the raised deck is dramatic. Some turbulence can be seen, but the flow pattern is considerably better than for the first two elevated-rooftop configurations.

Once success in maintaining attached flow had been achieved by the addition of rounded edges, fences were added to determine whether the flow would remain smooth and whether the crosswind profile above the deck would change. The flow over the resulting configuration (fourth in the elevated-rooftop series in fig. 3) is shown in figure 7. One must not confuse the spreading oi the smoke due to turbulence and unsteadiness with the spreading due to low velocities. The lazy drifting action of the smoke in this figure indicates low velocities.

Figure 8 shows that the flow over the solid parallelepiped building alone is separated and turbulent. In fact, it seems to be slightly worse than the flow over the basic-raised-deck configuration (fig. 4).

Again, the effect of adding rounded edges is dramatic. Figure 9 shows that over the solid building with rounded edges the flow is attached and fairly smooth and steady everywhere; it seems to be as smooth as the flow over the raised-deck configuration with rounded edges (fig. 6). At this stage of the study, it was concluded that the raised deck is not necessary to obtain good attached flow but that the rounded edges are the important factor. However, later investigations showed that the elevated deck may be desirable. This will be discussed in a later section. Although not illustrated, it should be noted that the addition of fences to the solid building with rounded edges produced favorable results. The flow remained smooth and the crosswind velocities near the building rooftop were greatly reduced. Most of the subsequent work has been without raised decks on the models.

This first qualitative phase of the research effort gave encouragement to the expectation that smooth, attached flow over an elevated STOLport could be achieved and that the crosswind profile could be modified in some desirable fashion.

QUANTITATIVE INVESTIGATION

The next phase of the study was a some*hat more detailed experimental investigation carried out at the University of Virginia. Results concerning the influence of fence structure and geometry on changes in crosswind velocity are presented.

Figure 10 shows schematically the type of effect one expects fences on either side of a STOLport runway to have on the crosswind velocity profile. The left-hand sketch shows the tunnel flow with the tunnel boundary layer. In the right-hand sketch, the dashed line indicates the profile on the STOLport model at the centerline with no fences. With fences, the profile is modified as shown by the solid curve. The curves in this figure are just illustrative.

The effects of a crosswind velocity on an aircraft attitude and airspeed can be seen in figure 11, which is a schematic diagram of a STOLcraft, designed to land at an airspeed of 60 knots, landing at a STOLport between fences in a 30-knot crosswind. The right-hand side of the figure indicates the situation initially in the full 30-knot crosswind. The airspeed is 67 knots; the ground speed is 60 knots; and the crab angle is 27 . The left-hand side indicates the situation at a place where the fences have reduced the crosswind speed to 15 knots, with the assumption of perfect decrabbing and a constant ground speed of 60 knots. The airspeed is now 62 knots, and the crab angle is 14 . The effect of crosswind angles of other than 90 could be examined in a similar fashion. Some concern had been expressed about the potential loss of airspeed as the crosswind component is removed. It can be seen from figure 11 that even when the relatively large crosswind of 30 knots (50 percent of ground speed) is decreased by 50 percent, the airspeed is only decreased by about $7 \frac{1}{2}$ percent. Consequently, it seems that loss of airspeed is probably not a sufficient reason for not seeking to control crosswind profiles.

It seems obvious that if a pilot had to land such a STOLcraft an an elevated STOLport in a crosswind, he would be concerned about such factors as the following: At what height does the crosswind component begin to change? How rapidly does it change? At what height above the runway does the crosswind become negligible?

It should be noted that the results to be presented herein are not given as a "solution" to the crosswind problem. With a given, unfenced STOLport building and a given flow over it, there will be a certain crosswind velocity profile provided by nature. If this profile is acceptable to all concerned, there is no problem. If it is not acceptable, then some mechanism of making the crosswind velocity profile acceptable becomes of interest. The question to which the present work is addressed is simply this: What are the possibilities of crosswind profile modification by putting fences on either side of the STOL-port building?

Crosswind Investigation

Figure 12 shows the test setup for a building model that is 76 cm (30 in) wide and 15 cm (6 in) high. The rounded edges of the model are circular and of 7 cm (2.75 in). If the 76-cm (30-in) model width corresponds to a 152-meter (500-ft) full-scale building width, then the 15-cm (6-in) model height corresponds to a 30.5-meter (100-ft) building height. Also, the 7-cm (2.75-in) model overhang radius corresponds to a 14-meter (46-ft) building overhang radius, and the 7.6-cm (3-in) model fence height corresponds to a 15-meter (50-ft) full-scale fence height. The fences were constructed of one, two or three wire screens.

6

Figures 13 and 14 show the measured profiles at the model centerline for different fence configurations. The dashed line indicates the top of the fences. The model is 76 cm (30 in) wide, and all the fence configurations are 7.6 cm (3 in) high. It is obvious that increasing the number of screens causes the centerline velocities near the deck to decrease and causes the height to which the fence effect extends to become larger. It is apparent that fence structure has a large influence on centerline crosswind velocity profiles.

Figure 15 shows results of efforts to generate varied velocity profiles by proper fence design. The straight line profile is the result of a separate experiment conducted at Langley (ref. 1) where a pair of three screen fences were modified in a trial and error manner until a linear profile was produced. The other profile was generated at the University of Virginia in an effort to show that unusual profiles could be generated. These results indicate that centerline profiles are adjustable over a considerable range and suggest that one might learn how to predict profiles for given fence structures and geometries.

It is also interesting to examine crosswind velocity profiles at positions other than the centerline. The investigations at the University of Virginia included experiments to determine the effects of measurement position. Figures 16 through 21 compare profiles taken 11.4 cm (4.5 in) behind the leading-edge fence to profiles taken above the centerline. In general, there is a shift to the left and upwards with increasing distance. This indicates a slowing and diffusion of the flow with distance behind the fence. Figures 22 through 26 show variation of velocity profile with distance for different ratios of S/h_f. The trends shown by these graphs are similar to those seen in figures 16 through 21. Figure 22 corresponds to the maximum S/h_f tested. It can be seen that there is less difference between the 1/2 S and the 3/4 S profiles than between the 1/4 S and the 1/2 S profiles. This seems to indicate that the flow is approaching an equilibrium condition.

In an effort to determine the effect of screen mesh and wire size, similar fence configurations were constructed from two different mesh and wire size screens. The solidity or ratio of projected wire area to projected total area was constant at about 0.30 for each of the screens. Results for similar fence configurations are shown on figures 27 through 32. The data taken above the centerline show negligible variation with type of screen for the one screen and two screen profiles. However, that taken at 11.4 cm (4.5 in) behind the screen shows appreciable differences. This is in agreement with other similar tests performed at the University of Virginia (ref. 2) which indicated that the equilibrium profile behind a screen depends only on the solidity of the screen, but that the distance to equilibrium depends on the wire and mesh size. The graphs also hint that equilibrium distance increases as the effective solidity of the fence increases by the addition of more screens. In other words, comparison of the three fence configurations tested at the centerline indicates small but increasing differences in velocity profiles with increasing number of screens.

An additional experiment showed that the centerline profile was essential-
ly the same with and without the downstream fence. Thus, one tentatively
concludes that the profiles in the runway area are fixed by the upstream fence
and are nearly independent of the downstream fence. Some additional evidence
on this point is provided in figure 33. A single two-screen fence was placed
approximately at the centerline position, and profiles were measured 5 cm (2 in)
upstream and 5 cm (2 in) downstream of the fence (that is, 0.07b upstream and
downstream of the fence). The other curve (through the square symbols) is the
no-fence profile at the fence position. The data clearly show that a fence
alters the downstream flow velocity very much more than it does the upstream
velocity. These results provide some insight into the mechanism by which
fences alter the adjacent upstream and downstream flow fields.

Velocity Fluctuation Investigation

Throughout the quantitative test program, large-scale velocity or dynamic
pressure fluctuations were observed above the STOLport deck. These fluctua-
tions appeared and were similar for all configurations tested. They usually
died out on the order of 0.5 building heights above the deck. The predominate
frequency associated with them was approximately one hertz, but slower and
faster frequencies were superimposed on this. Unfortunately, no spectral
analysis was carried out due to the lack of proper instrumentation. For most
configurations, the gross appearance of the fluctuation was invariant over the
small Reynolds number range investigated (Re = 100,000 to 750,000). Figure 34
shows a typical variation of the fluctuations with height above the building.
These measurements were obtained using a pitot-static tube placed at different
heights above the centerline of the model. Approximately ±50 percent fluctua-
tion in dynamic pressure (±25 percent velocity fluctuation) can be seen in the
extreme case near the deck. It is realized that because of their relatively
slow response times pitot-static tubes are not the ideal instruments to use in
measuring flow unsteadiness. In this application, however, the low frequency
oscillations are of primary interest since they would have the greatest effect
on landing aircraft. The response time of the pitot-static tube is sufficient-
ly fast to observe these low frequency oscillations.

In an attempt to determine scale effects, a single series of tests were
performed on a larger model (one that had been used in the earlier flow visual-
ization tests) in the Langley full-scale tunnel. The same instrumentation that
had been used at the University of Virginia was used in this investigation. A
Reynolds number one full order of magnitude higher (5×10^6) was achieved.
Mean velocity profiles and velocity fluctuations were similar to those previous-
ly obtained at Re = 5×10^5. Extrapolation of these results to a full-scale
building with a Reynolds number of 5×10^8 is not possible. Hence the full-
scale existence of this phenomena has not been verified. However, it can not
be discounted on the basis of tests completed to date.

Qualitative description of velocity fluctuation.-One possible explanation
of the flow fluctuations is the existence of an unstable vortex located in
front of the building model. This is a flow pattern similar to that shown in

figure 35. The flow field is divided into two regions separated by a stagnation streamline which is attached to the leading-edge overhang. Adjacent to the deck and elsewhere in the upper region the speed is high. The speed below the stagnation streamline, however, is low. Associated with this difference in speed is a pressure gradient between regions 1 and 2 in figure 35. Under equilibrium conditions, this gradient is just balanced by the curvature of the stagnation streamline. If the pressure gradient is raised above this equilibrium condition, the stagnation streamline would detach as shown in figure 36. This would allow a "bubble" of turbulence to escape up over the rounded edge. When the bubble is released, the excess pressure gradient is relieved and the stagnation streamline reattaches. This allows the pressure gradient to rise again and the cycle is repeated. This heuristic explanation has been substantiated by the use of flow visualization. Smoke injected under the rounded edge in front of the building escapes in distinct bubbles. It was further hypothesized that if the above explanation is true, the velocity fluctuation could be eliminated simply by continuously relieving the pressure gradient. With this in mind, a building configuration such as that shown in figure 37 was installed in the tunnel. It was found that if the second deck is raised high enough, and if proper rounded edges are used, the velocity fluctuations can be virtually eliminated. Another interesting means of alleviating the fluctuation (although it may not be practical in actuality) is shown in figure 38. The wedge in front of the building can be adjusted so that the stagnation streamline has a stagnation point at A and another at B. With this situation, the stagnation streamline is stabilized and the vortex is stable. Consequently, the flow over the deck is smooth.

Building induced turbulence measurements.-Since the magnitude and frequency of the velocity fluctuations are such that it would be potentially hazardous (depending o.. scaling, of course), it was decided that the phenomena should be more carefully investigated. Consequently, an experimental program was initiated to determine important parameters associated with the velocity fluctuation. The test set up was similar to that used earlier at the University of Virginia, the only difference being the use of hot wire anemometry for velocity measurements. Both mean velocity and RMS turbulence were measured with height above the deck for various building configurations. This program was not as complete as anticipated largely because of difficulties in using hot wires in the University of Virginia low-speed tunnel. The primary difficulty being the inability to adequately temperature compensate for the large scale temperature variations which occurred in this closed tunnel. Turbulence measurements, however, are insensitive to this problem, and consequently these data are presented.

Figures 39 and 41 show the height versus turbulence variation at stations above the deck for various rounded edges. A basic building configuration (no second elevated deck) was used for these tests. Each of the figures shows greater differences between the leading edge and centerline data than between the centerline and trailing edge data. This seems to indicate that some equilibrium is being approached. Figures 42 and 44 show differences due to different rounded edges. With increasing distance from the leading edge, data due to the $0.75h_b$ Dia and $0.916h_b$ Dia rounded edges become more similar.

Next an elevated deck was installed above the basic building deck. The spacing between the basic building and the elevated deck was 7.6 cm (3 in) or 1/2 building height. Tests were made with various rounded edge extensions on both the basic building and the deck. Figures 45 through 50 show the variation of turbulence with height for a given model configuration at different tunnel speeds. In each case there is a general decrease in turbulence with increasing wind velocity. The shape of the profile, however, seems to remain the same for a given configuration. There is no indication that a constant turbulence profile, independent of Reynolds number, is being approached. It should be remembered, however, that the maximum tested Re is two orders of magnitude smaller than that for an actual building so no real conclusions about scaling can be drawn. Figures 51 through 53 show turbulence profiles obtained by placing different rounded edges on the building edge while keeping a given rounded edge on the upper deck. The profiles on each graph are similar. This indicates a relative insensitivity to building rounded edges for a given deck edge. Figures 54 through 56 show results for different deck edges and a constant building edge. In each of these figures, the profiles fall into two groups. In each case, the similar profiles have similar arc length to radius ratios (a/r). These graphs indicate, therefore, that the rounded edge on the upper deck has a greater effect on the turbulence than the rounded edge on the lower section of the building. They also indicate the quantity a/r is important and should be investigated. Unfortunately, this could not be done in this program. The spacing of the elevated deck above the building is another important parameter that was not, but should be, investigated. It would also be desirable to perform frequency and spectral-energy analyses on the turbulence above the deck. This investigation has shown that the building configuration has a marked effect on the turbulence above the building.

Basic Fence Research

During the elevated deck turbulence program, it was noticed that mean velocity profiles took different shapes than corresponding profiles obtained with similar fence configurations on the basic building model. This indicated that the building configuration itself, or possibly the building-fence interaction, has an effect on the velocity profile. In an attempt to isolate this effect and gain knowledge into the basic mechanism by which fences alone affect velocity profiles, a basic fence investigation was initiated.

Experimental program.-The experimental part of this investigation utilized the test set-up shown in figure 57. In this arrangement, the fence was placed on a ground board above the tunnel boundary layer. Reasonably uniform flow was therefore incident on the fence as long as the fence was fairly close to the leading edge of the ground board. Figure 58 shows velocity profiles taken at various distances behind a simple one element fence. Near the screen the velocity profile is very irregular. This is because effects of individual wires are being seen. As the distance behind the fence increases, these differences are smoothed and a uniform profile is established. Figure 59 shows results for a more complicated two element fence configuration. Data were taken for this configuration up to 91 cm (36 in) (12 fence heights) downstream. As was the case with the simple one element fence, an equilibrium profile is established downstream and maintained until the boundary layer growing from the leading edge

of the ground board becomes thick enough to affect the profile. At 91 cm
(36 in) downstream, a large boundary-layer effect can be seen in these data up
to about 1/2 fence height. Figure 60 shows velocity profiles in front of the
fence for this 2 element configuration. It can be seen that there is very
little upstream effects of the fence at 23 cm (9 in) (3 fence heights) in front
of the fence. This is similar to results obtained in front of the fence on
the building model.

The striking difference between these results with fences on a ground
board and those obtained with similar fences on building models is that the
height to which the fence affects the flow is much less in the absence of the
building. This could have important practical ramifications since it is
structurally and economically desirable to build fences as low as possible.
Corresponding profiles obtained with fences on the building model and on the
rasied ground board also vary somewhat in appearance because of the differe'.t
characteristics of the boundary layer associated with each case.

Analytical program. - Analytical investigations of incompressible flow
through wire gauze have been performed by Taylor and Batchelor in 1949 (ref. 3)
and by Owen and Zienkiewicz in 1957 (ref. 4). The Taylor-Batchelor work deals
with the effect of woven wire gauze on small disturbances to a uniform stream.
In this work, the drag coefficient of a uniform screen is defined by

$$K_o = \frac{P_1 - P_2}{1/2 \rho U_\infty^2} \tag{1}$$

Owen and Zienkiewicz's analytical work on screens was performed as part of
an attempt to produce uniform shear flow in a wind tunnel. They were able to
predict the solidity distribution necessary to generate constant shear.

The objective of the present work is to predict the fence solidity distri-
bution necessary to generate a predetermined nonlinear velocity profile. In
addition to differing in profile shape, this work differs from Owen and
Zienkiewicz's in the boundary conditions on the fence. There is essentially
no upper boundary on the fence in the current work. Owen and Zienkiewicz's
grid spanned the entire test section of the wind tunnel.

Qualitatively, the effect of a fence on a flow field can be described as
follows. As a streamline passes through the fence, fluid momentum is lost.
This corresponds to a decrease in stagnation pressure at the fence. Conserva-
tion of mass requires that fluid velocity through the fence be continuous,
therefore, the change in stagnation pressure must appear as a static pressure
drop across the fence. Farther downstream an equilibrium condition is reached
where static pressure does not vary vertically. At the equilibrium condition
an exchange between static pressure and velocity has occurred so that the
momentum (or stagnation pressure) decrease appears as a decrease in velocity.

Bernoulli's equation written for a streamline passing through a fence is

$$P_{\infty_1} + \frac{1}{2} \rho U_\infty^2 - P_{\infty_2} - \frac{1}{2} \rho u^2(y) = p_1 - p_2 \qquad (2)$$

where p_{∞_1} and p_{∞_2} are the static pressures far upstream and far downstream, respectively, and $u(y)$ is the local equilibrium velocity downstream. In the absence of an upper boundary on the fence, p_{∞_1} and p_{∞_2} are equal. This allows equation (2) to be rearranged as

$$\frac{p_1 - p_2}{1/2\rho U_\infty^2} = 1 - \frac{u^2(y)}{U_\infty^2} \qquad (3)$$

In a manner analogous to equation (1), a local drag coefficient can be defined by the left hand side of equation (3) so that

$$K(y_o) = 1 - \frac{u^2(y)}{U_\infty^2} \qquad (4)$$

It has been demonstrated that for practical solidities, streamlines passing through the fence are "essentially" straight so that $y_o \simeq y$.

For any arbitrary, single-element screen or parallel-rod grid in an incompressible flow, it can be shown that the drag coefficient, $K(y_o)$ is related to the solidity, ξ, by

$$K(y_o) = \frac{\xi(y_o) \, C_D}{[1 - \xi(y_o)]^2} \qquad (5)$$

where C_D is a drag coefficient based on the blocked area of the grid and the average interstitial velocity (see Appendix I). Experimental results have shown that in the absence of an upper boundary $C_D = 0.5$ for uniform grids of 30 percent and 15 percent solidity. When the solidity is increased to 60 percent, however, the C_D decreases to approximately 0.14. This indicates that C_D is approximately constant at 0.5 for solidities less than approximately 30 percent. For higher solidities, however, it becomes a function of fence solidity. The following results are limited to maximum solidities of 0.3. Using $C_D = 0.5$. and combining equations (4) and (5) leads to

$$\frac{\xi(y_o)}{[1 - \xi(y_o)]^2} = 2 \left[1 - \left(\frac{u}{U_\infty}\right)^2 \right] \qquad (6)$$

Figure 61 shows a nonlinear velocity profile measured behind a parallel-rod grid installed in the University of Virginia Low Turbulence Wind Tunnel. The ratio of grid height to tunnel test section height was approximately 0.14. The experimental values of u/U_∞ from figure 61 were used in equation (7) to compute the solidity distribution. The computed solidity is compared to the actual measured solidity in figure 62. Figures 63 and 64 show similar results for another fence of approximately the same height, but constructed from a variable solidity screen. The average error is approximately 5 percent for the parallel-rod arrangement and approximately 15 percent for the screen. Most of this error can be attributed to wind tunnel blockage effects that prevent p_{∞_1} and p_{∞_2} from being exactly equal. Results are also sensitive to accurate measurement of U_∞. It should also be pointed out that these results cannot be extended to higher Reynolds number cases until Reynolds number effects on C_D can be determined.

CONCLUSIONS

The problem of rooftop STOLport aerodynamics is a large and complicated one. Consequently, the initial investigation has generated more questions than it has answers. There are, however, some relatively firm conclusions which may be stated as follows.

1) At the scale of these experiments, it is possible to modify STOLport building models so that in a steady (wind tunnel) crosswind there is smooth attached flow over the models. This is achieved by attaching rounded-edge extensions to the upper lateral edges of the model.

2) At the scale of these experiments, it is possible to modify the steady crosswind profile above the building model, by attaching vertical porous fences to the upper edges of the model. By varying the fence geometry, a wide range of profiles can be obtained.

3) By a not well-understood mechanism, some model configurations produce large levels of turbulence at low frequencies (1 Hz at this scale) above the STOLport deck.

4) A simple theoretical analysis of the effect of a single element fence on a uniform velocity profile has been validated for low solidity fences (up to 0.30 area blockage).

5) There are several important questions that have been raised, but left unanswered because of the limited scope of this research. The most important of these pertain to both fences and buildings and are:

   a) The determination of scale effects

13

b) The determination of effects derived from the natural
unsteadiness in actual atmospheric flow.

c) The determination of effects derived from the unique
character of the earth's boundary layer.

The above questions can only be answered by large scale atmospheric
testing.

APPENDIX A

Relationship Between Solidity and Drag Coefficient

The solidity of a uniform screen or parallel-rod grid is defined as the ratio of blocked area to total area. If a wire screen has grid dimensions of ℓ by h where ℓ is the grid length and h is the grid height and the diameter of the wire is d, the following can be written for each grid:

$$\text{Blocked Area} = hd + \ell d - d^2$$

$$\text{Total Area} = h\ell$$

$$\text{Open Area} = h\ell - (hd + \ell d - d^2)$$

Consequently, the solidity, ξ, is given by

$$\xi = \frac{d(h + \ell - d)}{h\ell} \tag{A1}$$

or if the grid is square so that $h = \ell$

$$\xi = \frac{d(2\ell - d)}{\ell^2} \tag{A2}$$

For the case of a parallel-rod grid, the solidity can be written as

$$\xi = \frac{d}{S} \tag{A3}$$

where d is the rod diameter and S is the spacing between successive rod centerlines. These equations are valid local solidity expressions for a non-uniform screen (or parallel-rod grid with variable spacing) if h and ℓ (or S) are given their local values.

The relationship between the drag coefficient and solidity for a screen can be developed by considering the aerodynamic force on one grid as follows:

$$\text{Force} = K(\tfrac{1}{2}\rho U_\infty^2)\, h\ell = C_D(\tfrac{1}{2}\rho U_{ave}^2)(hd + \ell d - d^2) \tag{A4}$$

where K is the drag coefficient based on total grid area and the freestream velocity, U_∞, and C_D is the drag coefficient based on the blocked area of the grid and the average interstitial velocity, U_{ave}. The average interstitial velocity can be found in terms of U_∞ by considering conservation of mass in a

rectangular (h x ℓ) stream tube intersecting the screen at the grid where K is to be determined. For incompressible flows, this gives

$$U_\infty \, h\ell = U_{ave} \, [h\ell - (hd + \ell d - d^2)]$$ A5

which can be combined with equation A4 to give

$$K = \frac{C_D[(hd + \ell d - d^2/(h\ell)]}{[1 - (hd + \ell d - d^2)/(h\ell)]^2}$$ A6

Similarly, it can be shown for a parallel-rod grid that,

$$K = \frac{C_D \, d/S}{[1 - d/S]^2}$$ A7

When written in terms of solidity, either of these equations reduces to the general result

$$K = \frac{C_D \, \xi}{(1 - \xi)^2}$$ A8

As mentioned in the text, $C_D = 0.5$ for solidities less than 30 percent (for the Reynolds numbers tested). Equation A8 can therefore be used to determine the resistance, K, of a screen or parallel-rod grid as a function of solidity.

16

REFERENCES

1. Parker, Hermon M.; Blanton, Jeffrey N.; and Grunwald, Kalman, J.: Some Aspects of the Aerodynamics of STOL-ports. Proceedings of a Conference on NASA Aircraft Safety and Operating Problems, Vol. 1, NASA Sp-270, 1971, pp. 263-276.

2. Hwang, Wen Shiuh: Experimental Investigation of Turbulent Shear Flow. Ph.D. Dissertation, University of Virginia, 1971.

3. Taylor, G.I.; and Batchelor, G.K.: The Effect of Wire Gauze on Small Disturbances in a Uniform Stream. Quart. Journ. Mech. and Applied Math., Vol. II, Pt. 1, 1949, pp. 1-29.

4. Owen, P.R.; and Zienkiewicz, H.K.: The Production of Uniform Shear Flow in a Wind Tunnel. J. Fluid Mech., Vol. 2, 1957, pp. 521-531.

CONCEPT OF AN ELEVATED STOL PORT
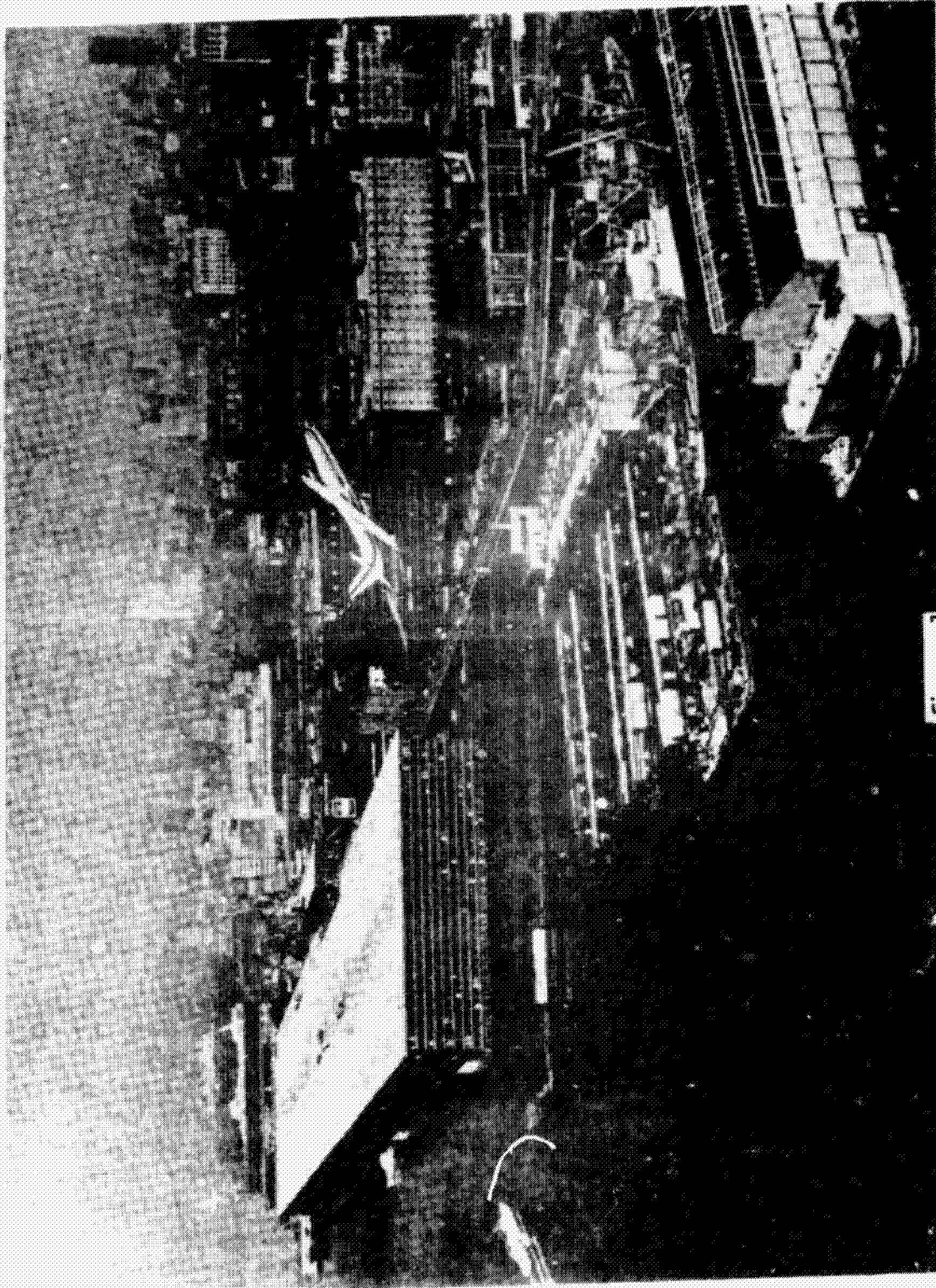
Figure 1

PRECEDING PAGE BLANK NOT FILMED

BUILDING MODEL IN TUNNEL
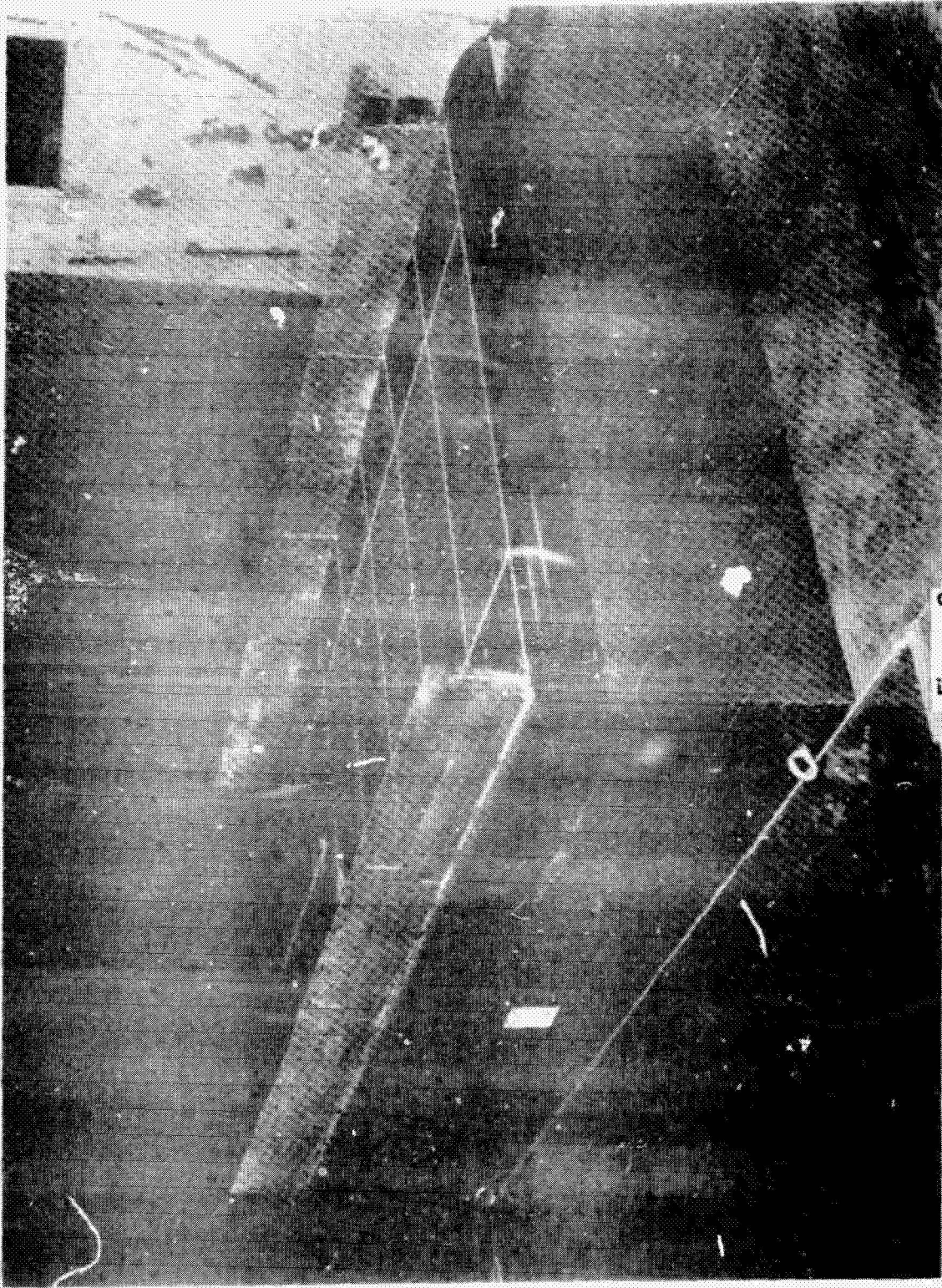
Figure 2

ELEVATED ROOFTOP RUNWAY

0.25b

b

2b

0.08b

BASIC

SIDE RAMPS

CURVED OVERHANG
0.08b RADIUS

CURVED OVERHANG
WITH POROUS SIDE
FENCES

SOLID BUILDING
CURVED OVERHANG
WITH POROUS SIDE
FENCES

ELEVATED ROOFTOP RUNWAY
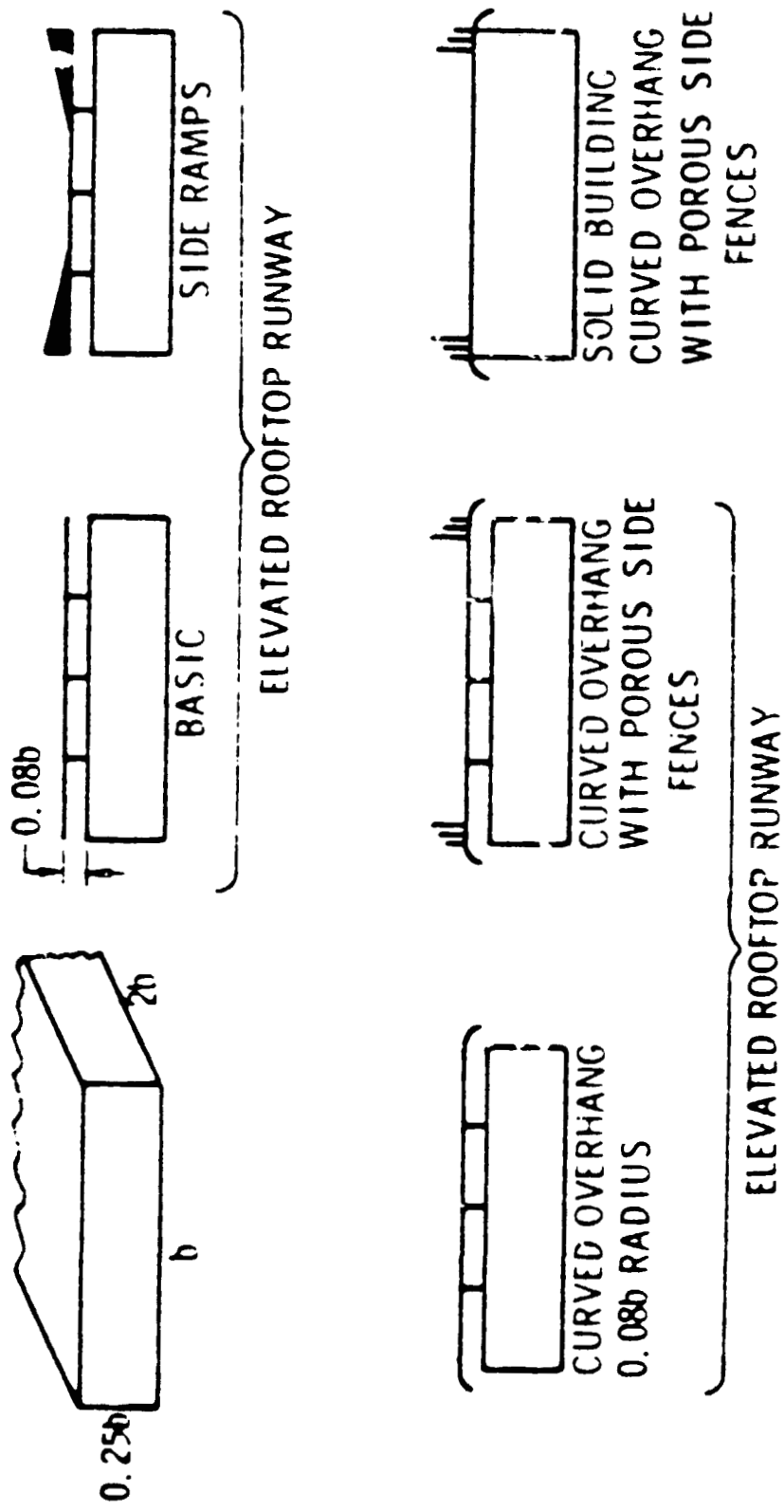
Figure 3

SMOKE FLOW
BASIC RAISED DECK
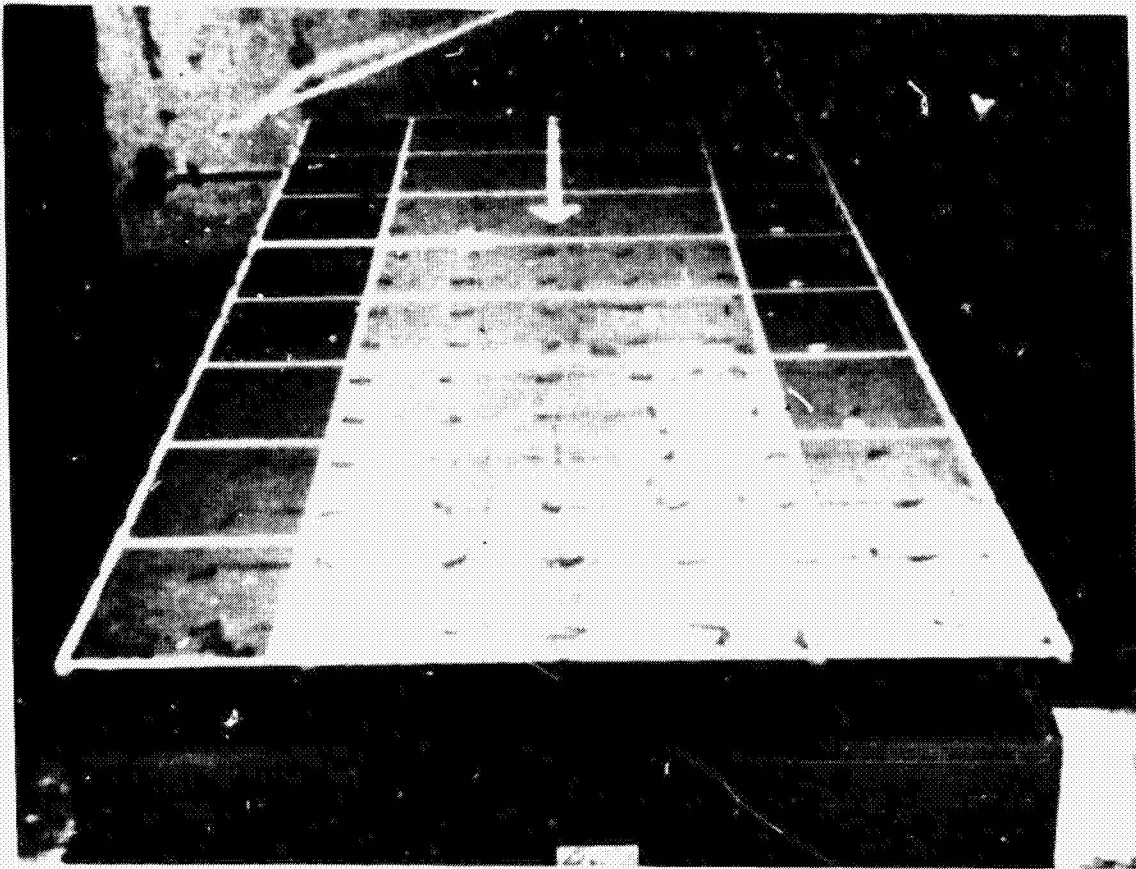
Figure 4

SMOKE FLOW
SIDE RAMPS ADDED
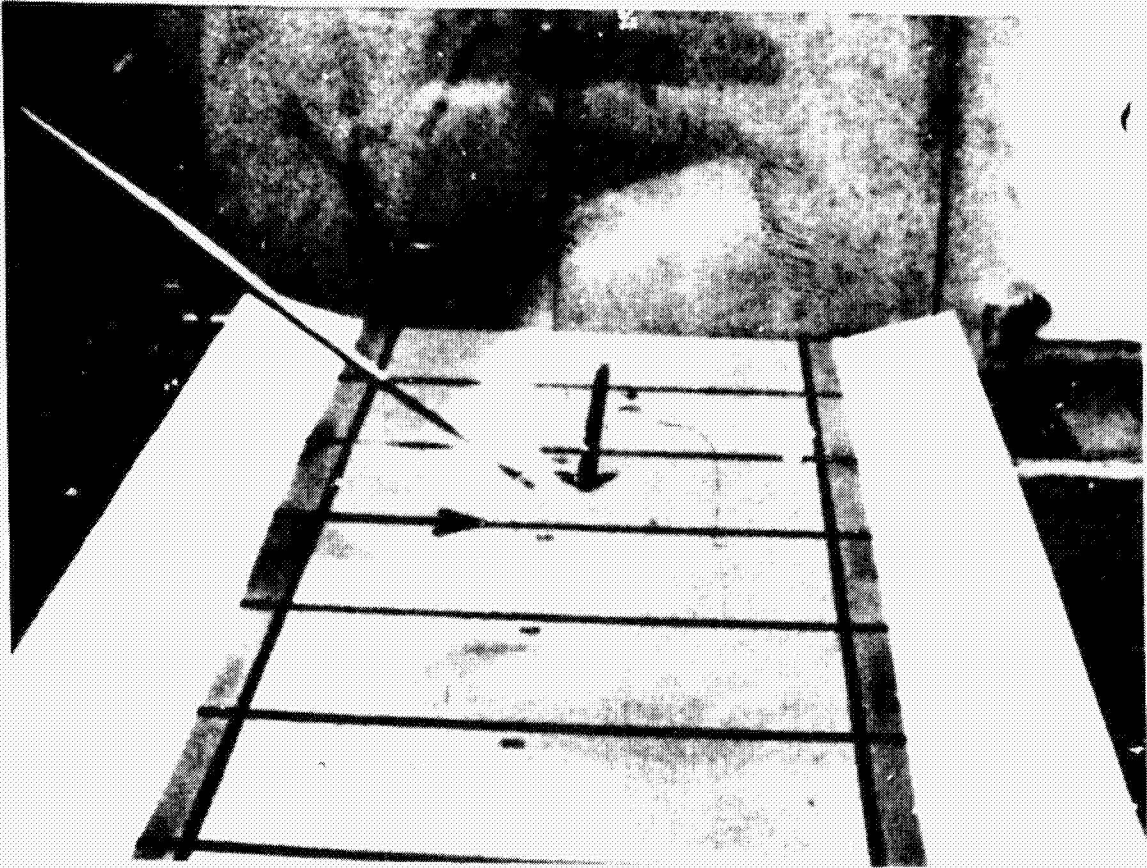
Figure 5
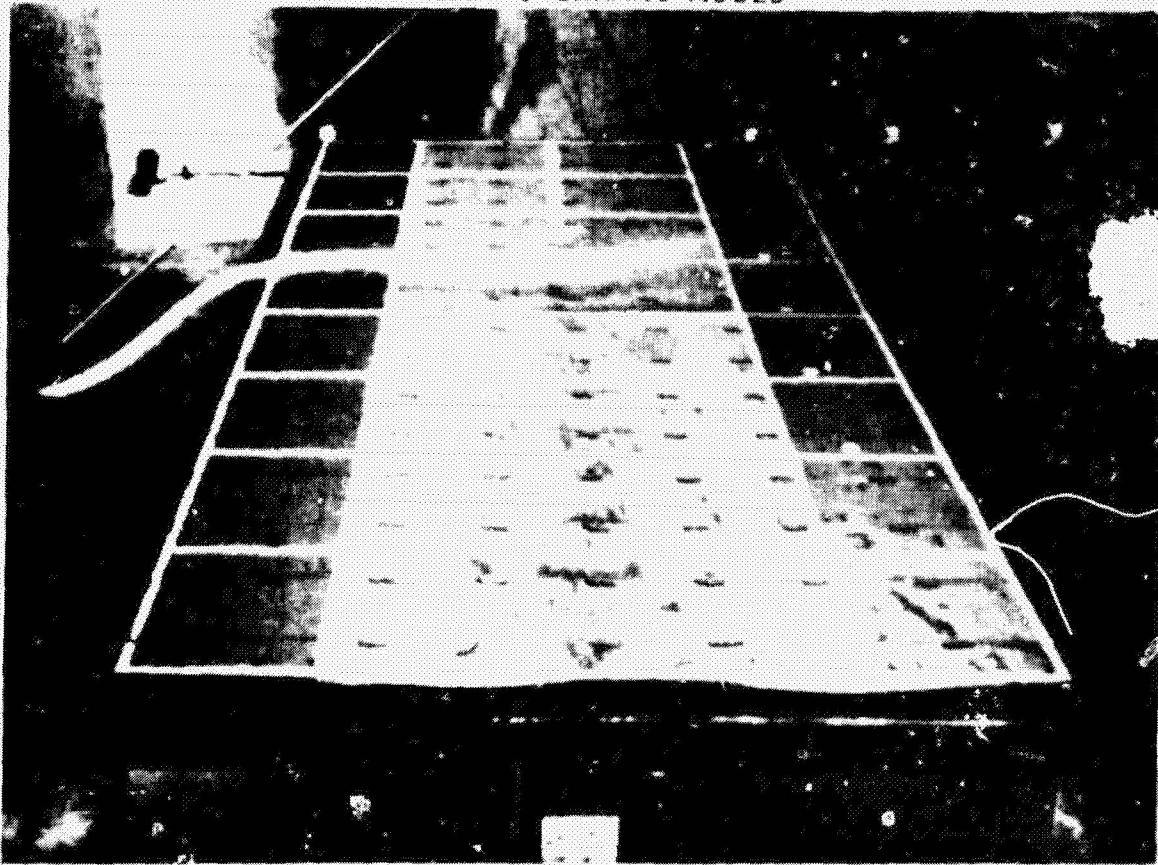
SMOKE FLOW
CURVED OVERHANG ADDED

Figure 6

SMOKE FLOW
FENCES ADDED
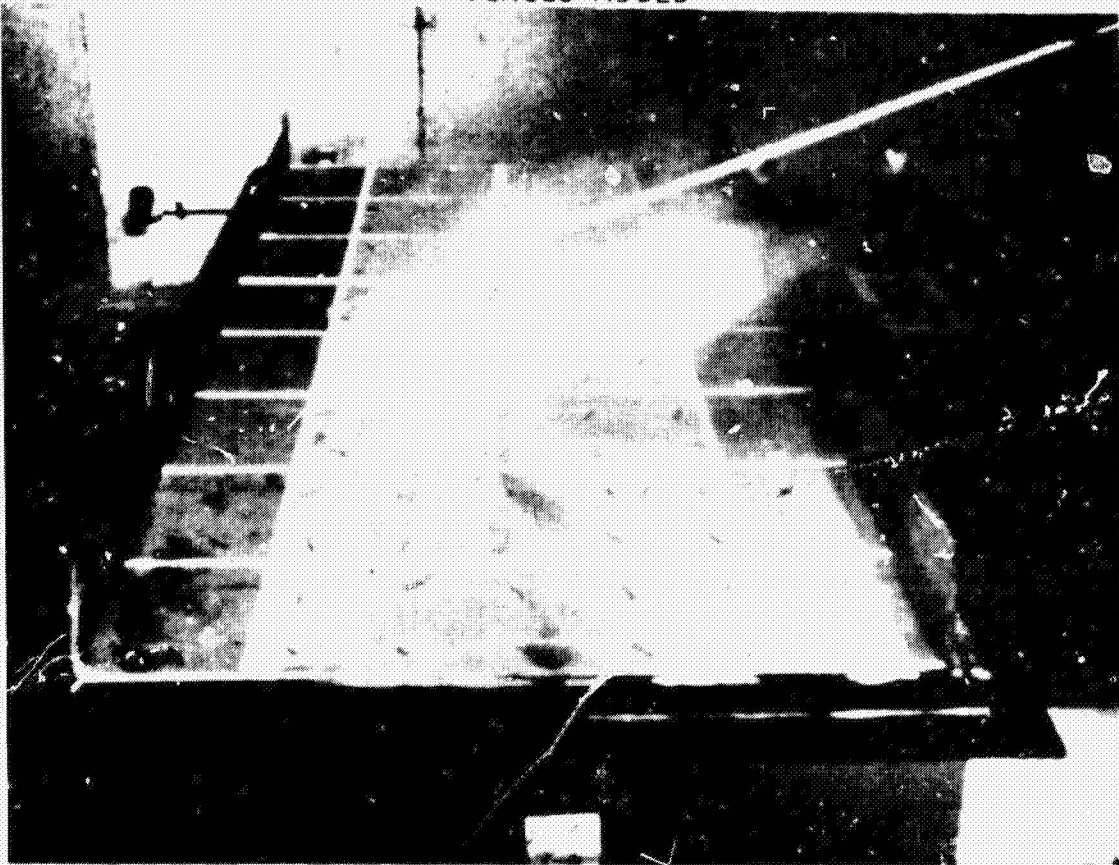
Figure 7

SMOKE FLOW
SOLID BUILDING
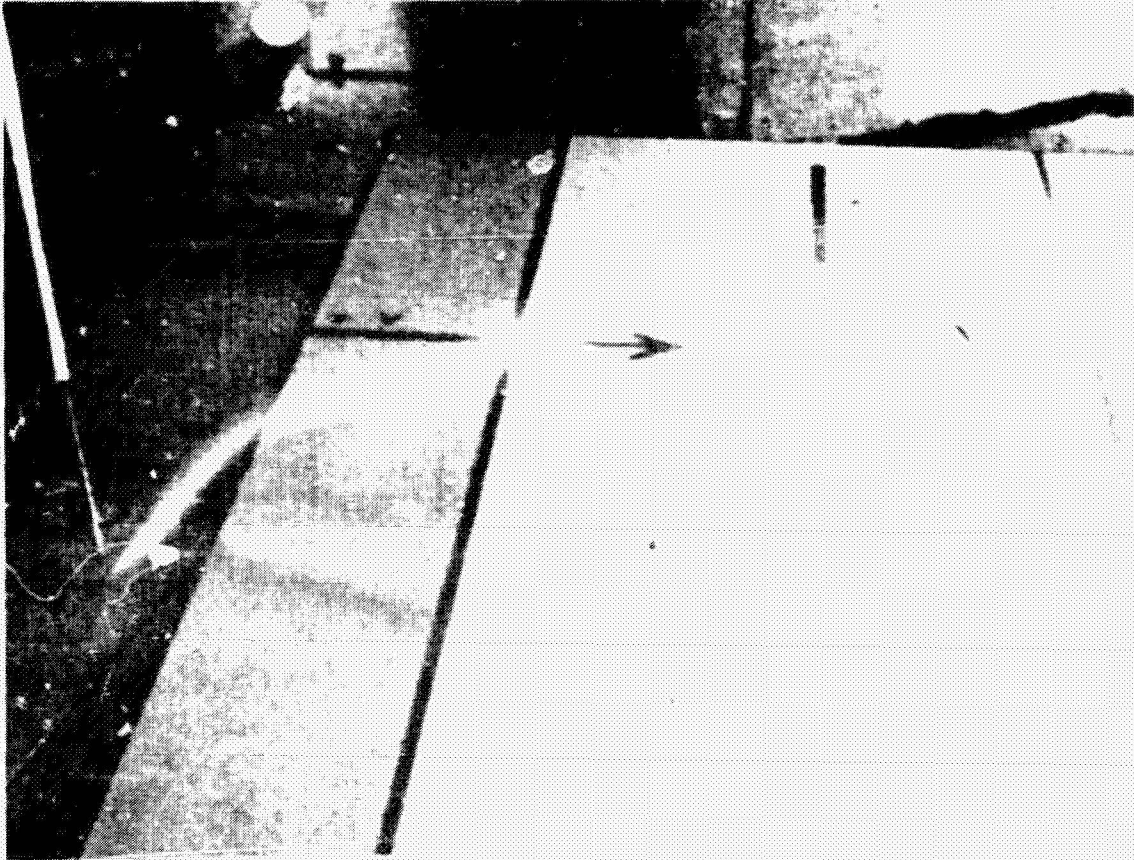
Figure 8

SMOKE FLOW
CURVED OVERHANG ADDED TO SOLID BUILDING
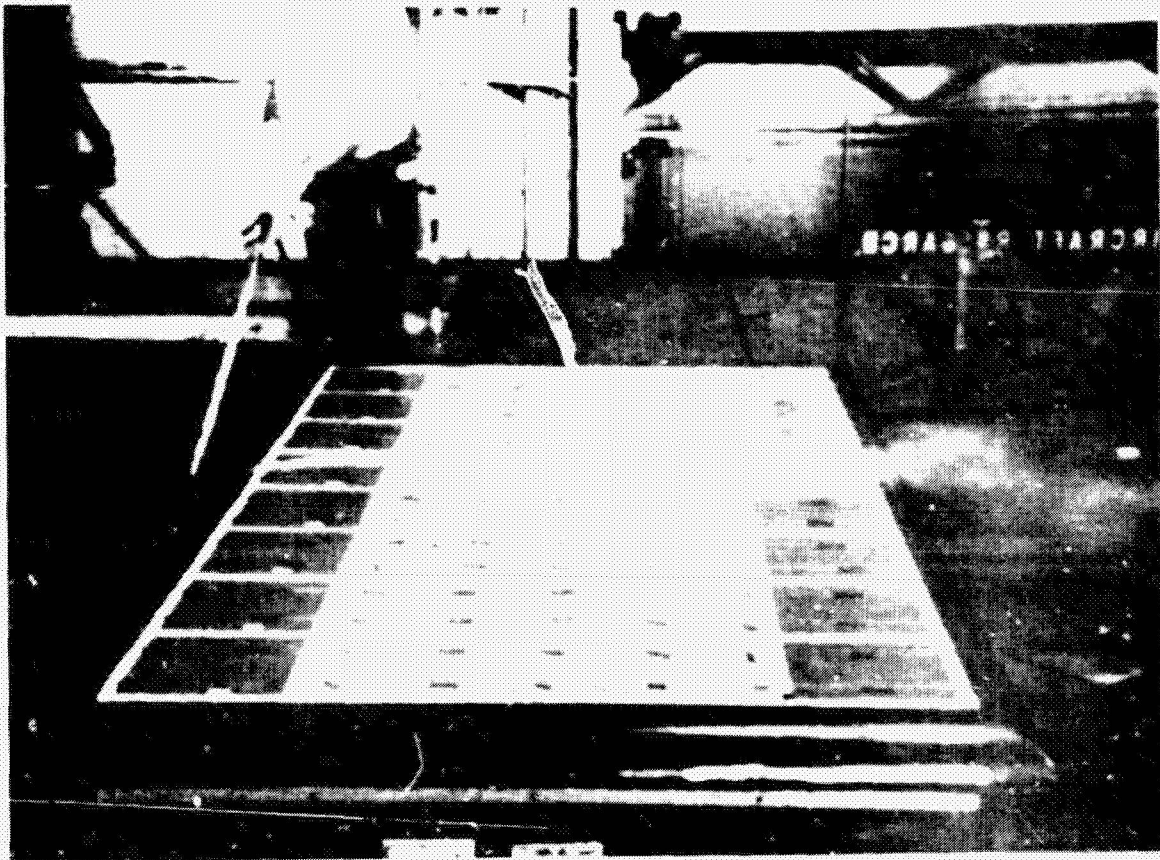
Figure 9

CROSSWIND VELOCITY PROFILE
AS A RESULT OF FENCE INSTALLATION

FENCES

BUILDING

GROUND
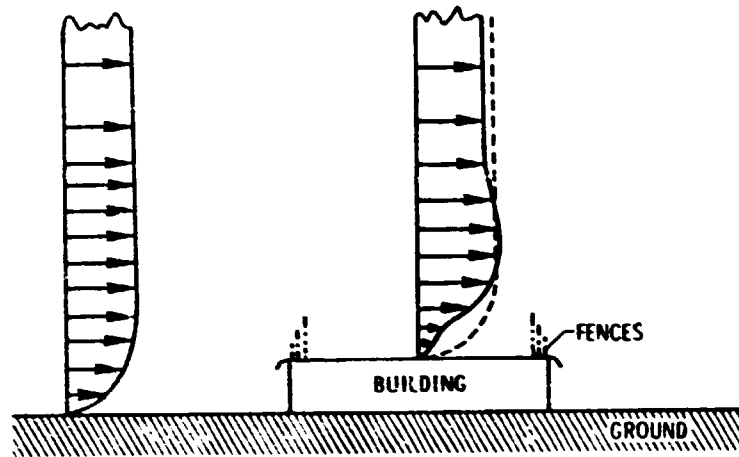
Figure 10

CROSSWIND LANDING FACTORS
30-knot CROSSWIND

V_g = 60 knots

V_{cw} = 15 knots

V_a = 62 knots

V_{cw} = 30 knots

V_g = 60 knots

V_a = 67 knots

STOL

14°

27°

7°

Figure 11

TEST SETUP

PITOT
STATIC
TUBE

FLOW

h_r

$0.0\% = 0.46h_b$

$.2b = h_b$

b

MODEL SCALE • 76 cm (30 in.)
FULL SCALE • 152 m (500 ft)
EACH POROUS SCREEN 30% SOLID
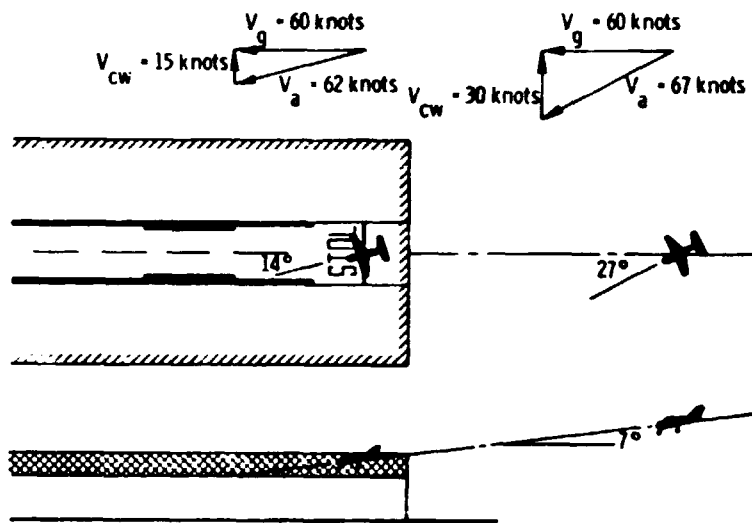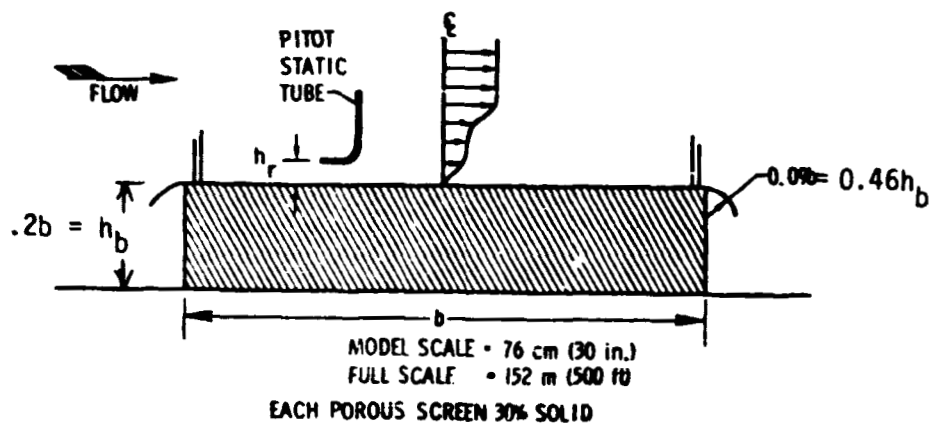
Figure 12
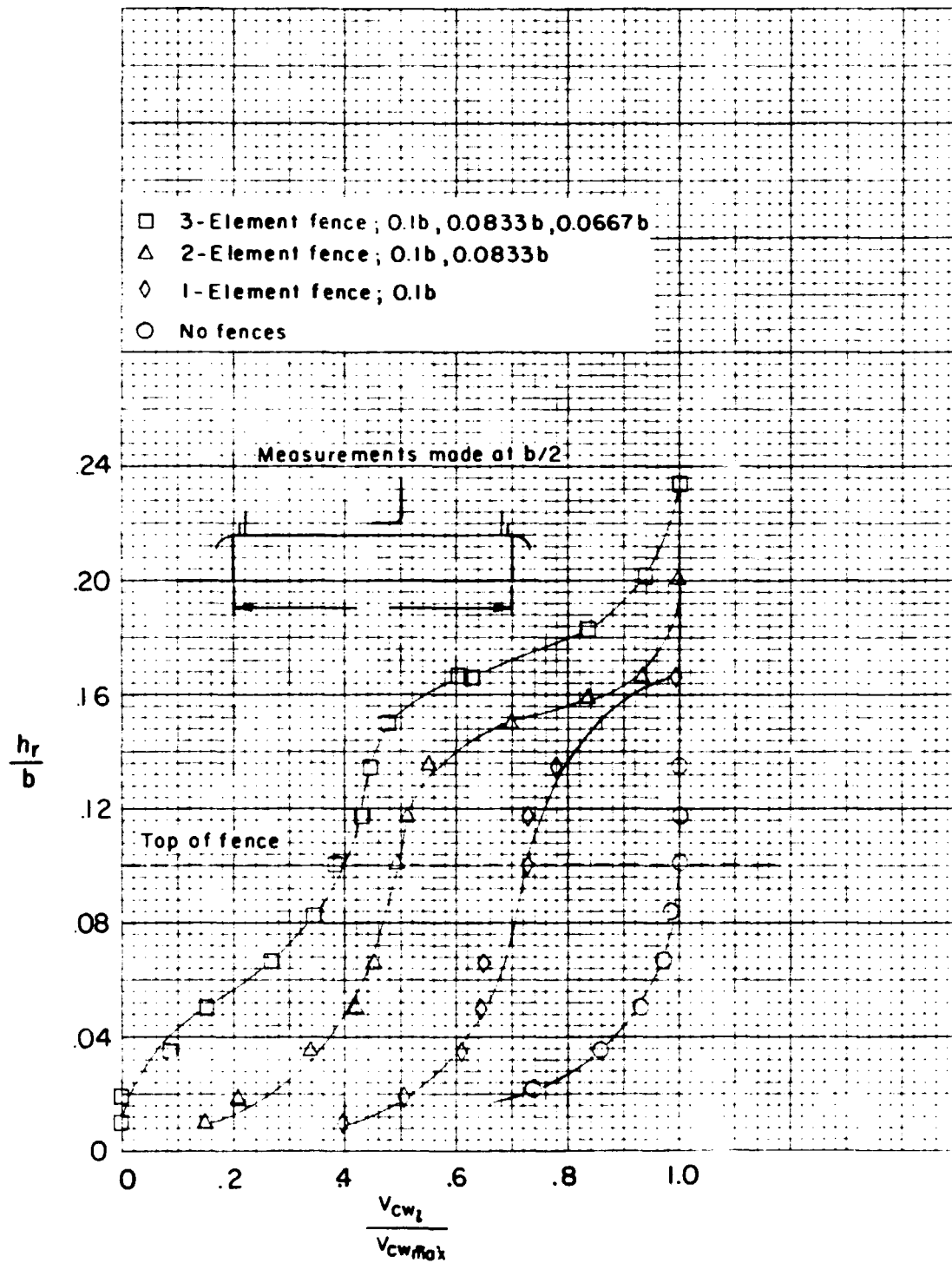
Fig. 13- Effect of fence configuration on cross wind profile
Fences constructed from 0.02" wire , 0.125" grid screen
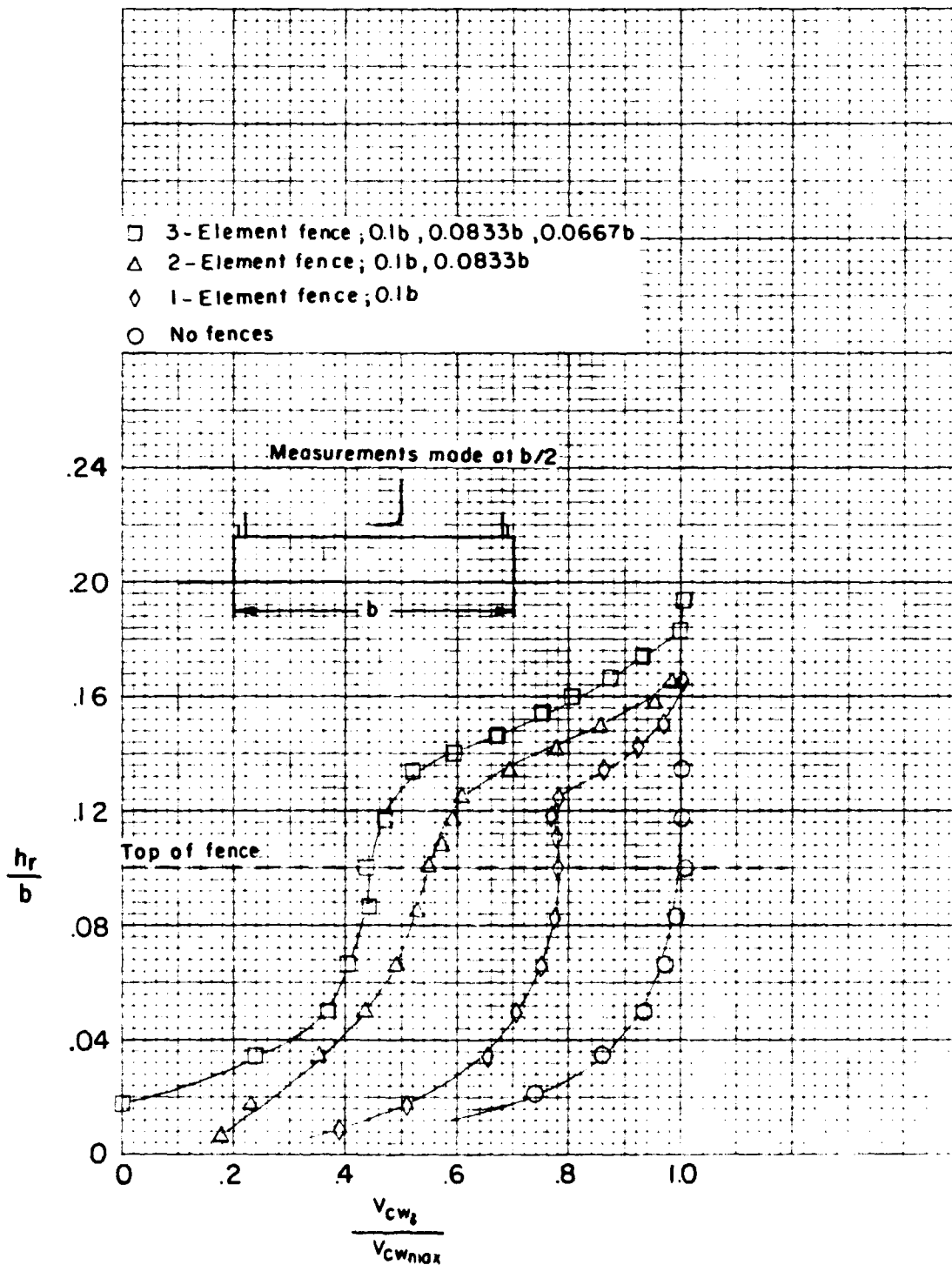
Fig. 14- Effect of fence configuration on cross wind profile fences constructed of 0.0009"wire, 0.0496"grid screen
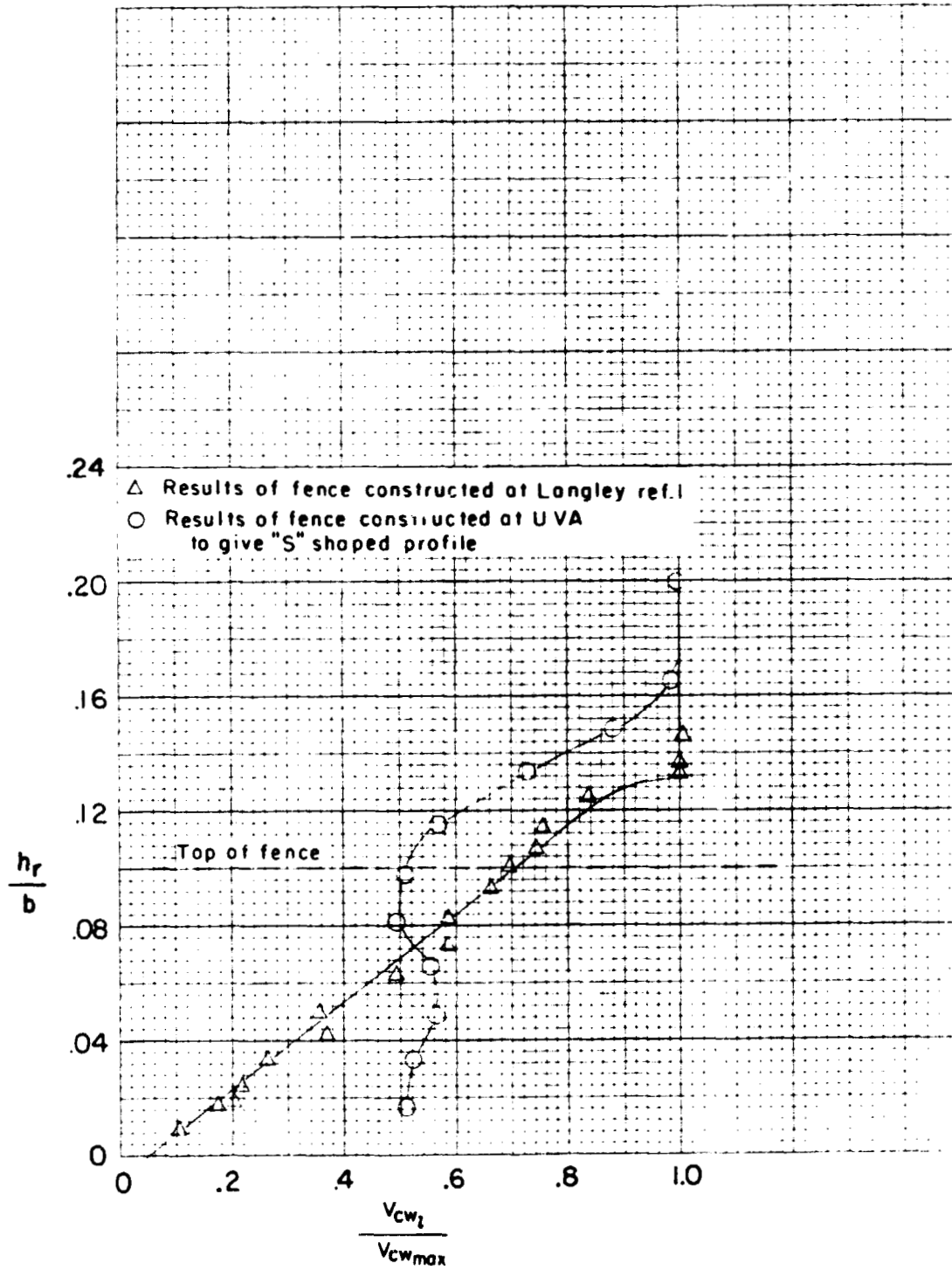
Fig. 15 - Demonstration of possibility of generating preconceived cross wind profile shapes
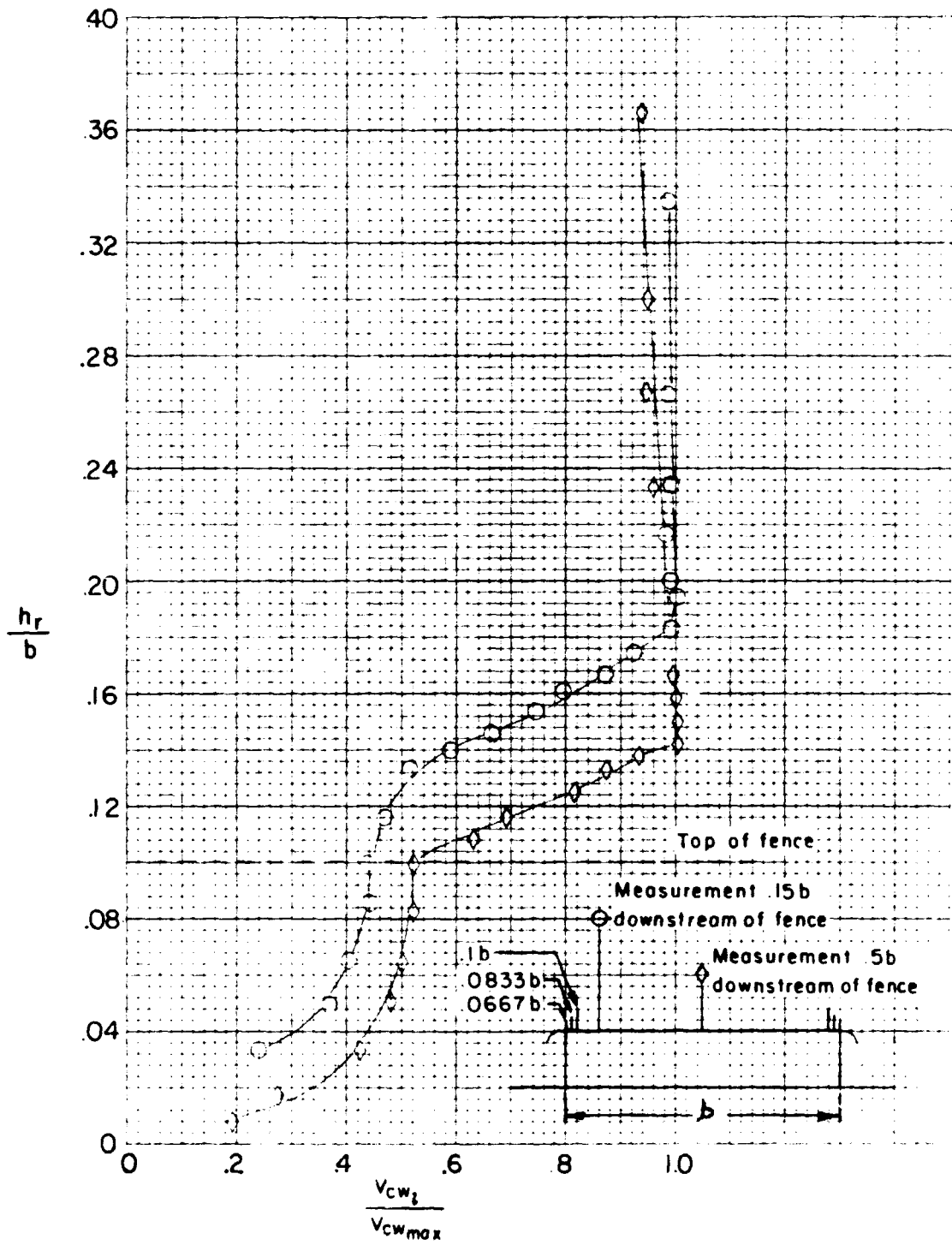
Fig. 16- Effect of distance from upstream fence on cross wind profile
3-Element fence. Each element constructed from
.009" wire , .0496" grid screen
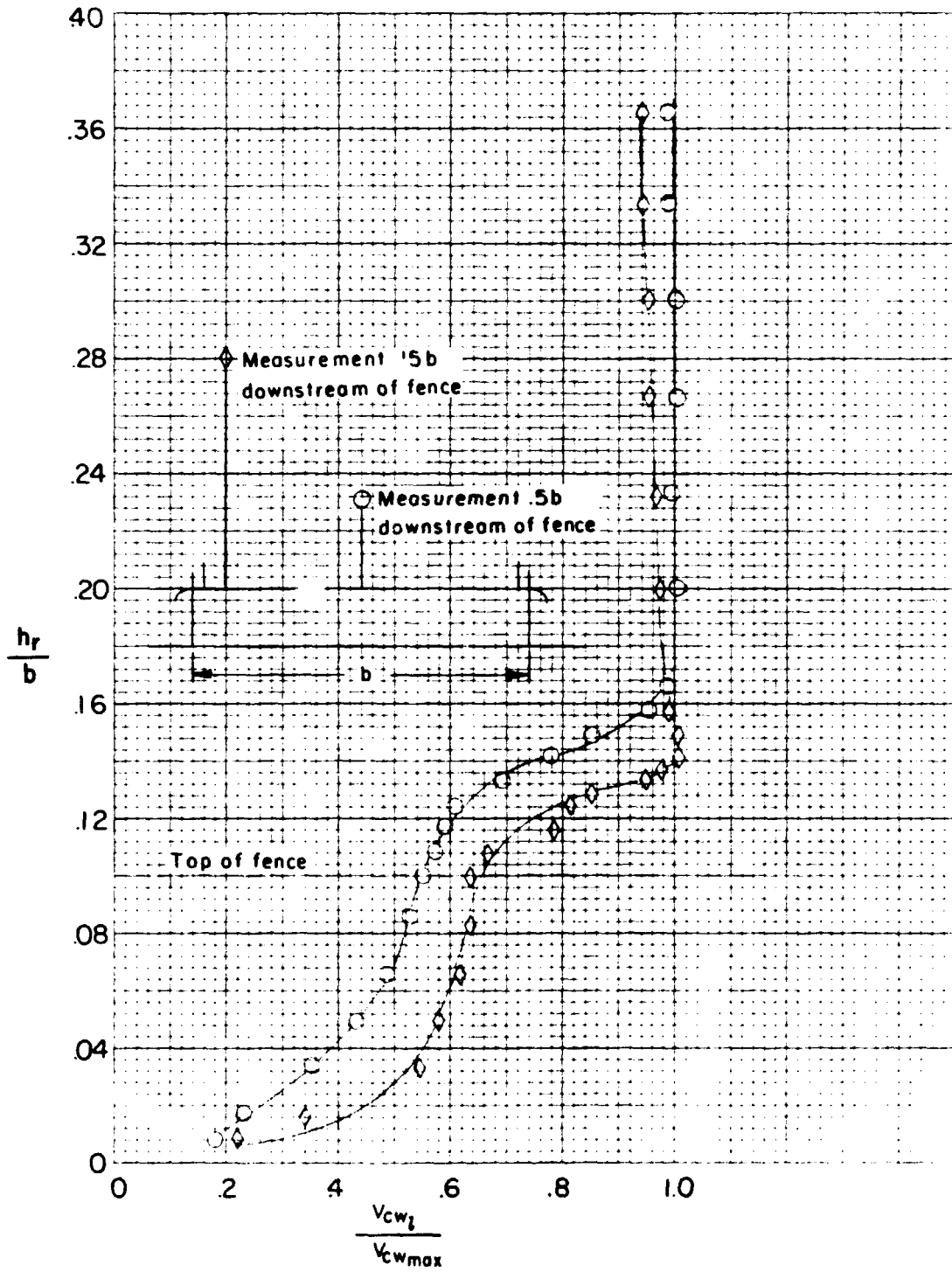
Fig. 17- Effect of distance from upstream fence on cross wind profile
2-Element fence. Each element constructed from
0.009" wire, 0.0496" grid screen
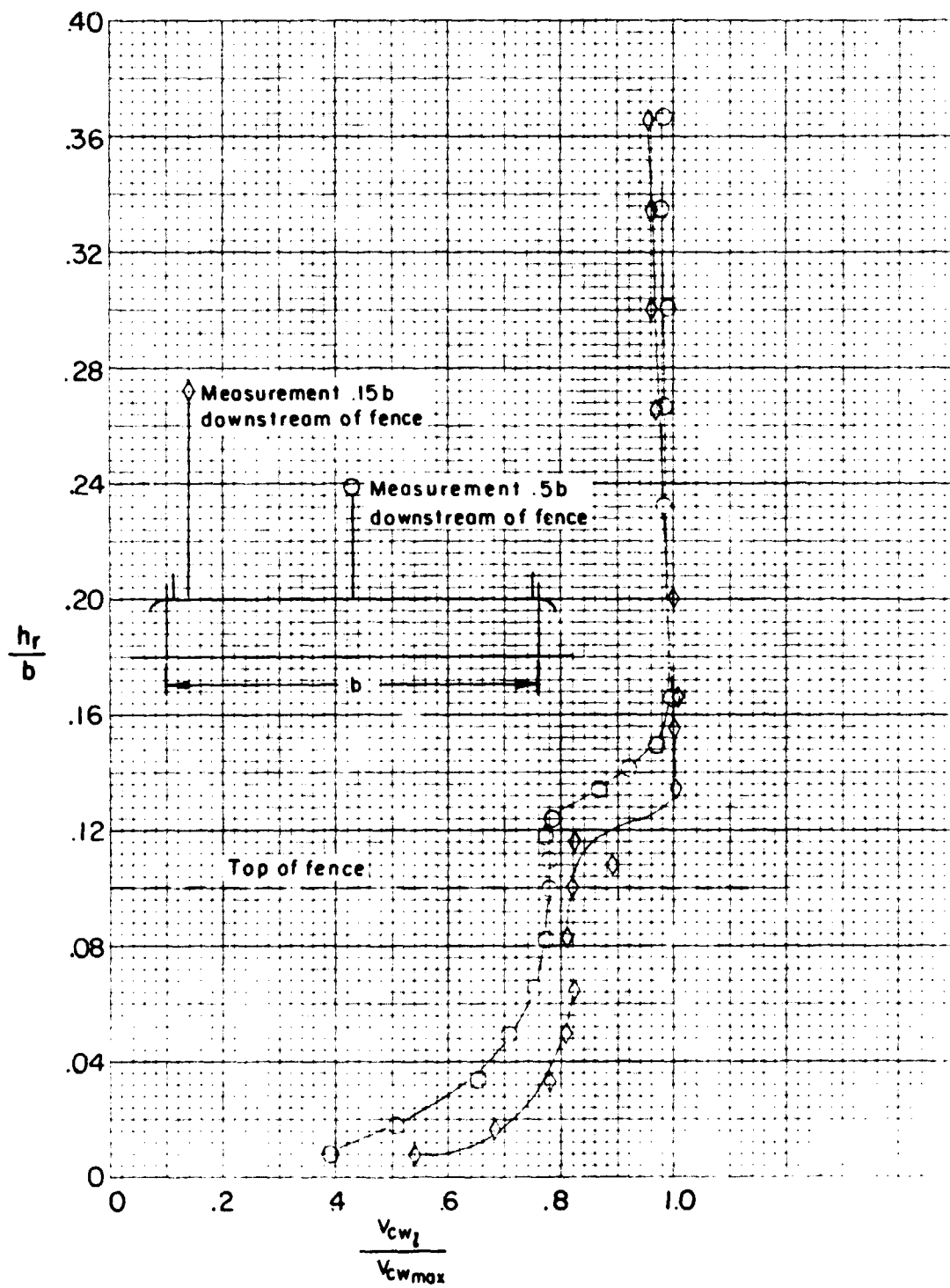
Fig. 18- Effect of distance from upstream fence on cross wind profile
b-Element fence constructed from 0.009" wire,
0.496" grid screen
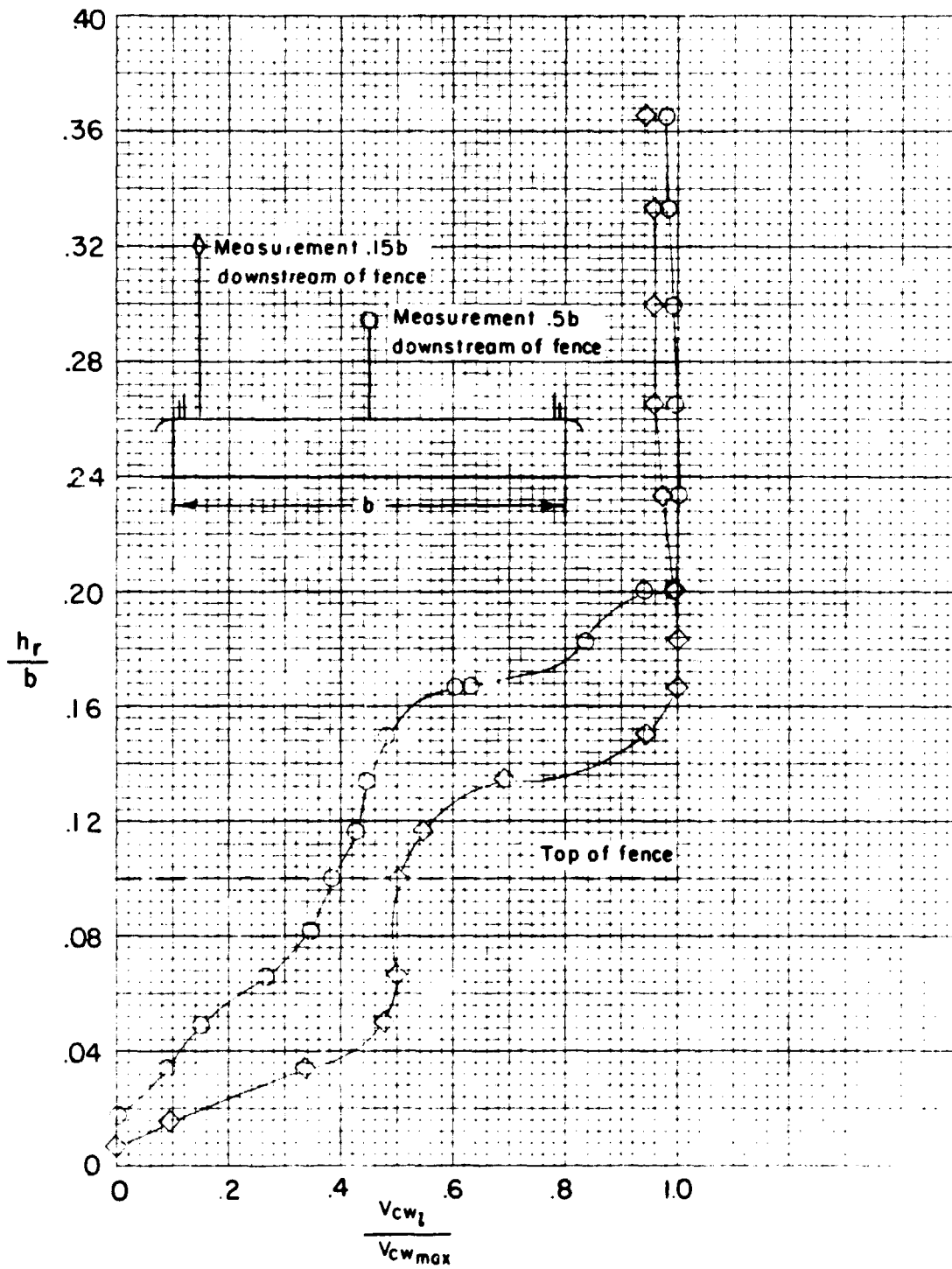
Fig. 19- Effect of distance from upstream fence on cross wind profile
3-Element fence; constructed from
0.02" wire, 0.0125" grid screen
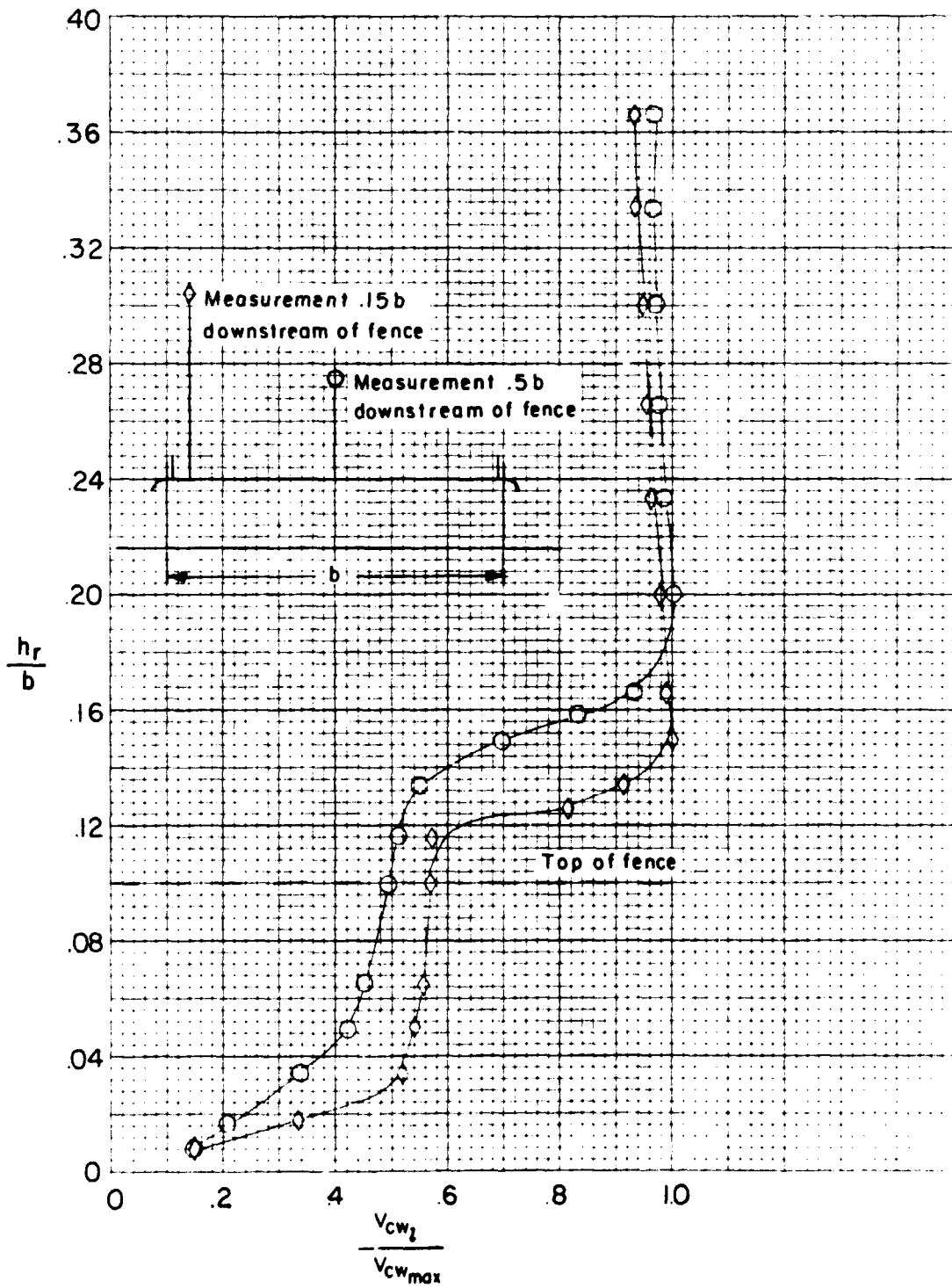
Fig. 20- Effect of distance from upstream fence on cross wind profile
2-Element fence ; constructed from
0.02" wire , 0.125" grid screen
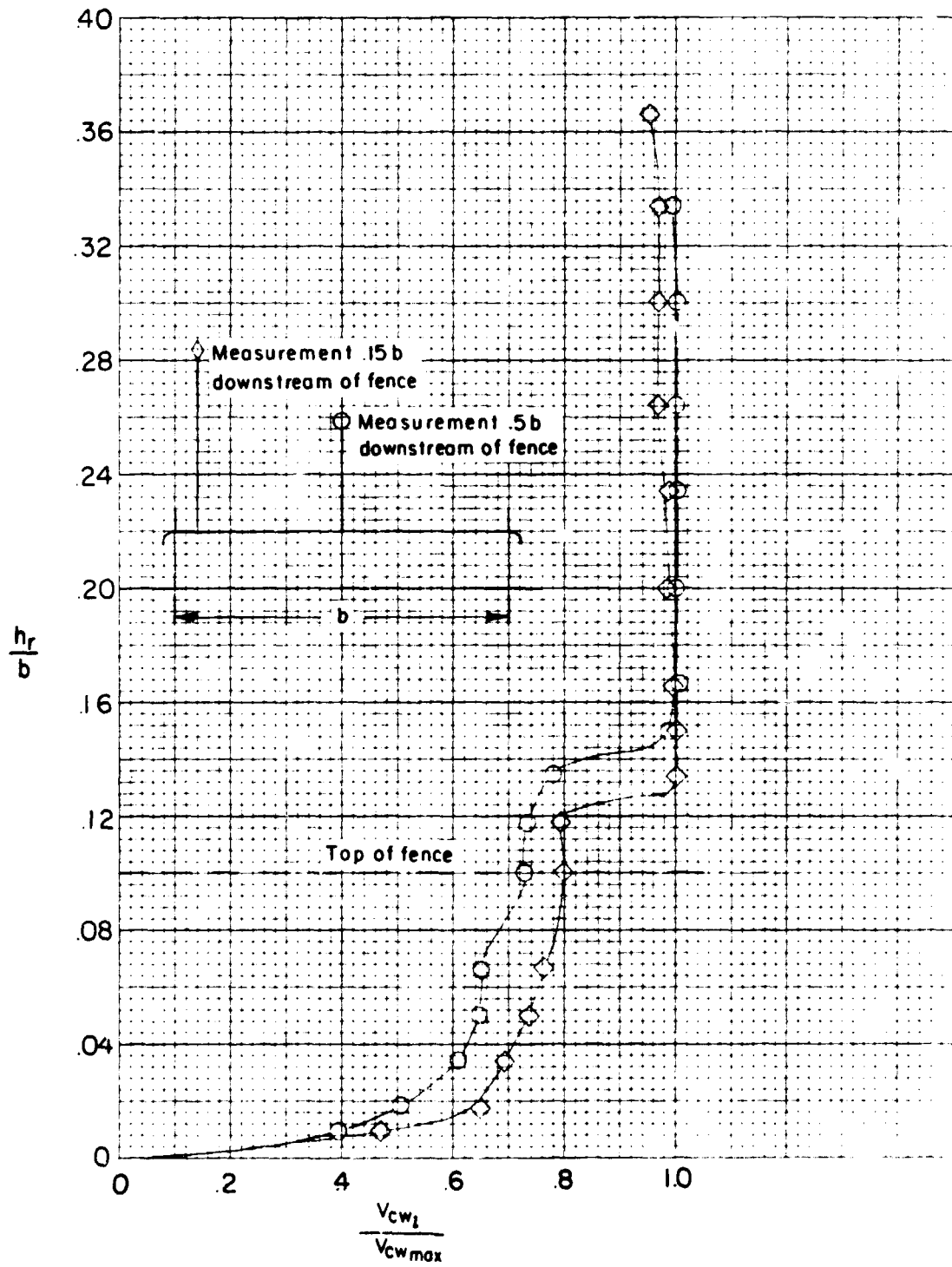
Fig. 21- Effect of distance from upstream fence on cross wind profile
1-Element fence ; constructed from 0.02"wire 0.25"grid screen
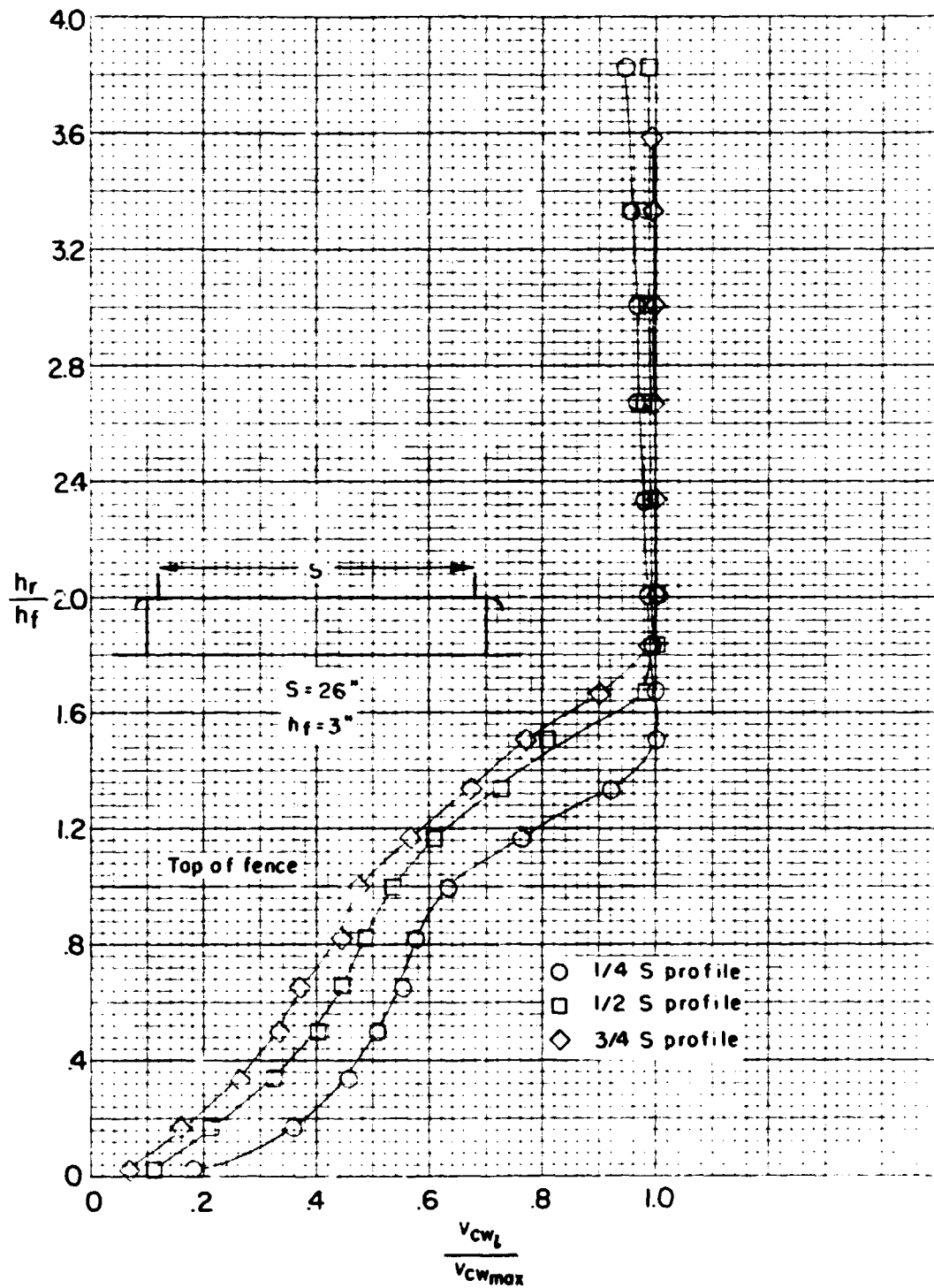
Fig. 22- Effect of distance from upstream fence on cross wind profile

(Distance between upstream and downstream fences, S) / (max fence height, h_f) = 8.67
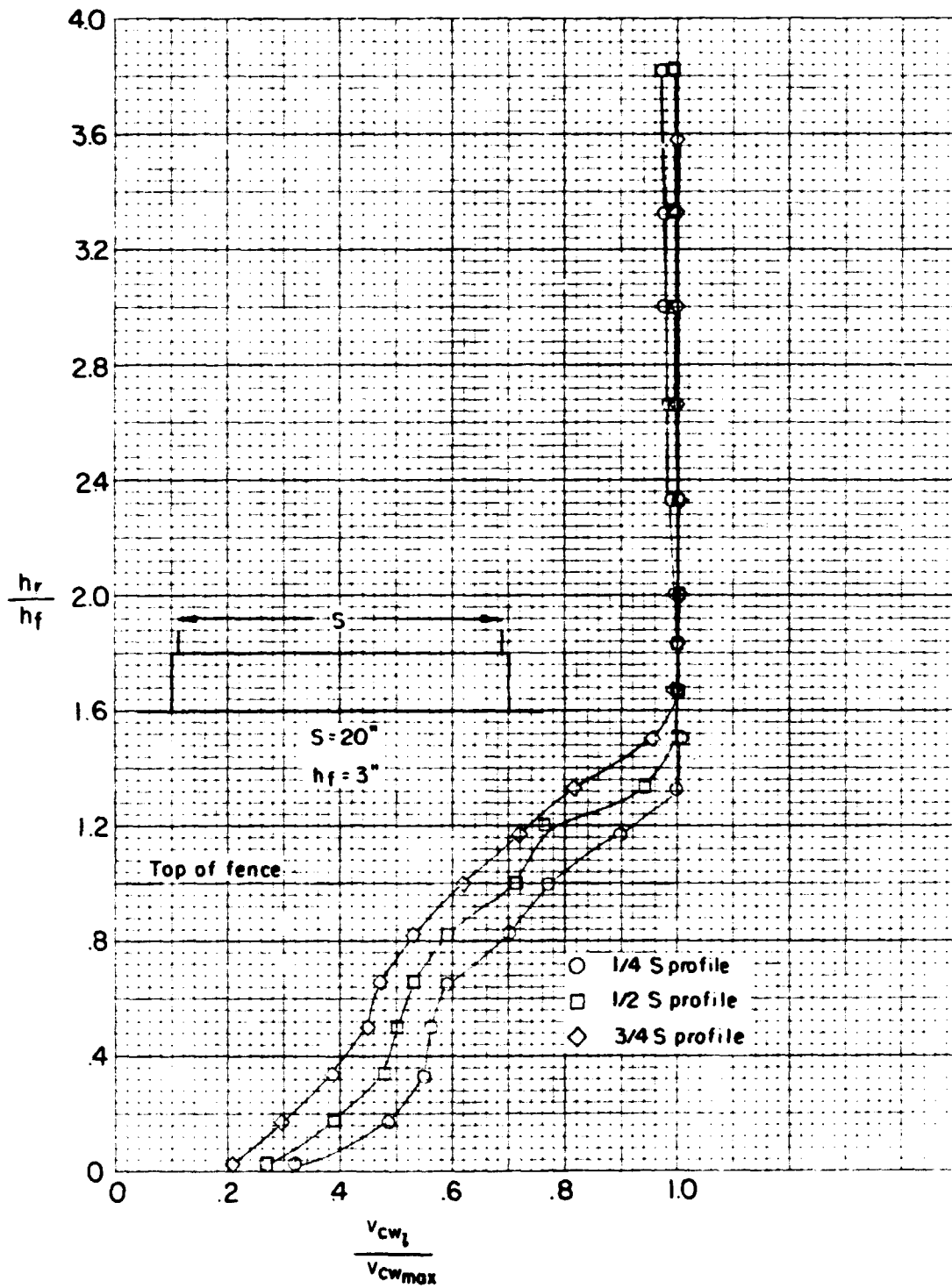
Fig. 23- Effect of distance from upstream fence on cross wind profile
(Distance between upstream and downstream fences, S)/(max fence height, h_f)=6.667
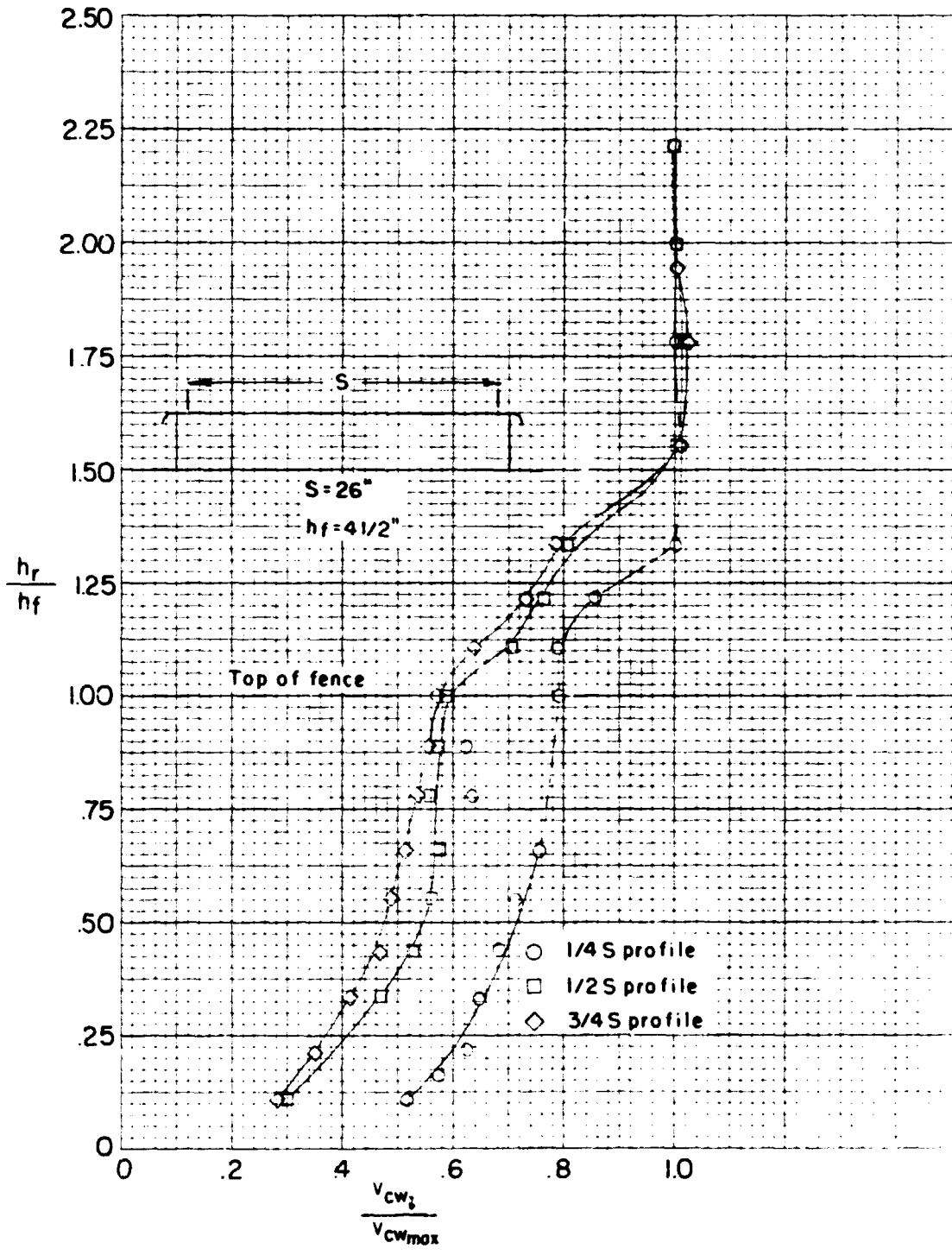
Fig. 24- Effect of distance from upstream fence on cross wind profile
(Distance between upstream and downstream fences, S)/(max fence height, h$_f$)=5.77
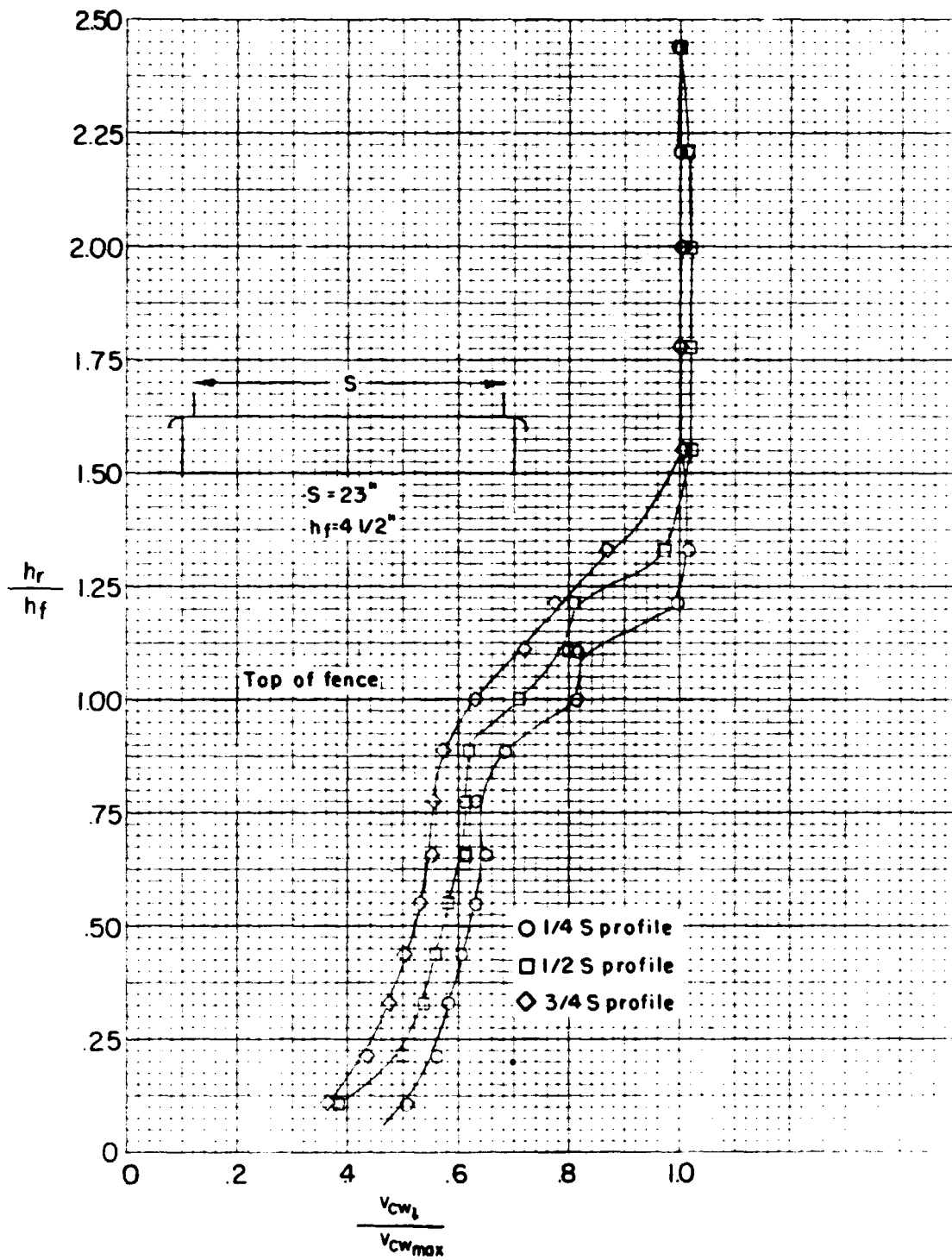
Fig. 25- Effect of distance from upstream fence on cross wind profile
(Distance between upstream and downstream fences, S)/(max fence height, h_f) = 5.11
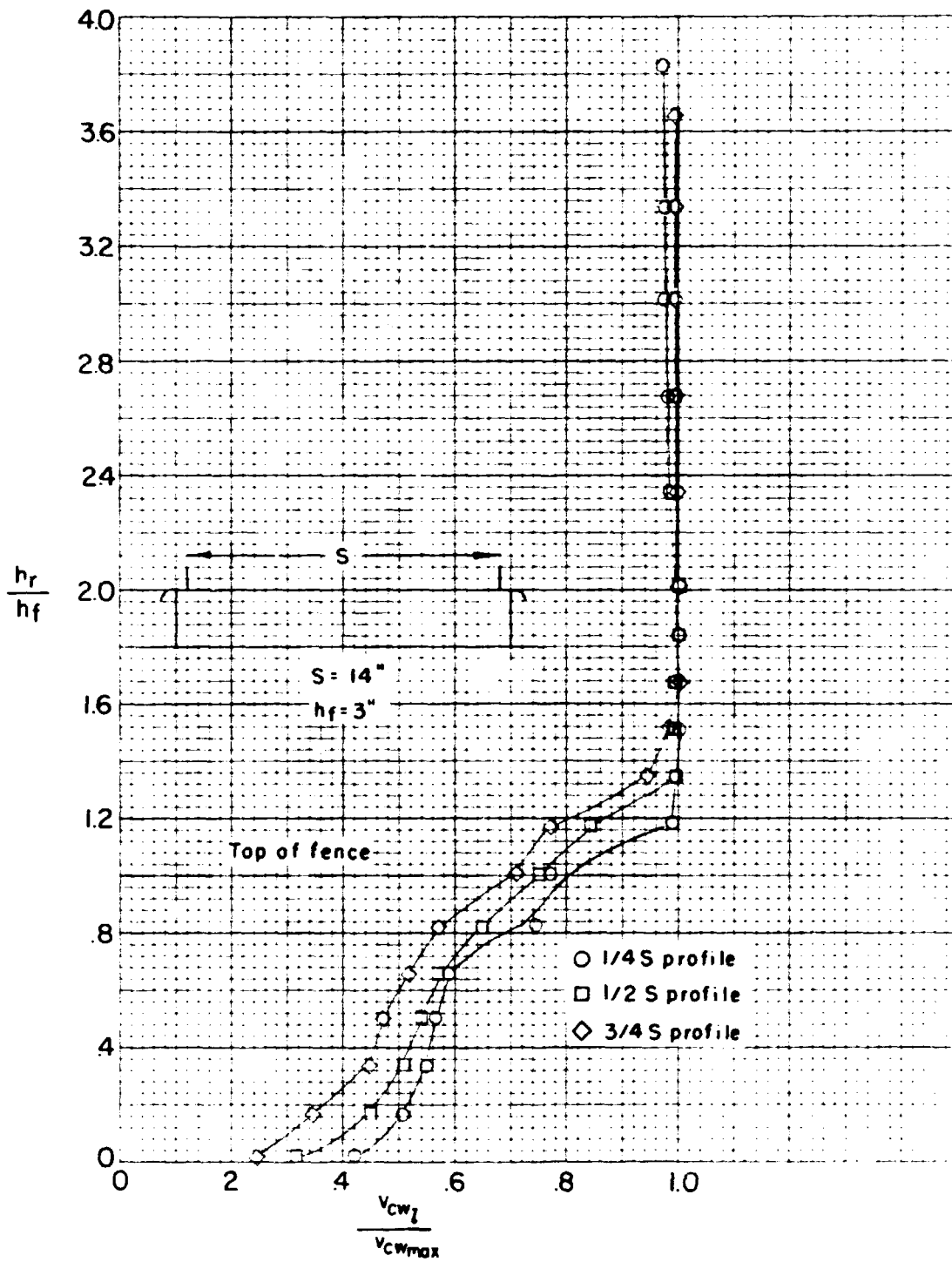
Fig. 26- Effect of distance from upstream fence on cross wind profile
(Distance between upstream and downstream fences,S)/max fence height,h_f)=4.67
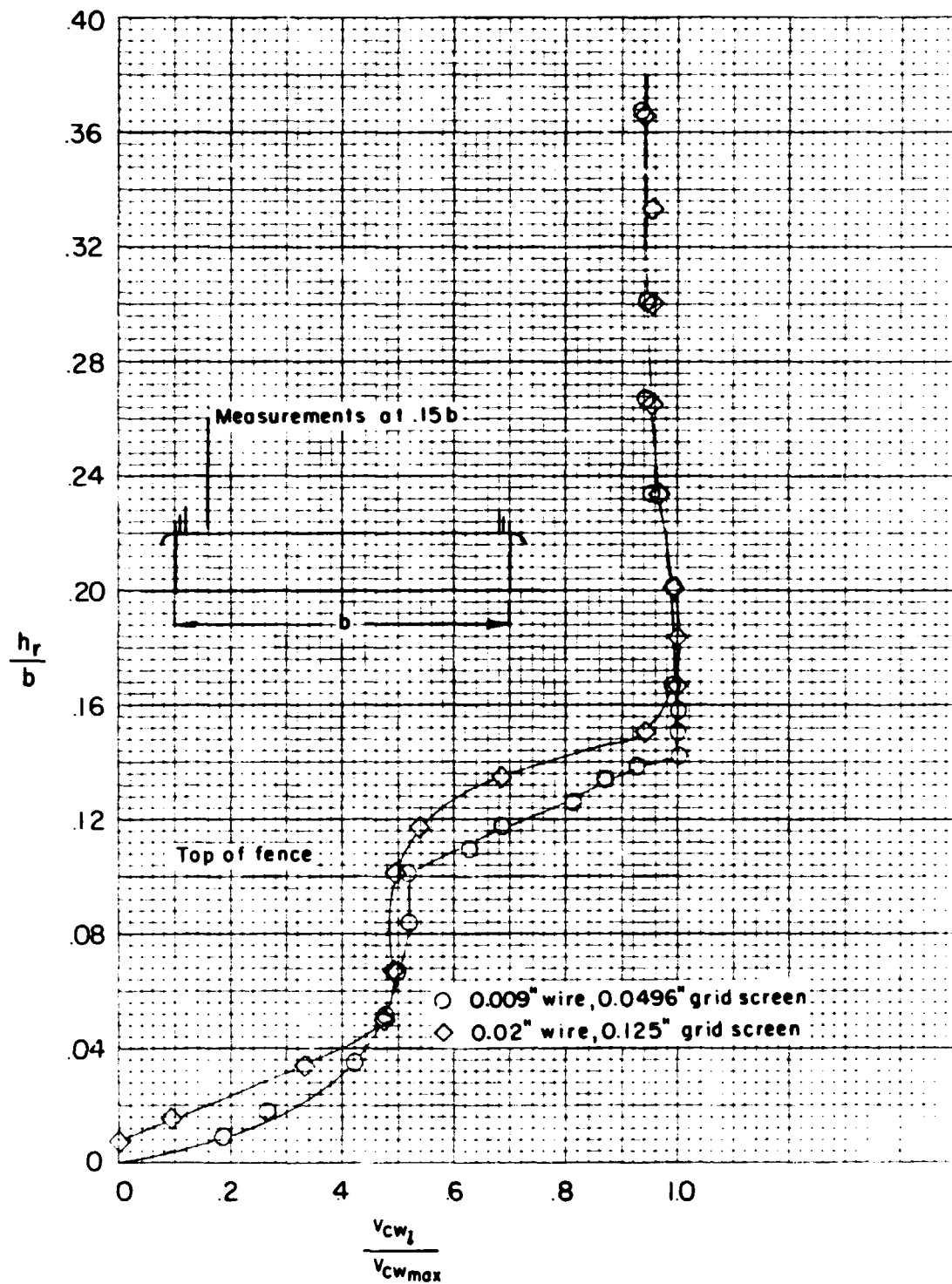
Fig. 27 - Effect of screen geometry 3-element fences
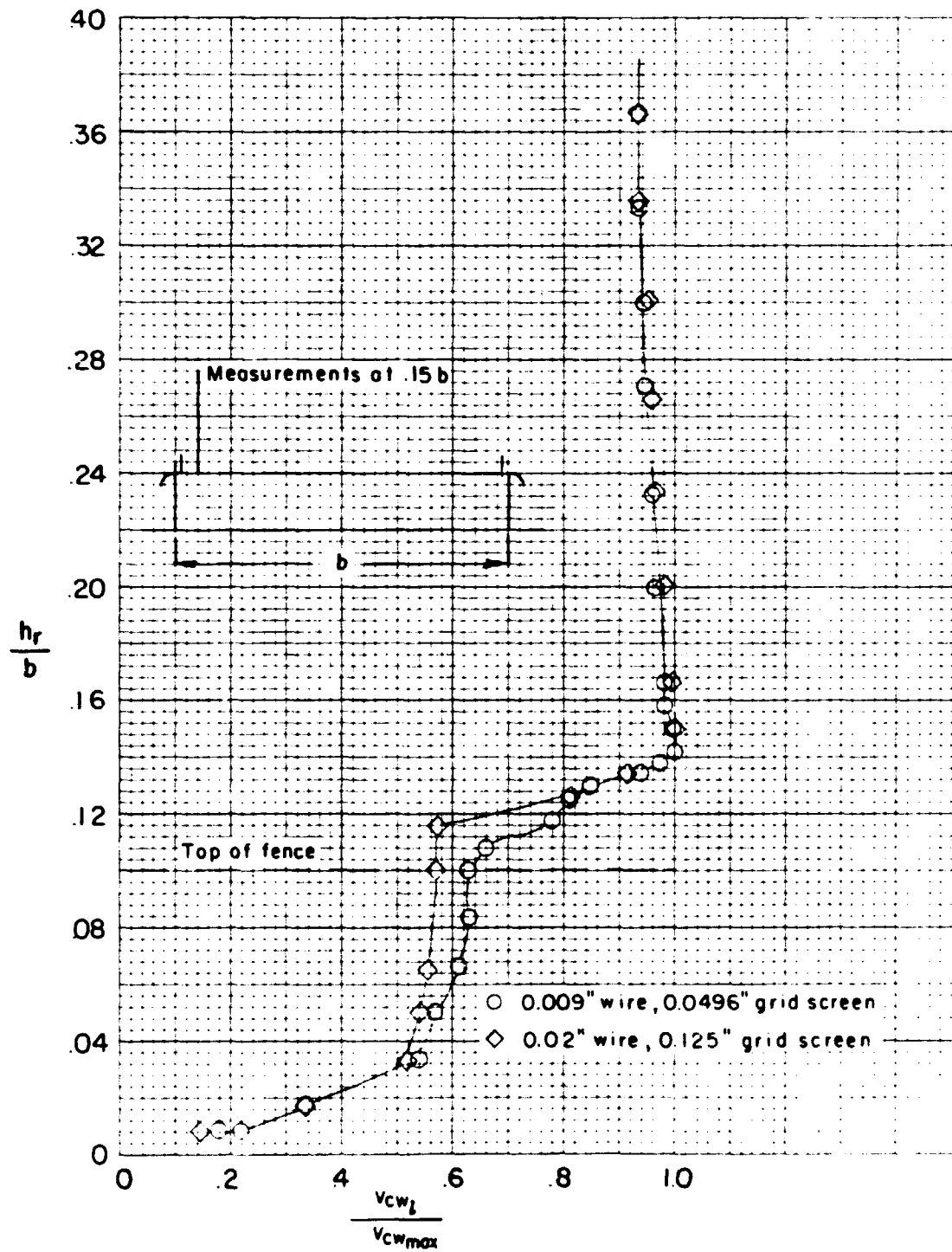
Fig. 28- Effect of screen geometry   2-element fences
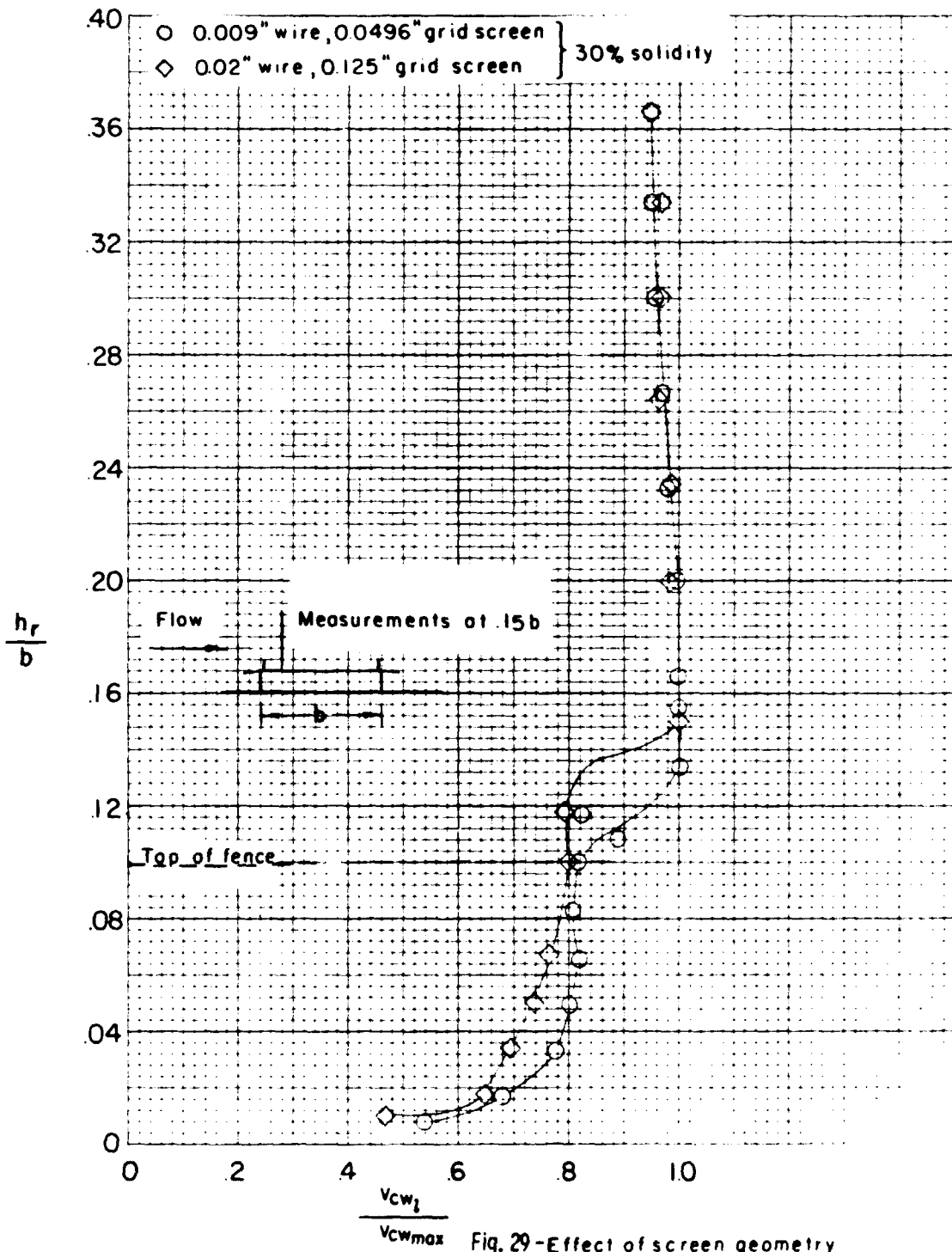
Fig. 29 - Effect of screen geometry
1-element fences ; 1 b
Measurements made 0.15 b
from upstream fence
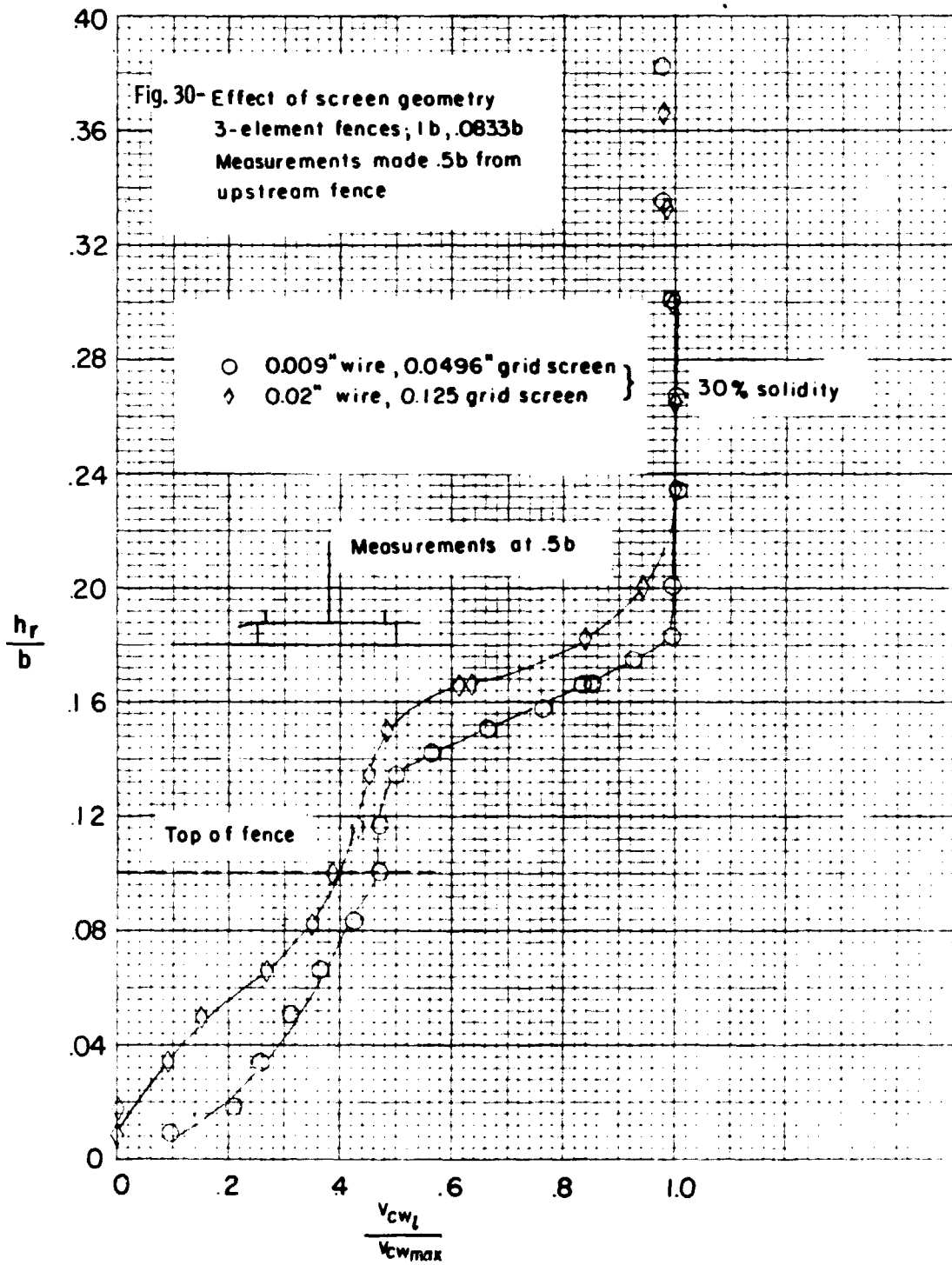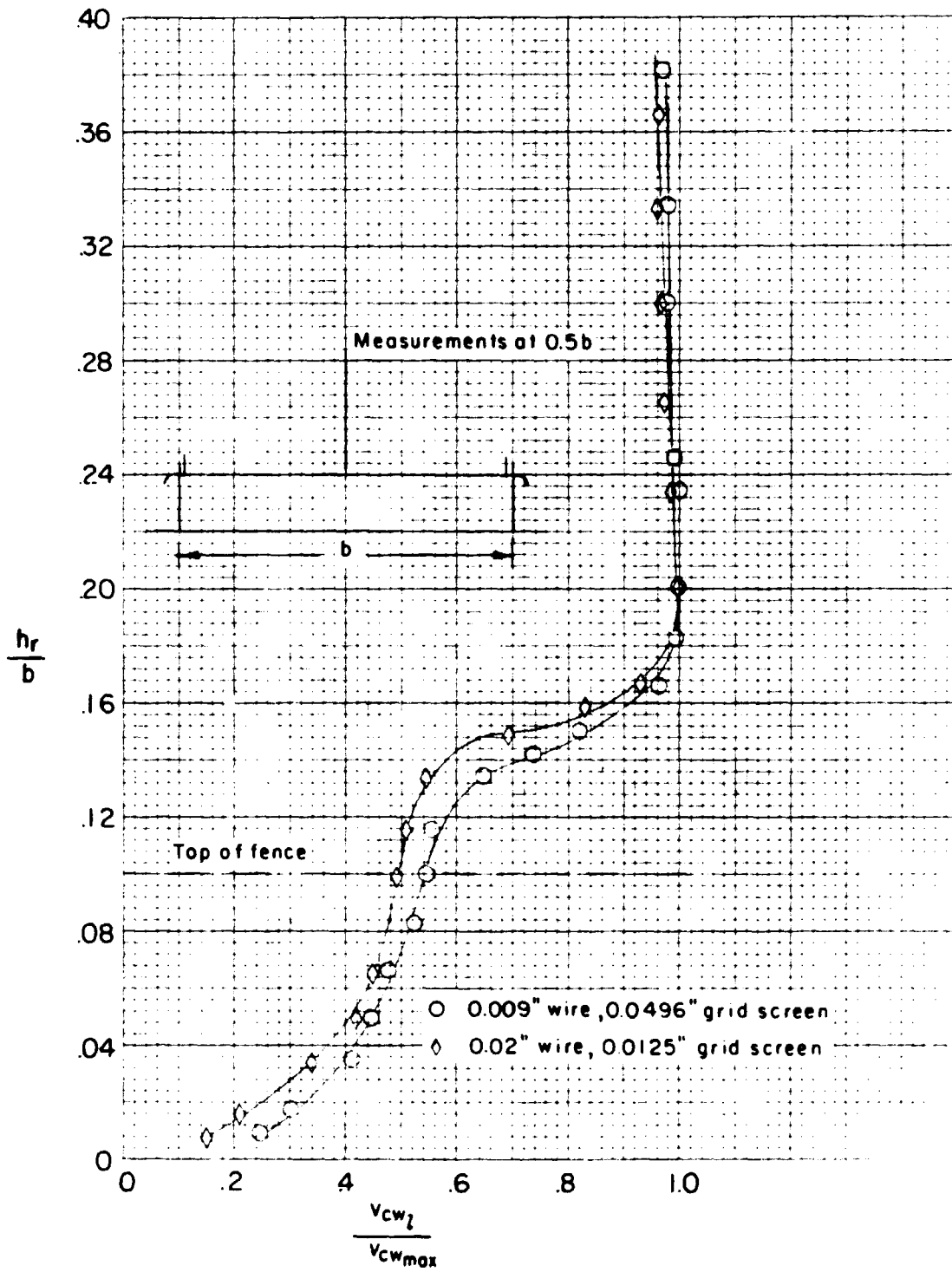
Fig. 30- Effect of screen geometry
3-element fences; 1b, .0833b
Measurements made .5b from
upstream fence

○ 0.009" wire , 0.0496" grid screen ⎫
◊ 0.02" wire , 0.125 grid screen   ⎬ 30% solidity

Measurements at .5b

Top of fence

$\dfrac{h_r}{b}$

$\dfrac{V_{cw_l}}{V_{cw_{max}}}$

Fig. 31- Effect of screen geometry 2-element fences

Fig. 32- Effect of screen geometry
1-element fences; .1 b
Measurements made .1 b
from upstream fence

O   0.009" wire, 0.0496" grid screen ⎤
◊   0.02" wire, 0.0125" grid screen ⎦   30% solidity

Measurements at 0.5 b

FLOW

b

Top of fence

$\frac{h_r}{b}$

$\frac{V_{cw_l}}{V_{cw_{max}}}$

EFFECT OF FENCE LOCATION
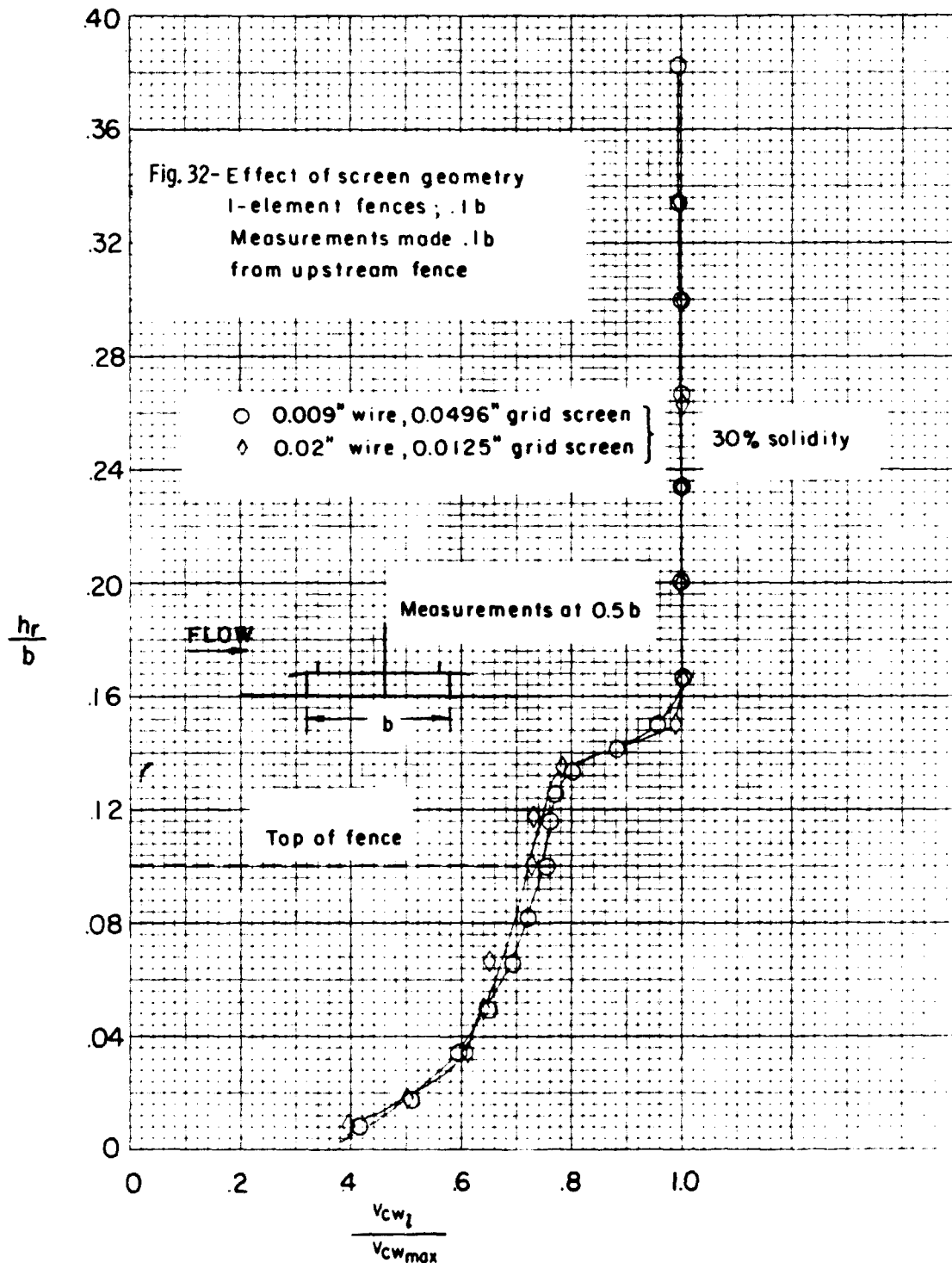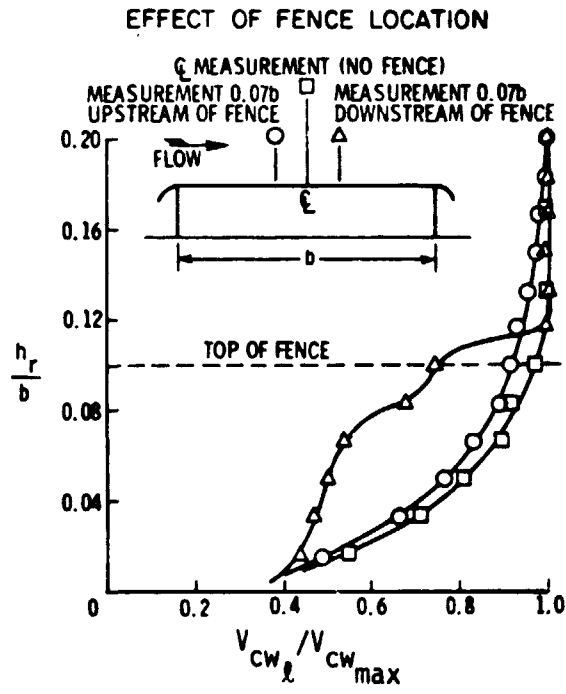
Figure 33
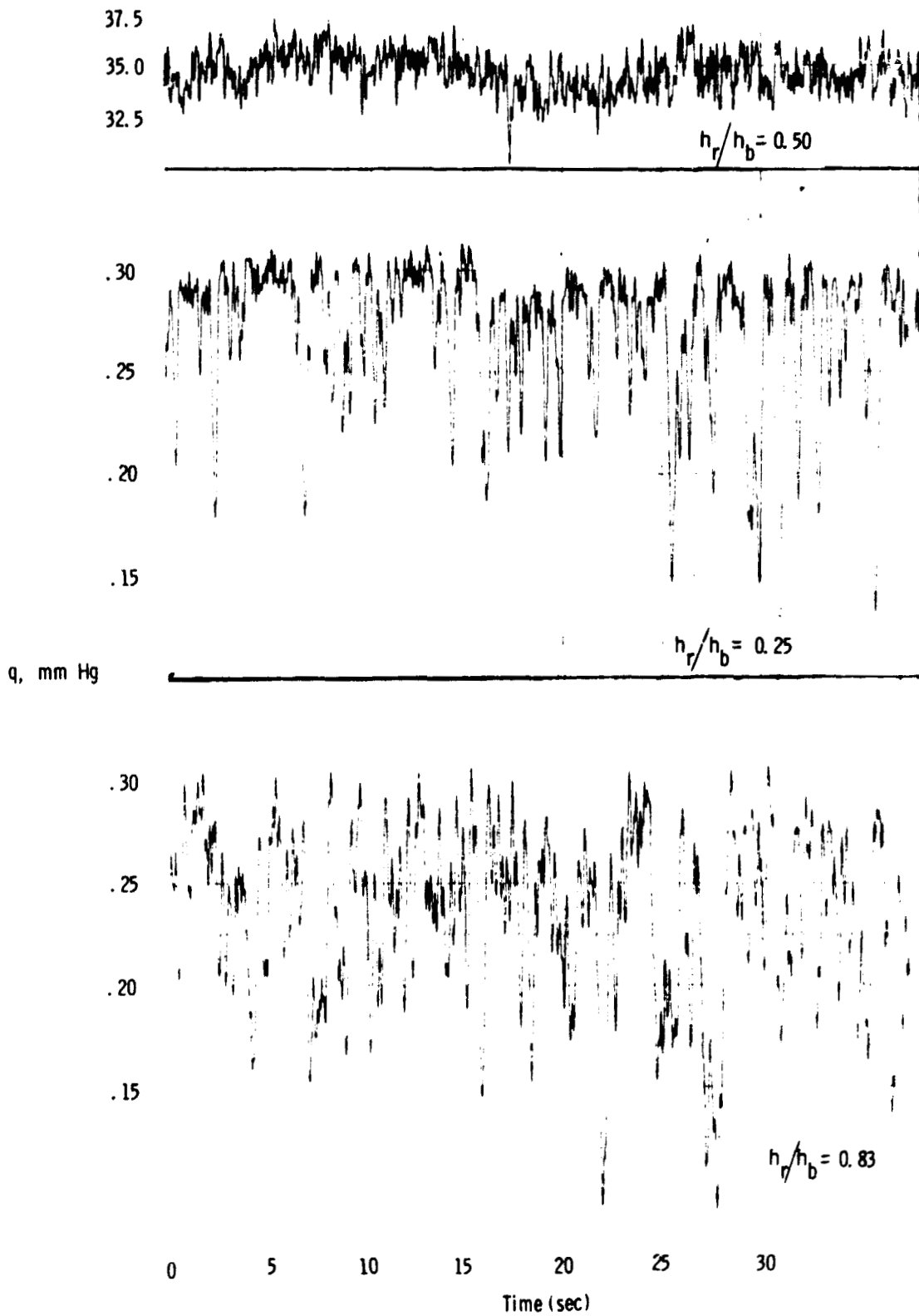
Fig. 34-Effect of height above building on turbulence
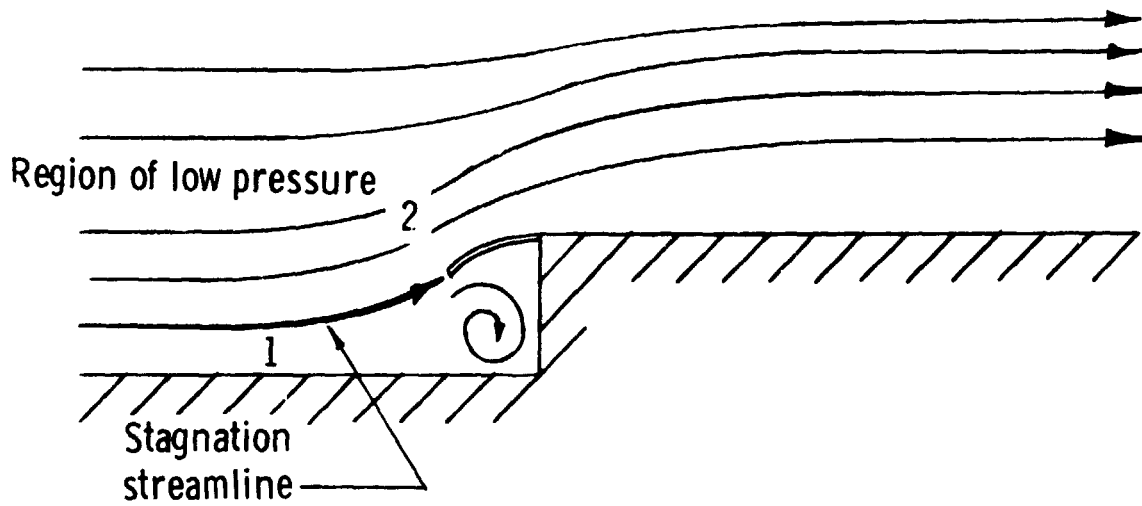
Fig. 35- Flow over building model when stagnation streamline is attached.
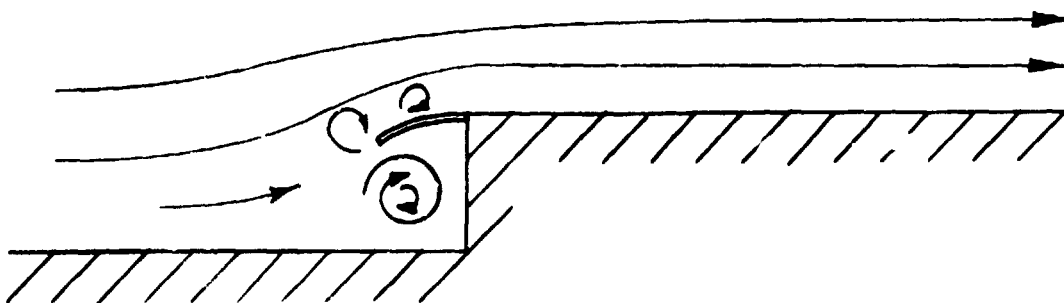
Fig. 36- Flow over building model when stagnation streamline has detached.
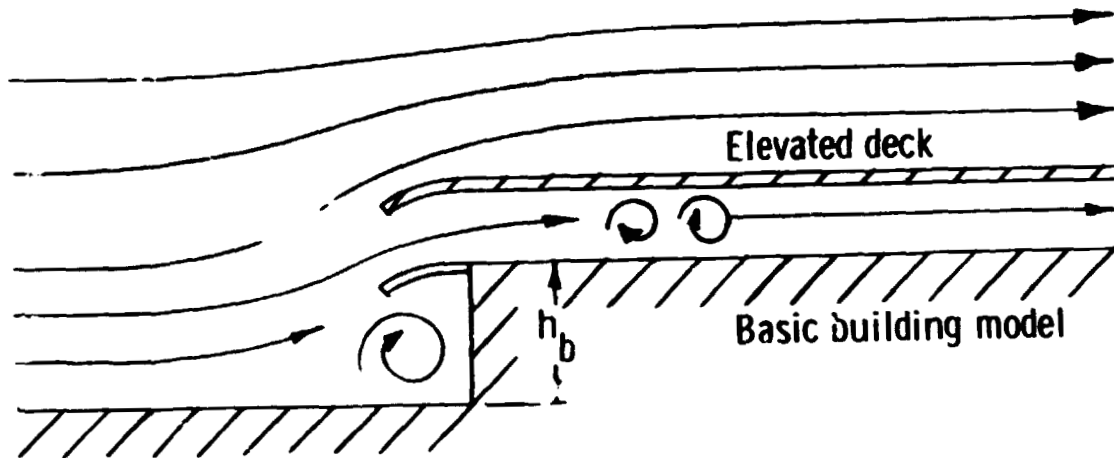
Fig. 37 - Flow over building model with elevated deck $h_b/2$ above basic building model.
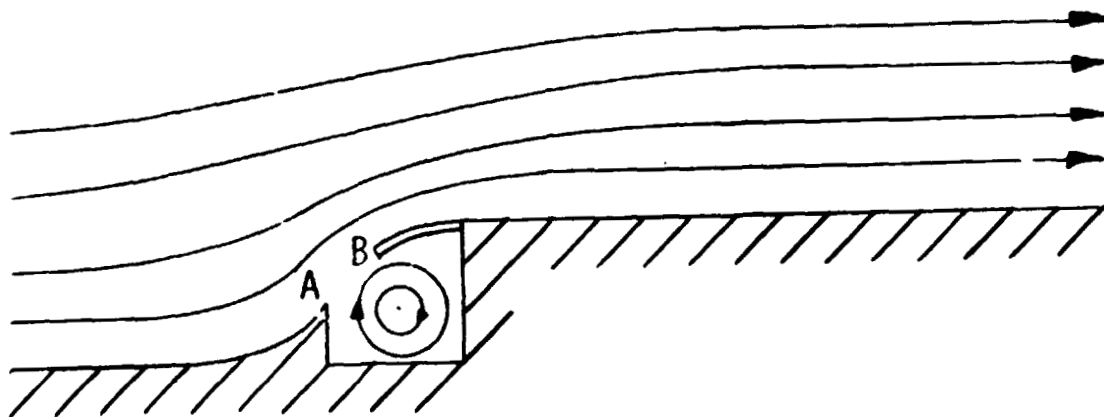
Fig. 38 - Flow over building model with "wedge" upstream.
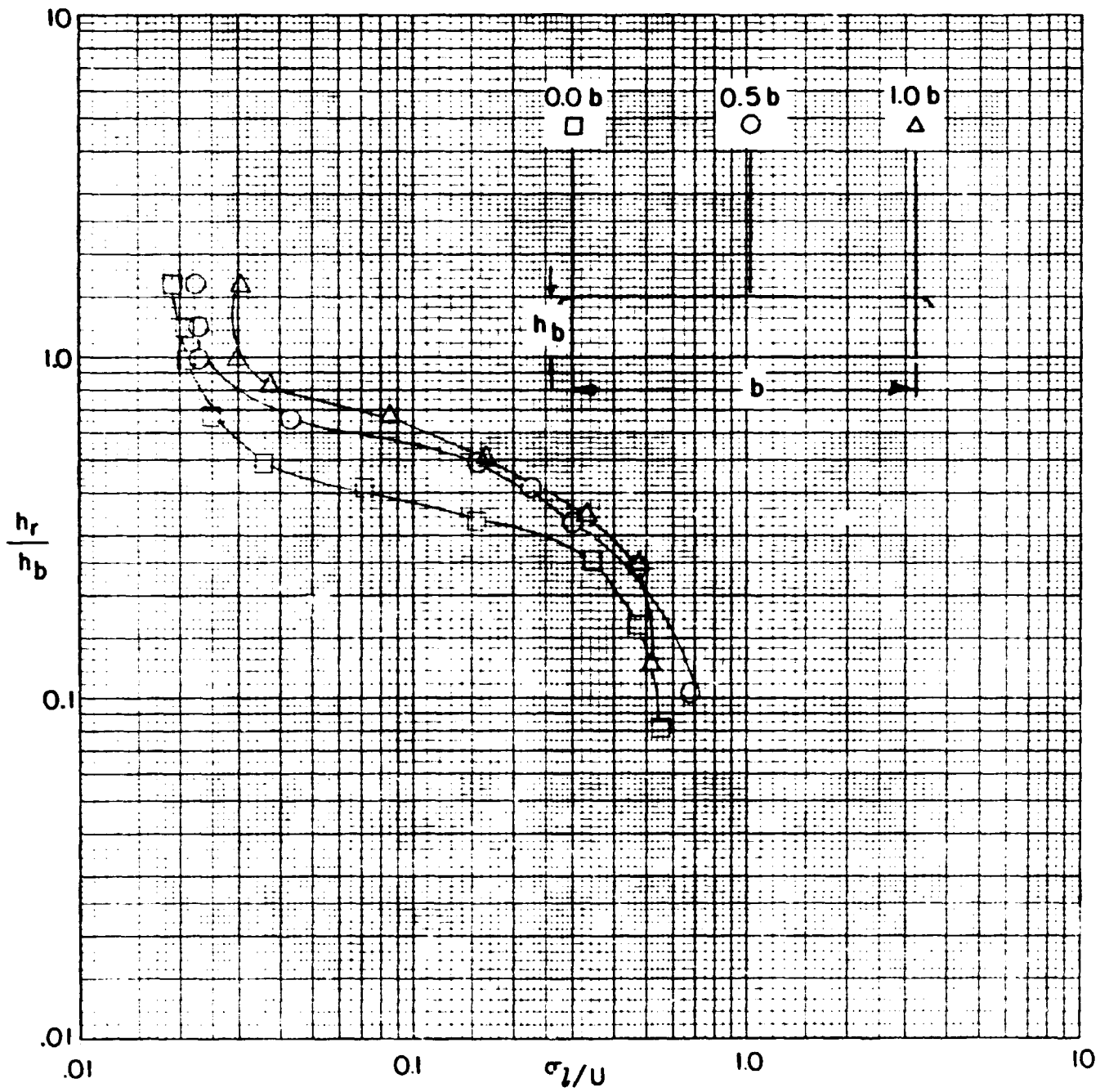
Fig. 39- Effect of distance from upstream building edge on turbulence profile
building rounded edges 0.916 h_b diam. and 0.5h_b are length. R_e =6.3x10⁵
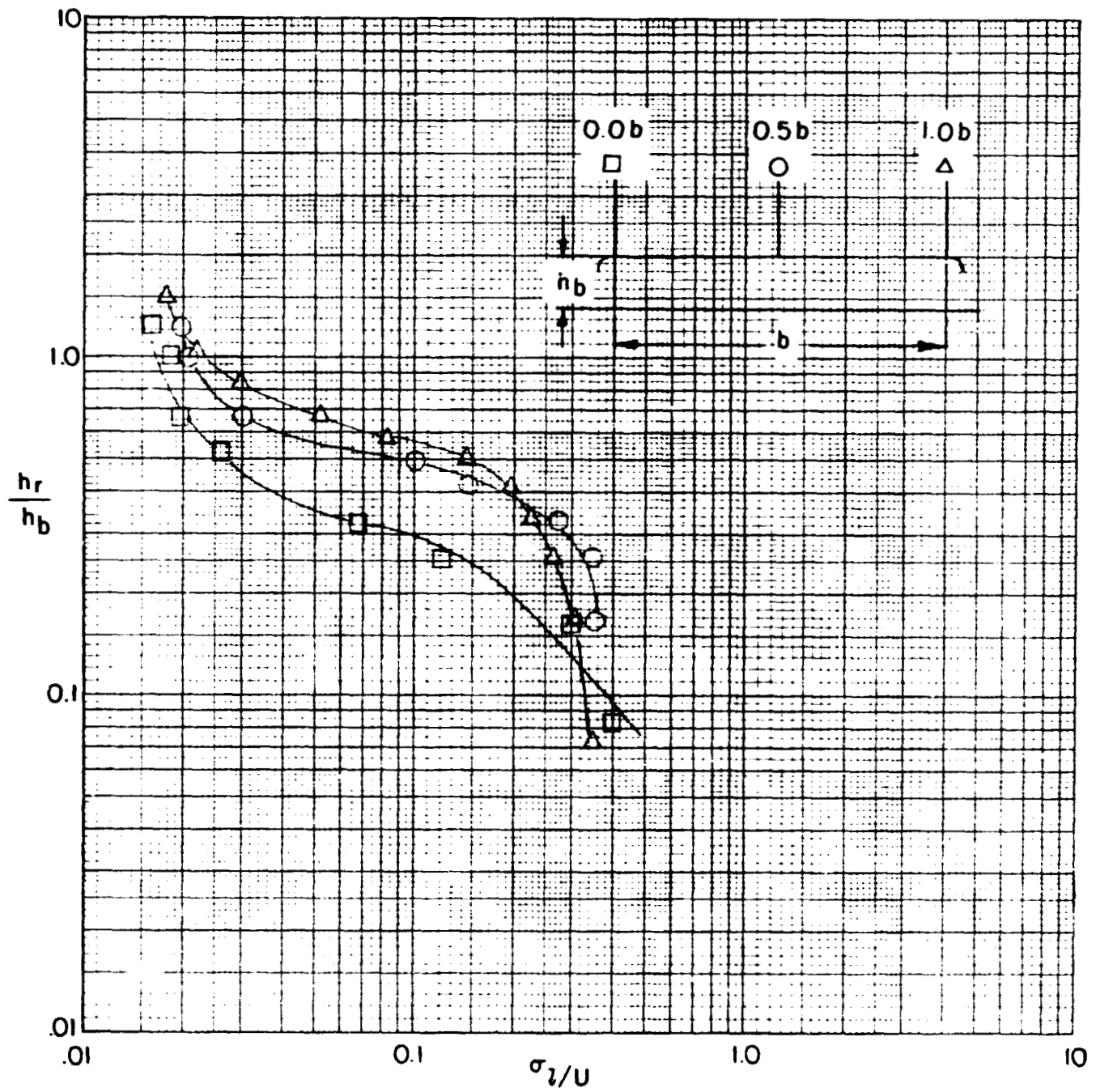
Fig. 40- Effect of distance from upstream building edge on turbulence profile building rounded edges 0.75 h_b diam. and 0.543 h_b are length. $R_e = 6.3 \times 10^5$
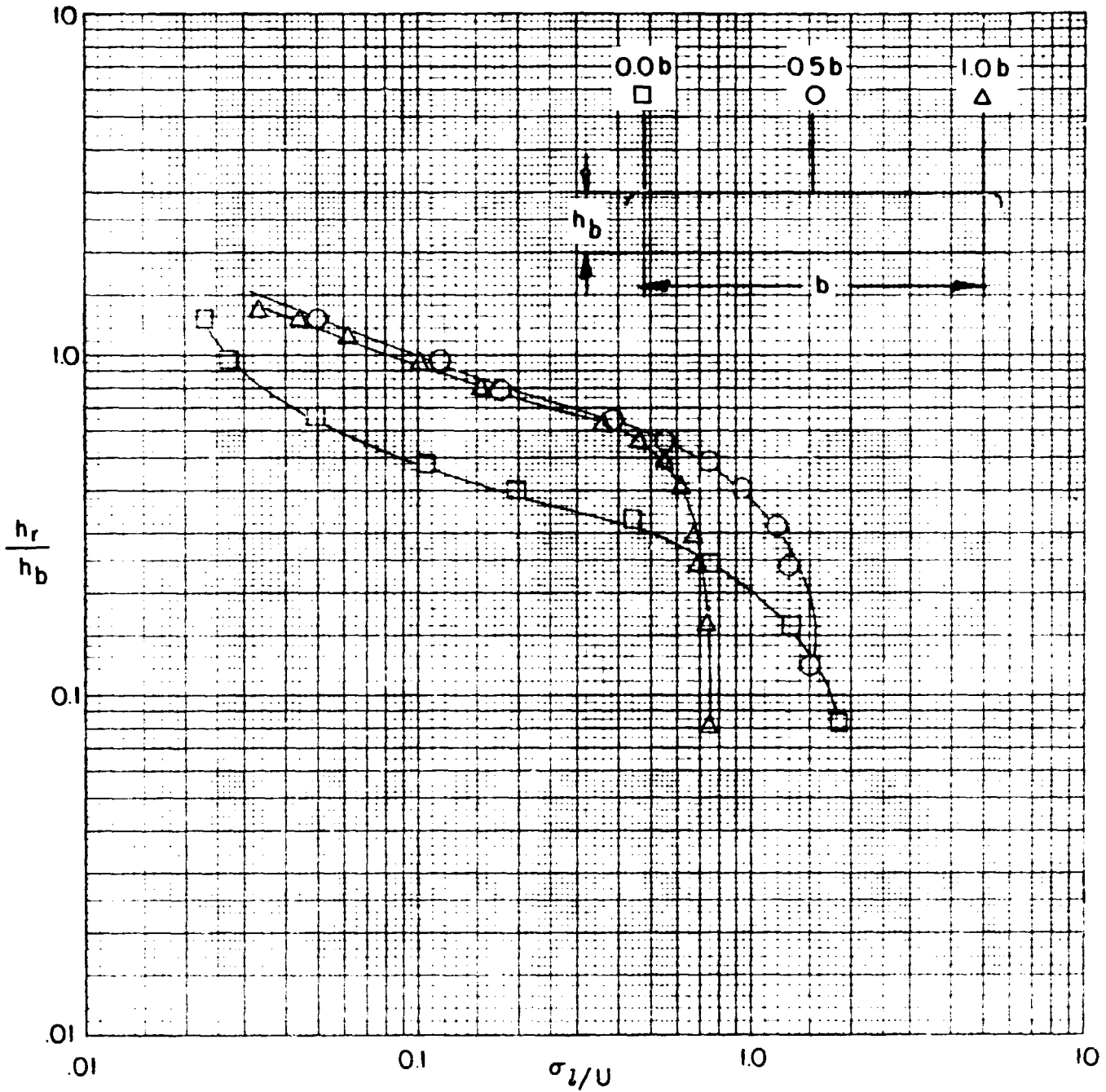
Fig. 41- Effect of distance from upstream building edge on turbulence profile building rounded edges $0.5h_b$ diam. and $0.292h_b$ are length $R_e = 6.3 \times 10^5$
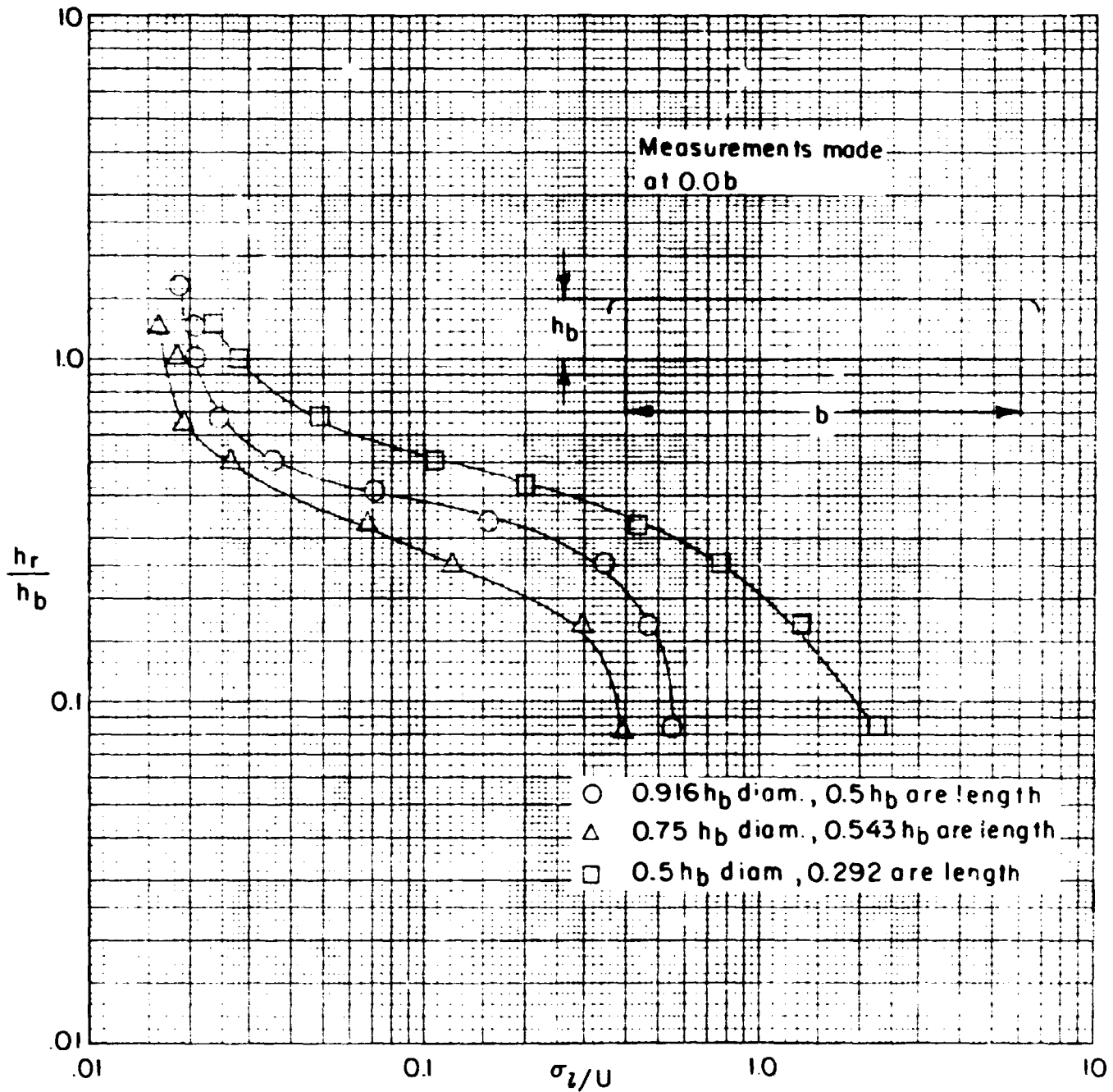
Fig. 42- Effect of building rounded edge on turbulence profile at leading edge.

$R_e = 6.3 \times 10^5$
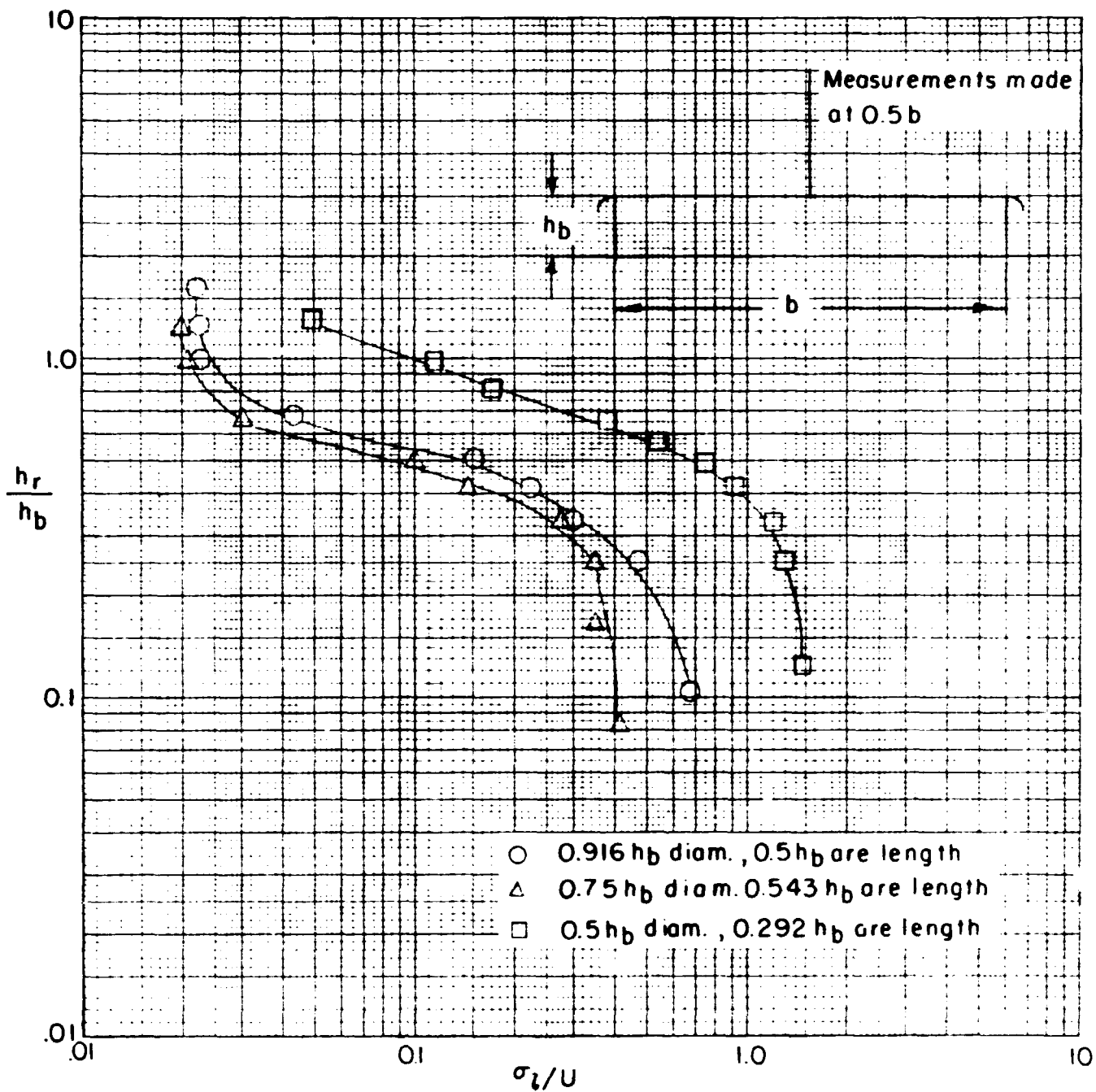
Fig. 43- Effect of building rounded edge on turbulence profile at centerline
$R_e = 6.3 \times 10^5$
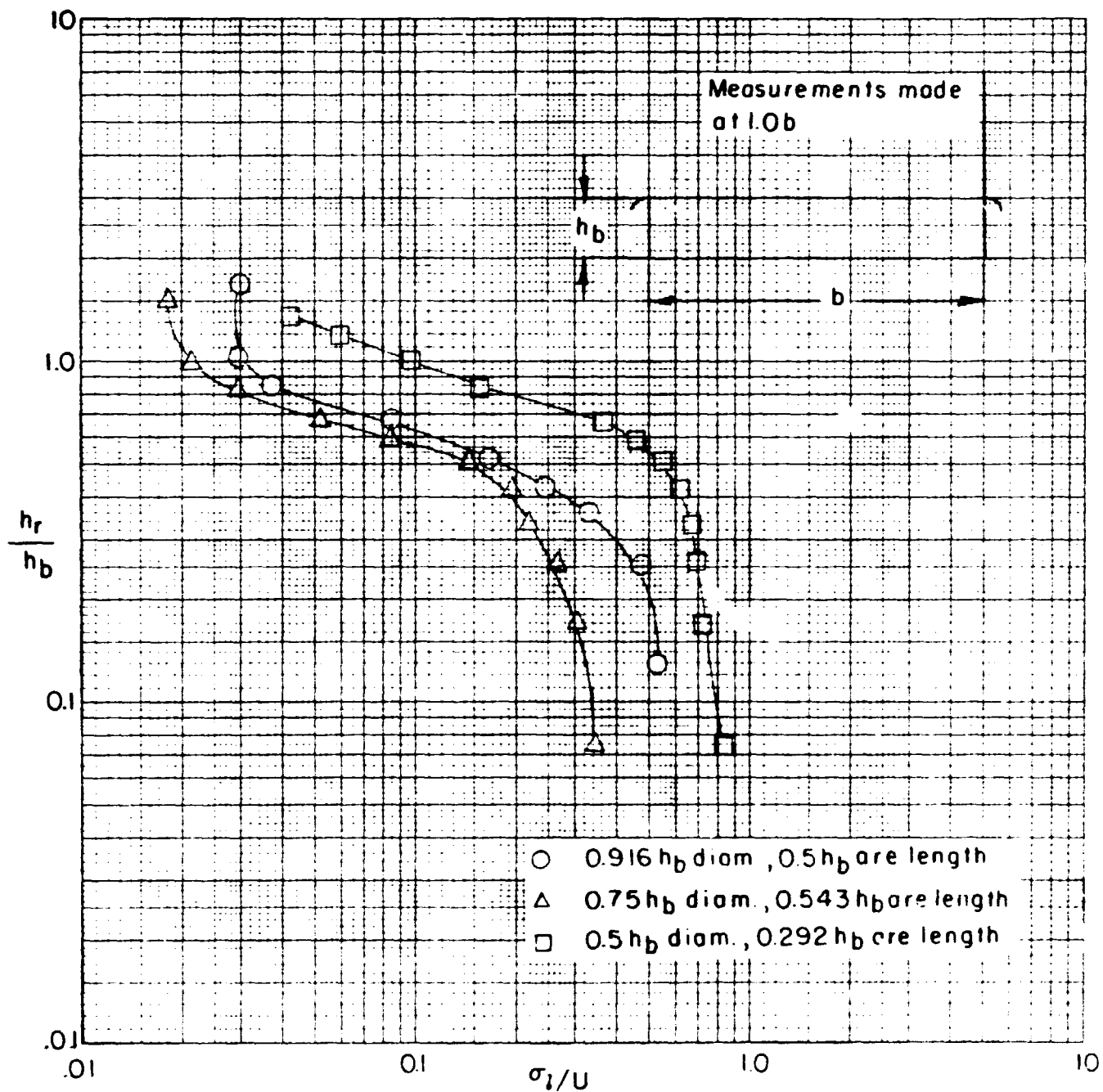
Fig. 44- Effect of building rounded edge on turbulence profile at trailing edge
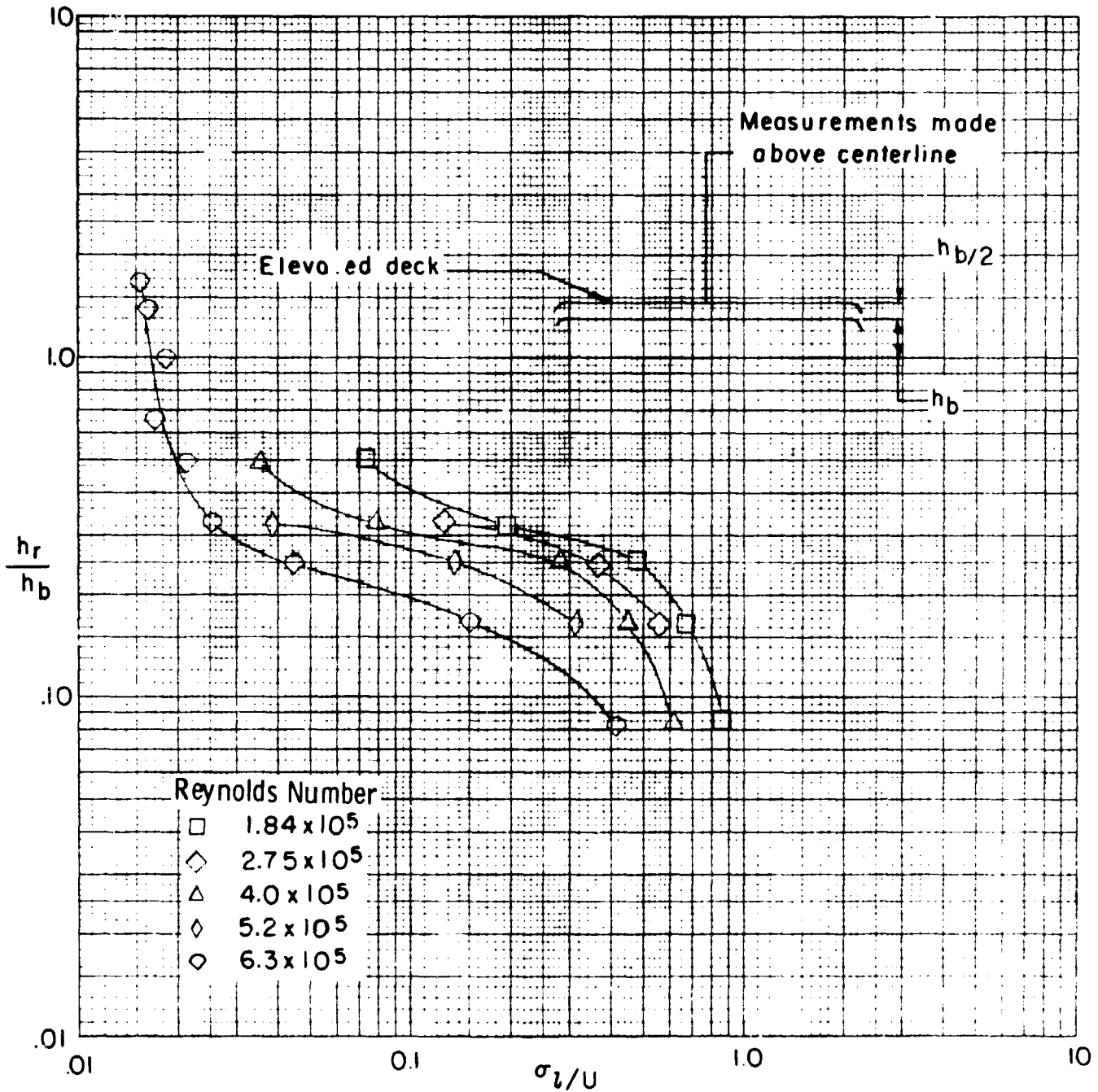$R_e = 6.3 \times 10^5$
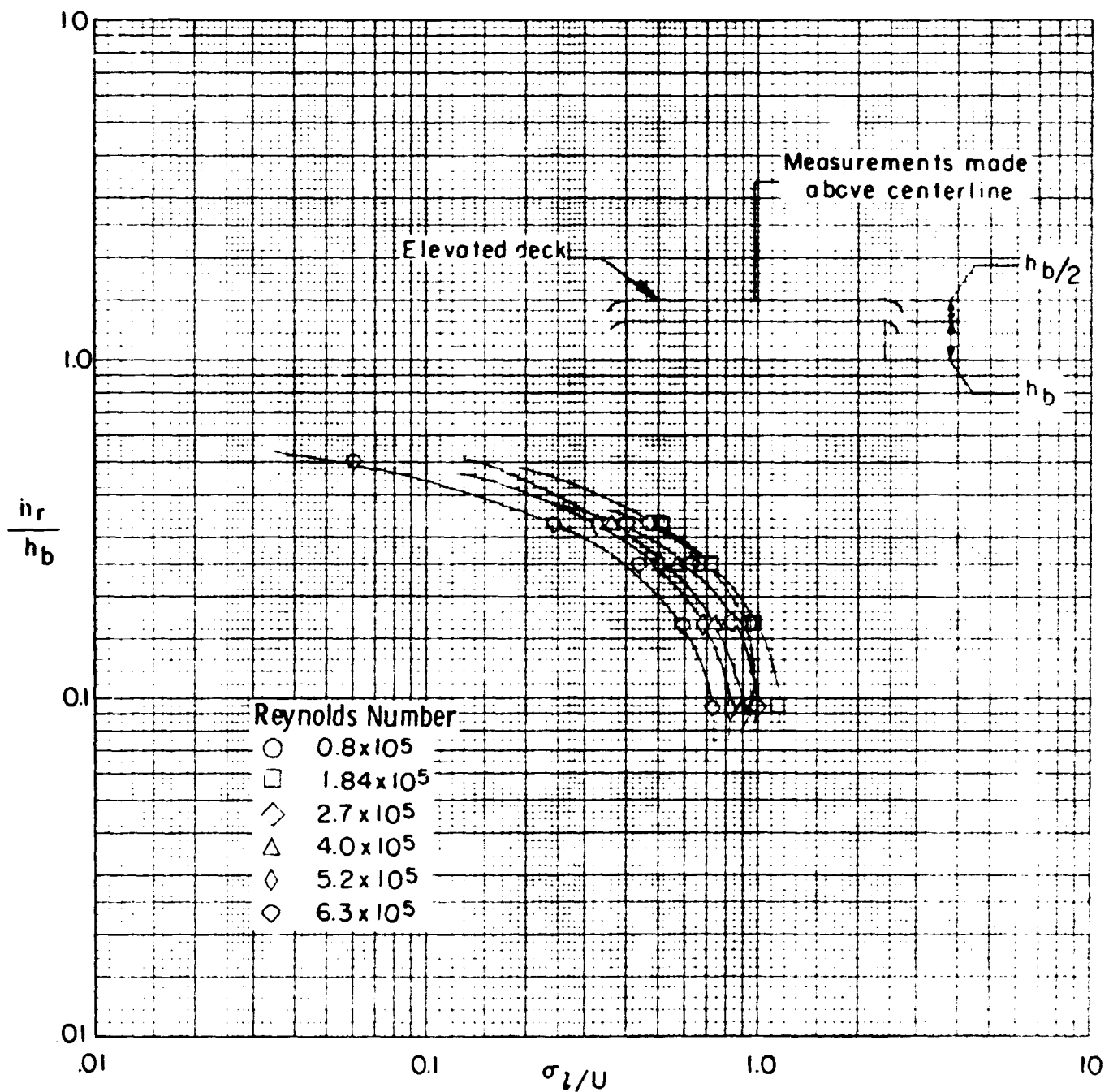
Fig. 45- Effect of Reynolds number on turbulence profile above building
centerline. Elevated deck configuration. Building rounded edge;
0.916 h_b diam. and 0.5 h_b are length. Elevated deck rounded edge;
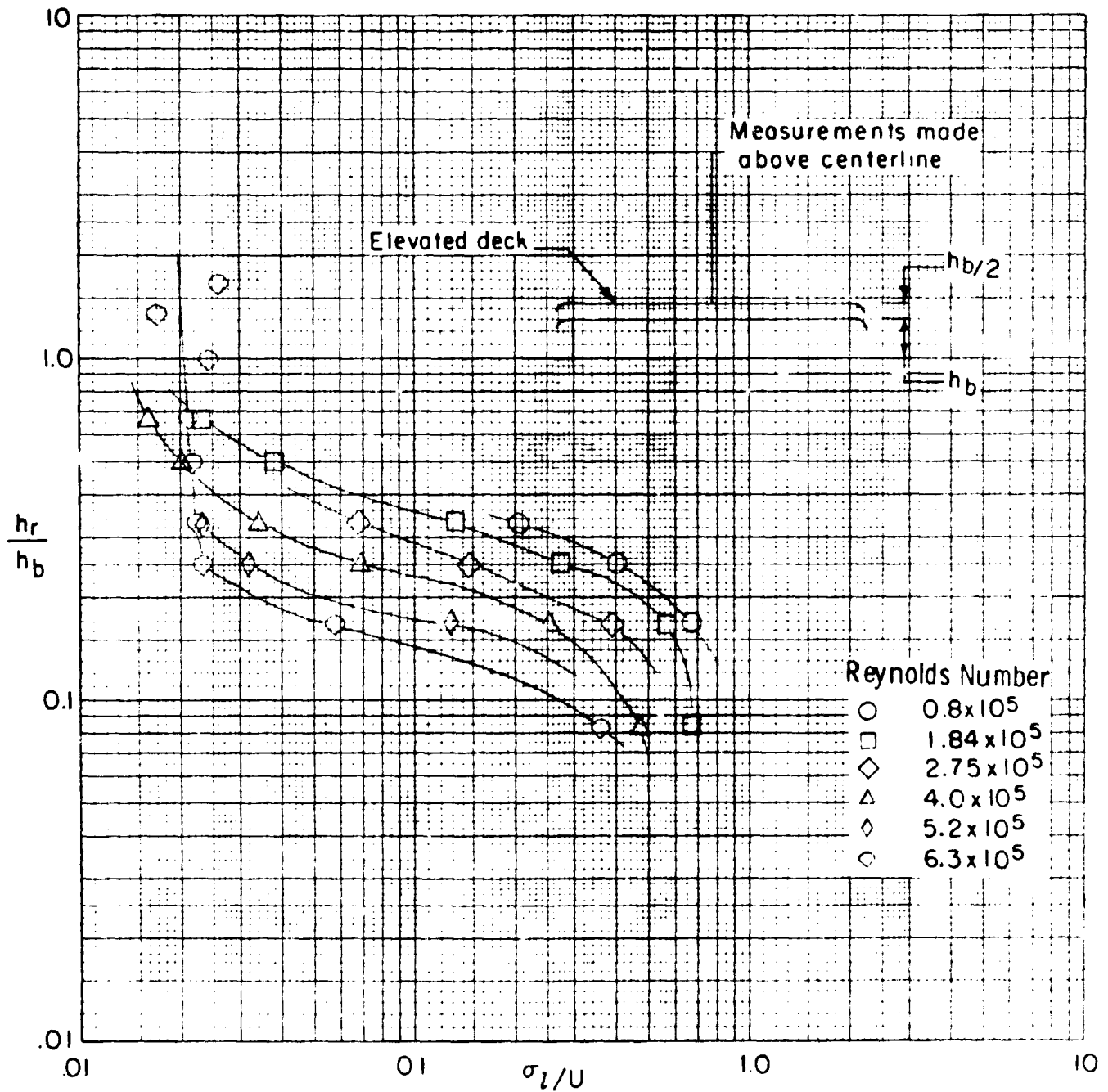0.75 h_b diam. and 0.543 h_b are length.
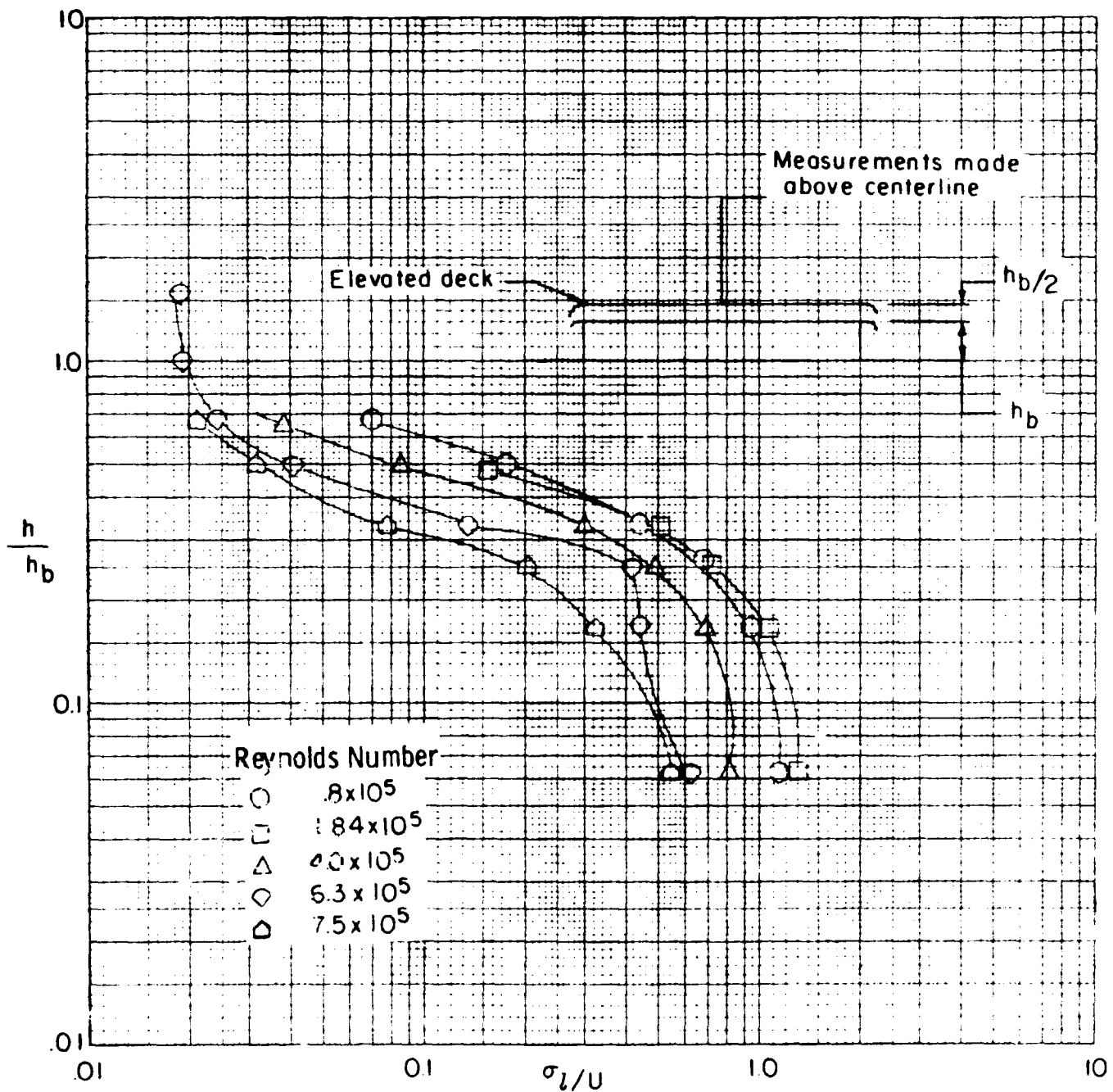
Fig. 46- Effect of Reynolds number on turbulence profile above building centerline
elevated deck configuration. Building rounded edge 0.75 h_b diam and 0.543 h_b
are length. Elevated deck rounded edge; 0.75 h_b diam and 0.543 h_b are length
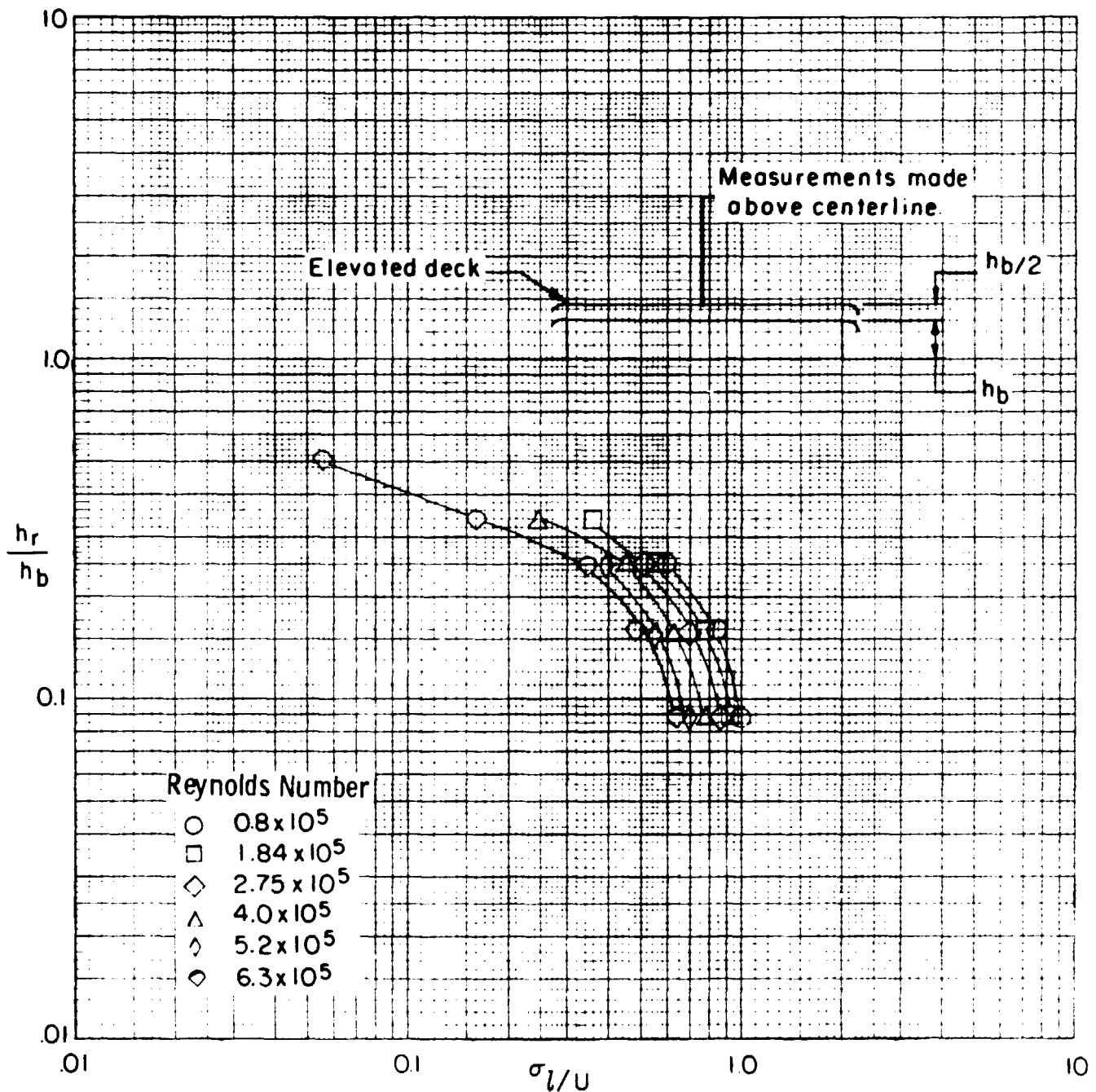
Fig. 47- Effect of Reynolds number on turbulence profile above building centerline elevated deck configuration. Building rounded edge ; 0.916 h_b diam and 0.5 h_b are length Elevated deck rounded ; 0.583 h_b diam and 0.438 h_b are length.
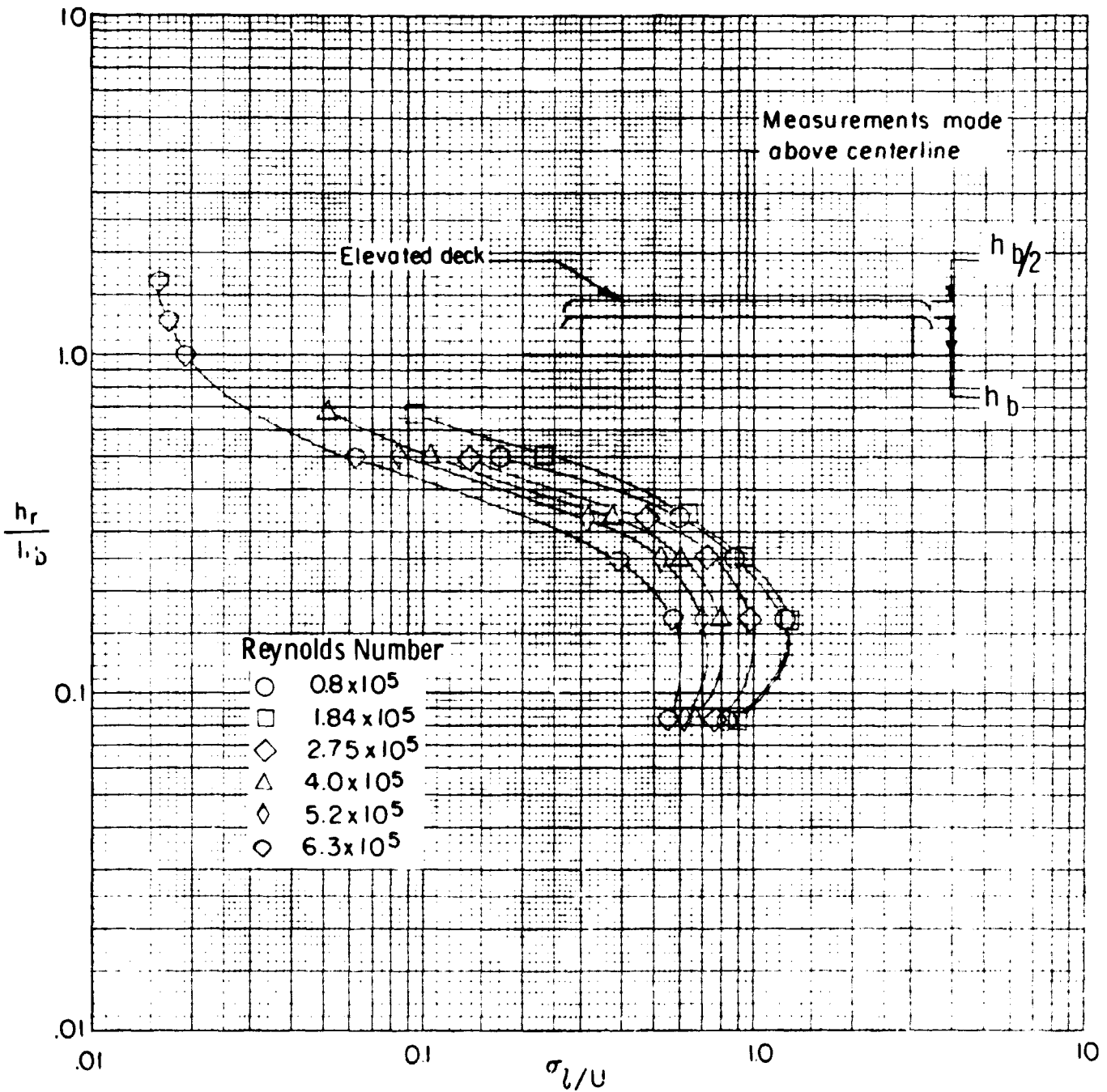
Fig 8- Effect of Reynolds number on turbulence profile above building centerline elevated deck configuration. Building rounded edge; 0.583 h_b diam and 0.438 h_b are length, elevated deck rounded edge; 0.75 h_b diam and 0.543 h_b are length.

Fig. 49- Effect of Reynolds number on turbulence profile above building centerline elevated deck configuration. Building rounded edge; $0.5 h_b$ diam and $0.292 h_b$ are length. Elevated deck rounded edge; $0.916 h_b$ diam and $0.5 h_b$ are length.

Fig. 50– Effect of Reynolds number on turbulence profile above building centerline elevated deck configuration. Building rounded edge; $0.583\,h_b$ diam and $0.483\,h_b$ are length. Elevated deck rounded edge; $0.916\,h_b$ diam and $0.5\,h_b$ are length
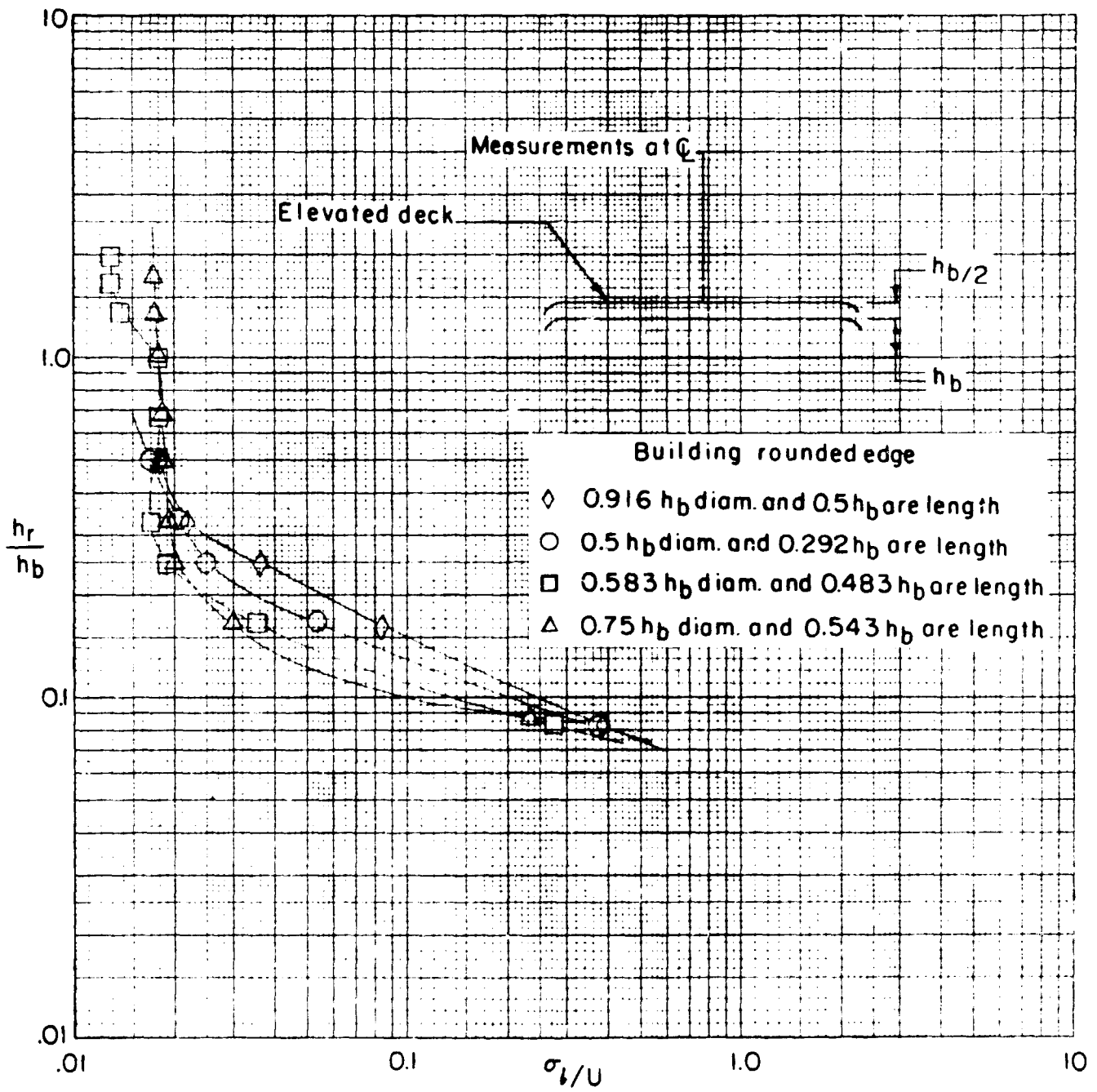
Fig. 51- Effect of geometry of building rounded edge on turbulence profile above
the centerline. Elevated deck rounded edge; 0.5h_b diam.,0.292 are length
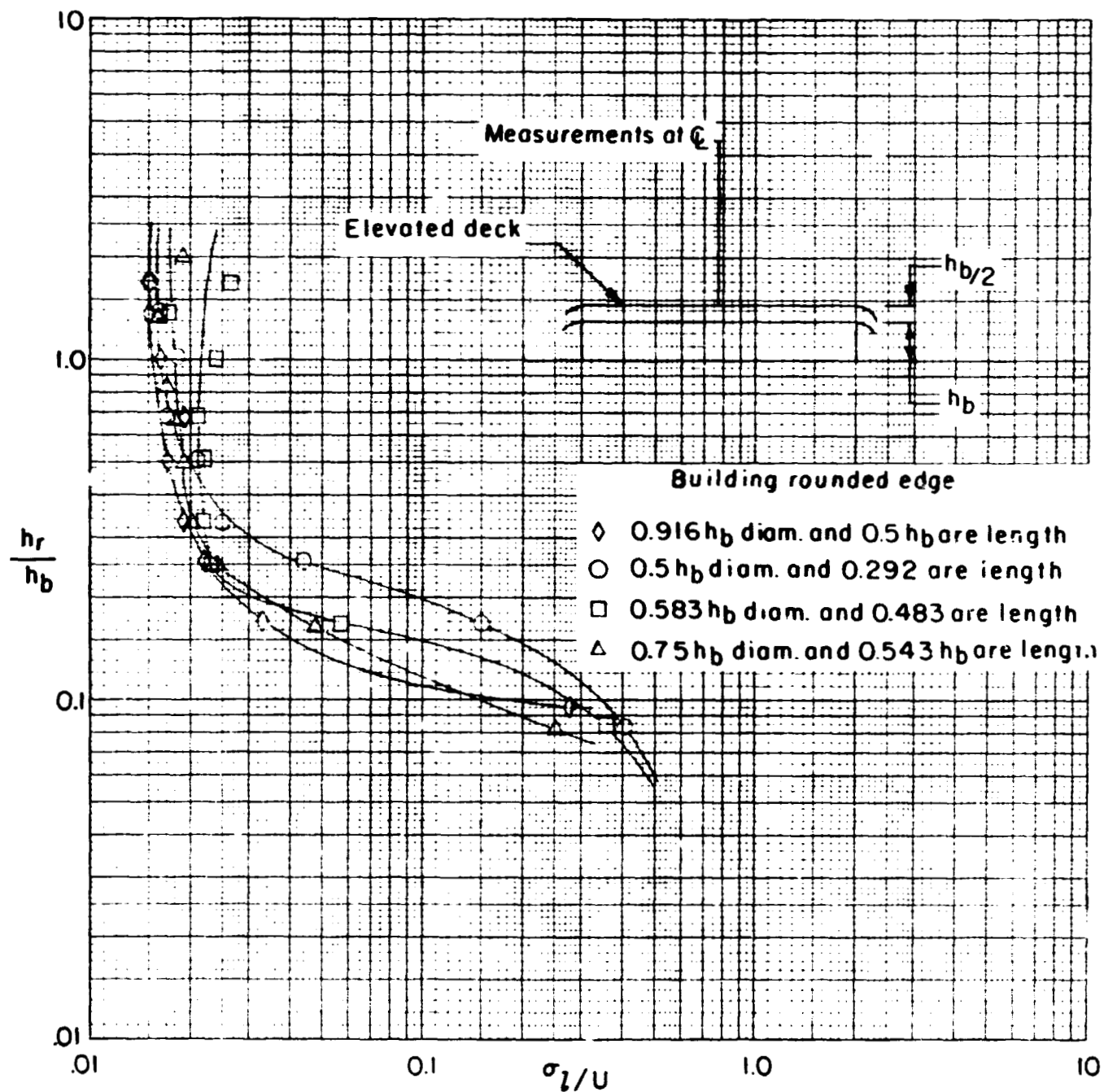$R_E = 6.3 \times 10^5$
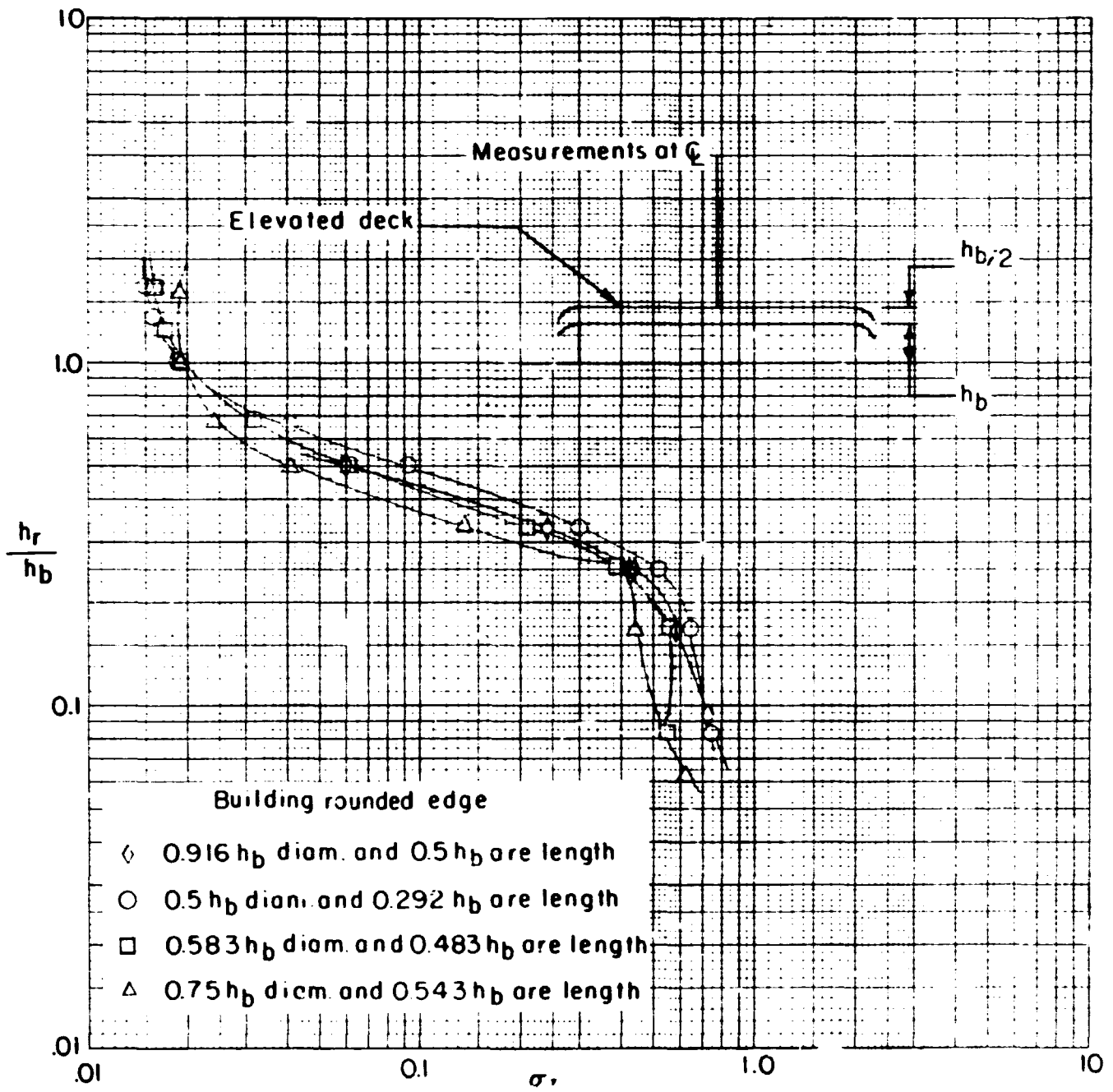
Fig. 52- Effect of geometry of building rounded edge on turbulence profile above the centerline. Elevated deck rounded edge ; 0.75 h_b diam. and 0.543 are length
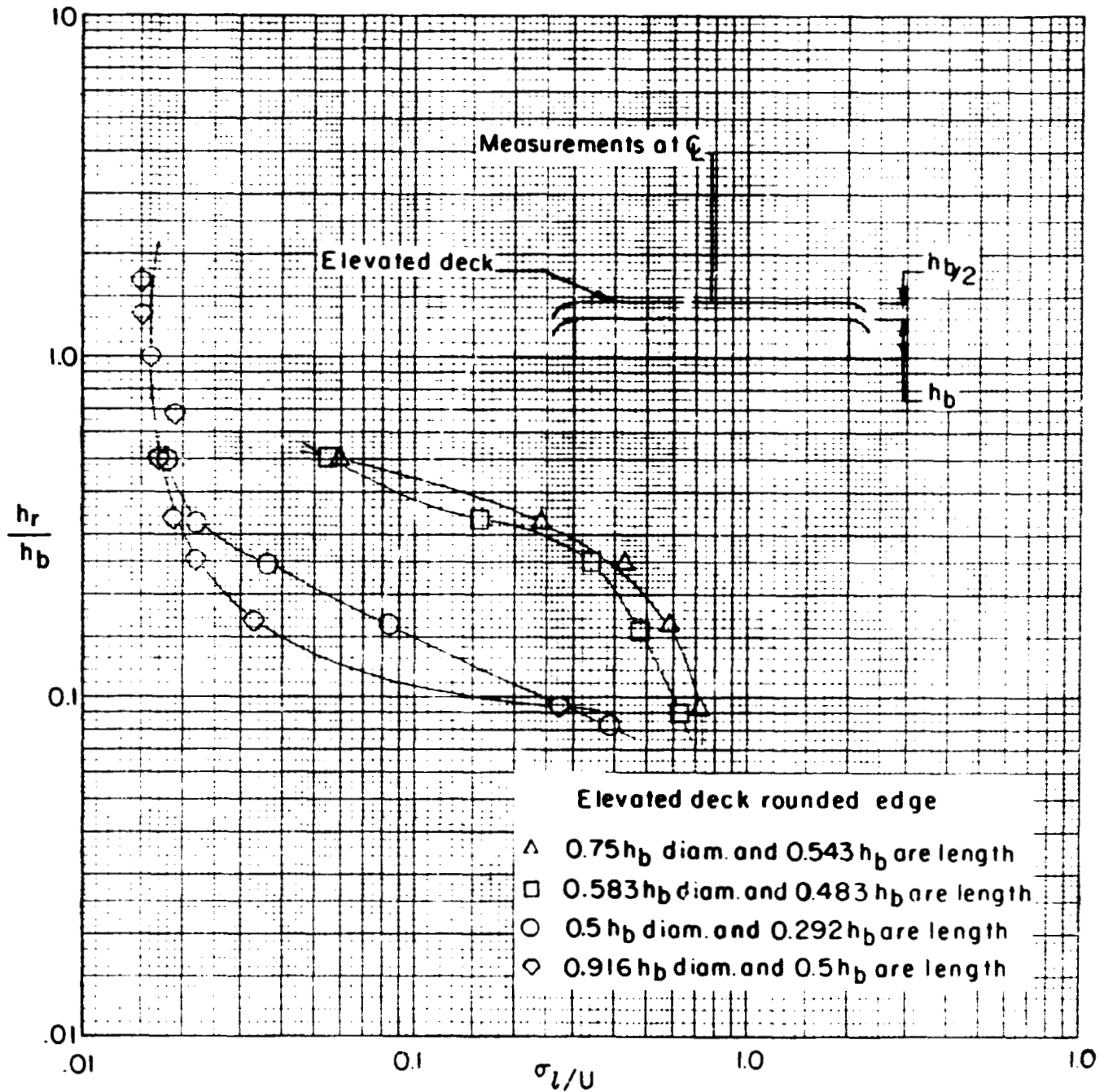$R_e = 6.3 \times 10^5$

Fig. 53- Effect of geometry of building rounded edge on turbulence profile above the centerline. Elevated deck rounded edge ; 0.916 h_b diam. and 0.5 h_b are length

$R_e = 6.3 \times 10^5$

Fig. 54- Effect of geometry of elevated deck rounded edge on turbulence profile above
the centerline. Building rounded edge; 0.916 h_b diam. and 0.5 h_b are length
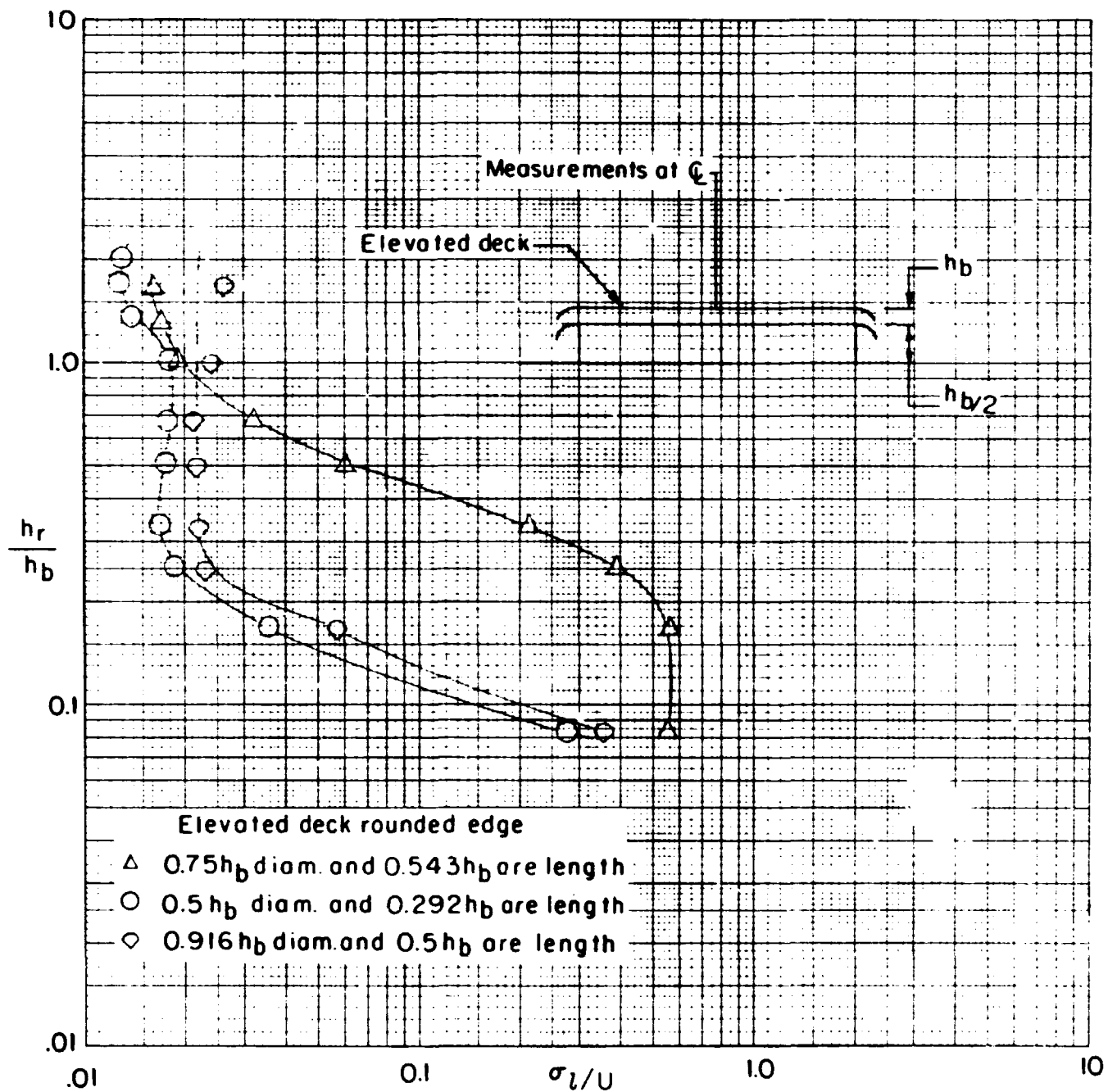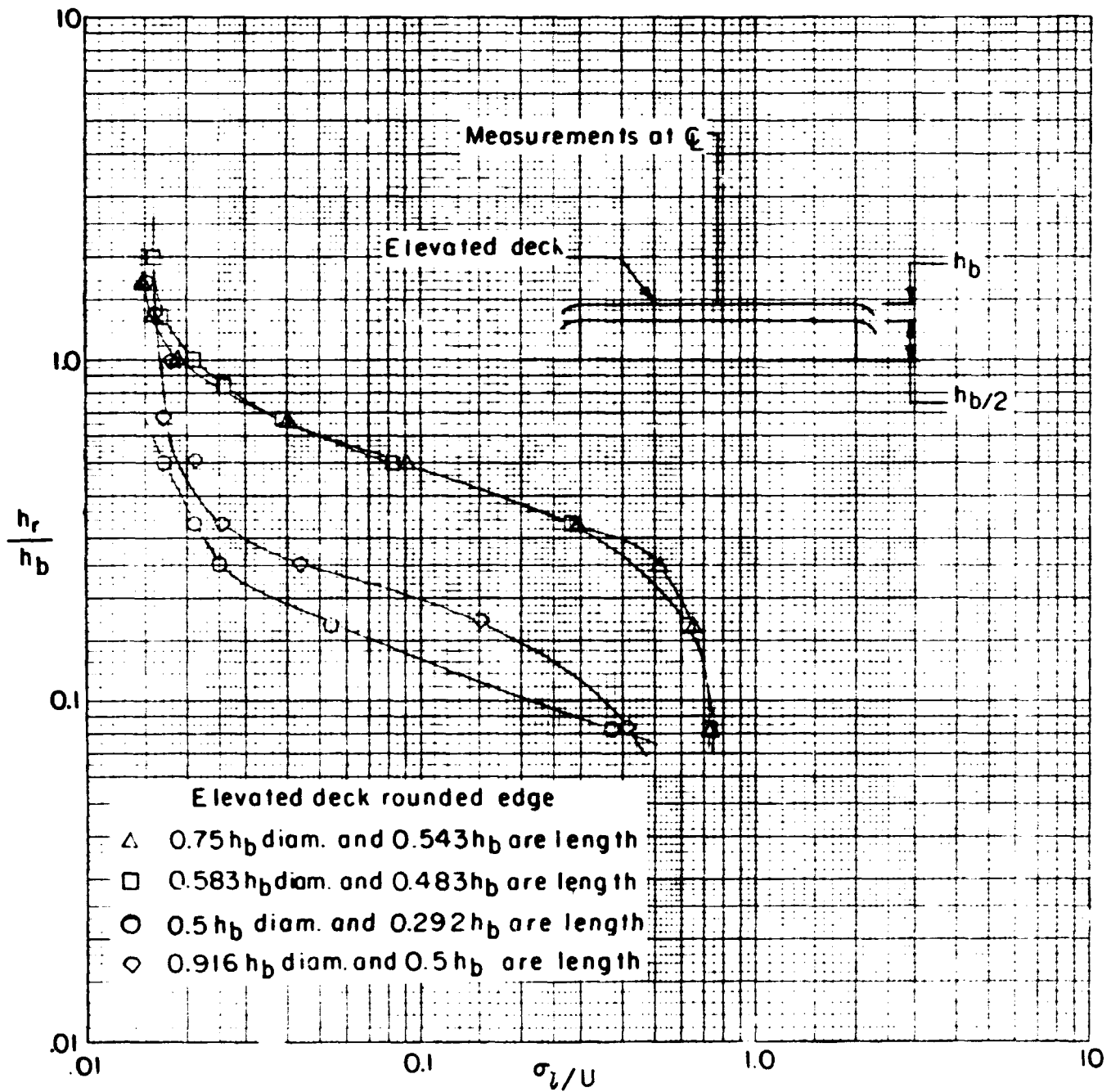
$R_e = 6.3 \times 10^5$

Fig. 55- Effect of geometry of elevated deck rounded edge on turbulence profile above the centerline. Building rounded edge; 0.583h_b diam. and 0.483h_b are length. R_e=6.3x10^5

Fig. 56- Effect of geometry of elevated deck rounded edge on turbulence profile above the center ne. Building rounded edge; 0.5 h_b diam. and 0.292 h_b are length

$R_e = 6.3 \times 10^5$

Wind tunnel test section

Fence
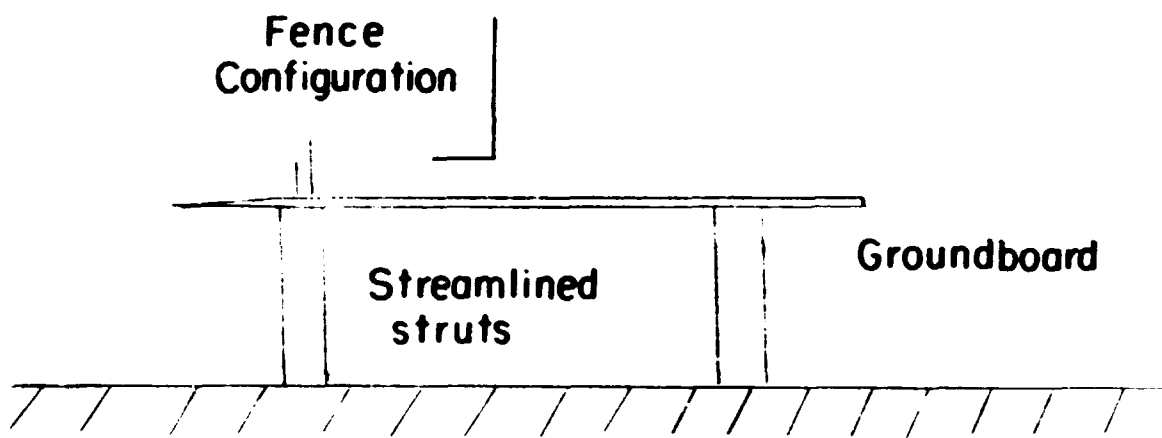Configuration

Groundboard

Streamlined
struts

Fig. 57 - Experimental test set-up

Fig. 58- Effect of distance from fence on velocity profile single element 3" high fence constructed from 0.02" wire, 0.125" grid screen.

Measurement immediately behind fence

Measurement 1 hf behind fence

Measurement 2 hf behind fence

Measurement 3hf behind fence
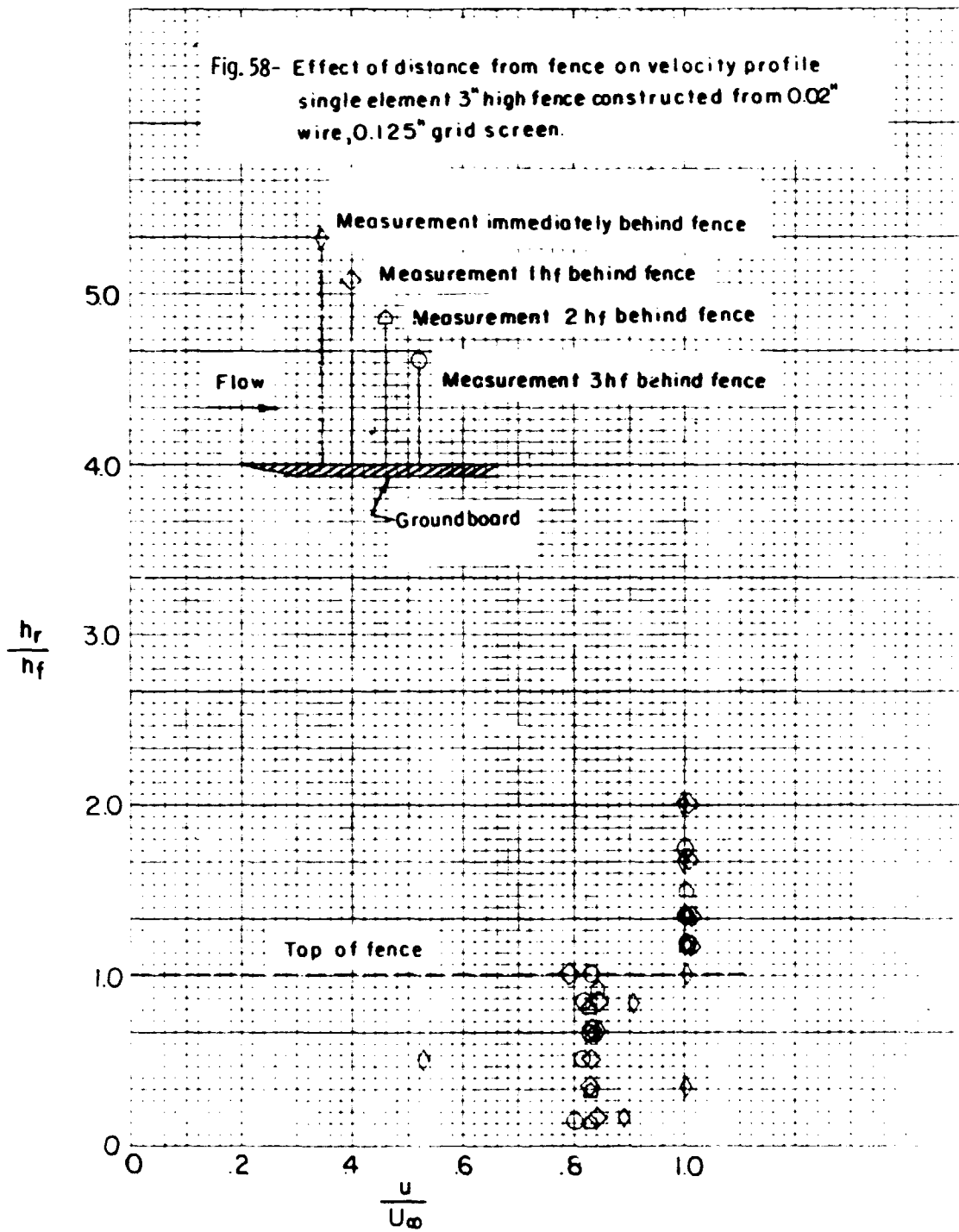
Flow

Groundboard

Top of fence

$\frac{h_r}{h_f}$

Fig. 59- Effect of distance from fence on velocity profile double element fence, 2" element and 3" element, constructed from 0.02" wire, 0.125" grid screen.
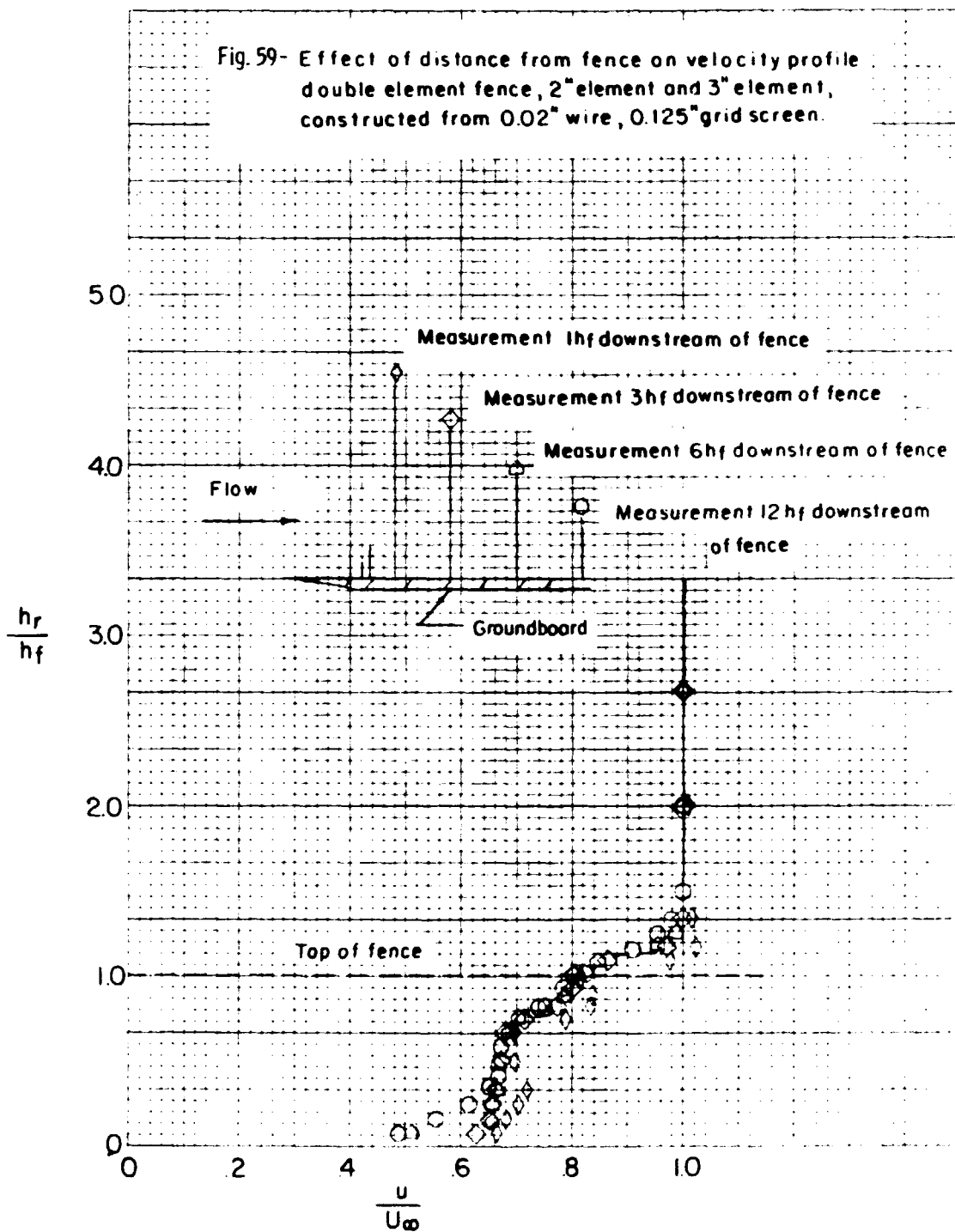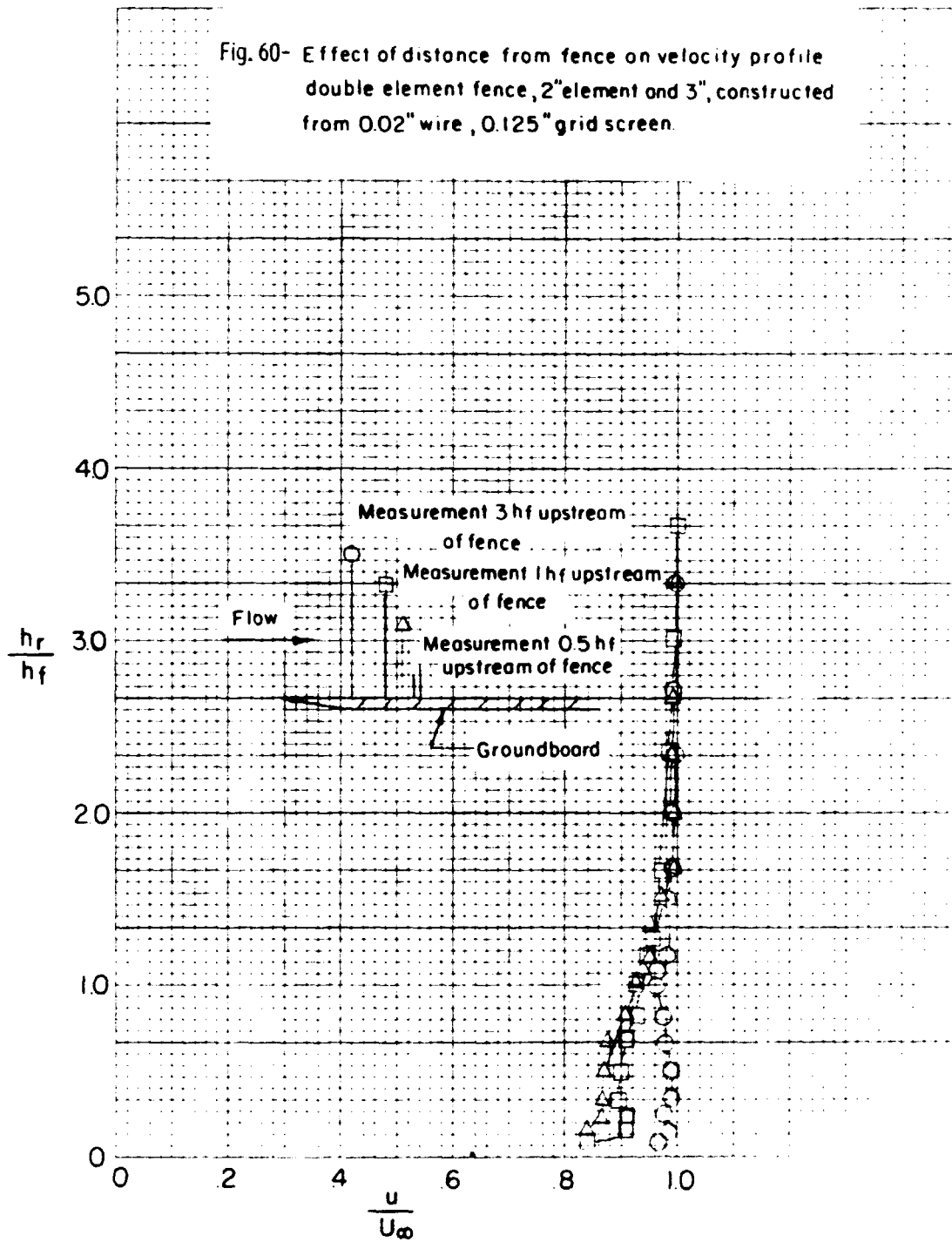
Measurement 1hf downstream of fence

Measurement 3hf downstream of fence

Measurement 6hf downstream of fence

Measurement 12hf downstream of fence

Flow

Groundboard

Top of fence

$\frac{h_r}{h_f}$

$\frac{u}{U_\infty}$

Fig. 60- Effect of distance from fence on velocity profile
double element fence, 2" element and 3", constructed
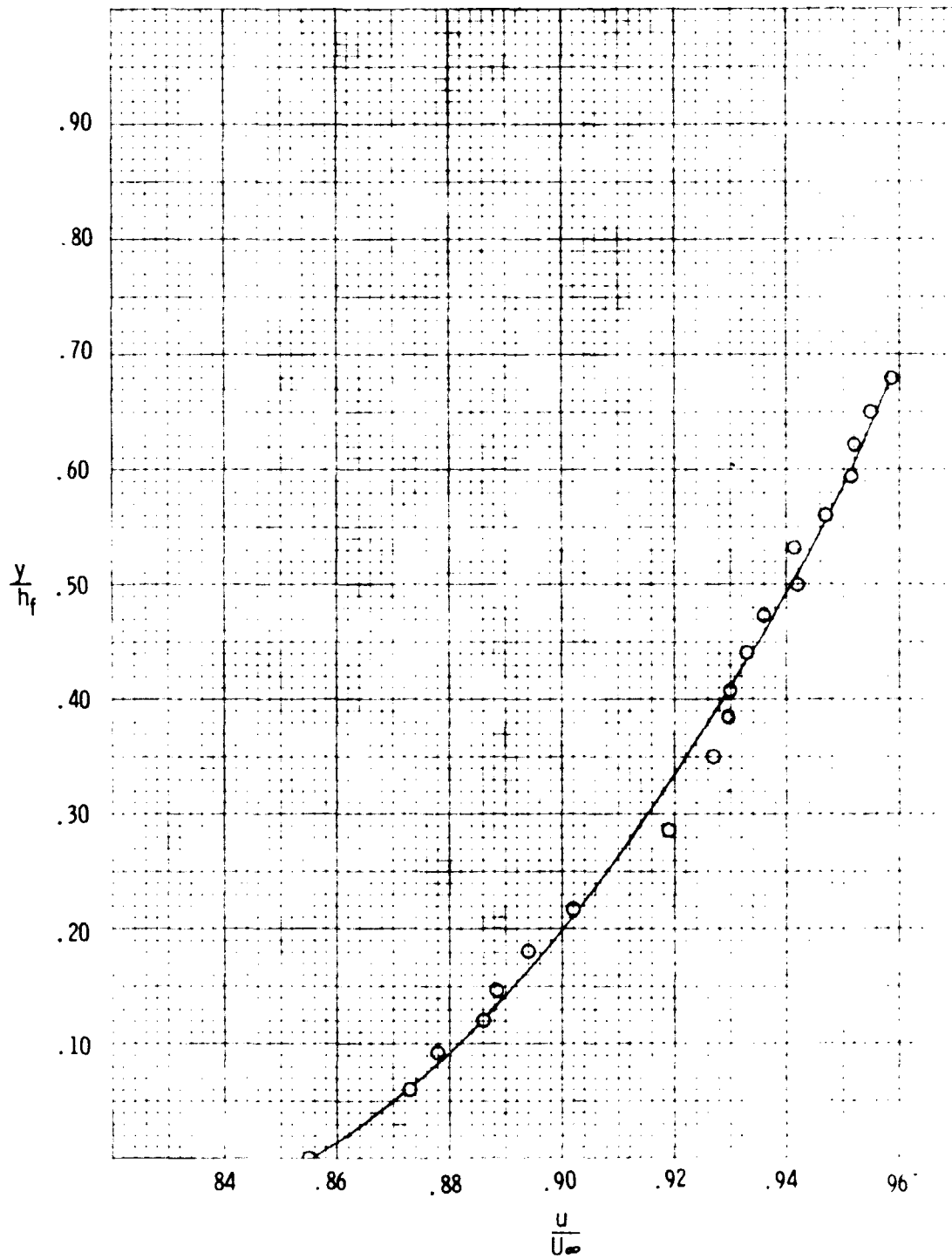from 0.02" wire , 0.125" grid screen.

Measurement 3 hf upstream
of fence

Measurement 1 hf upstream
of fence

Flow

Measurement 0.5 hf
upstream of fence

Groundboard

$\frac{h_r}{h_f}$

$\frac{u}{U_\infty}$

Fig. 61-Velocity profile behind variable solidity , parallel-rod grid.

$$2\left[1-\left(\frac{u'}{U_\infty}\right)^2\right] \cdot \frac{\xi}{(1-\xi)^2}$$
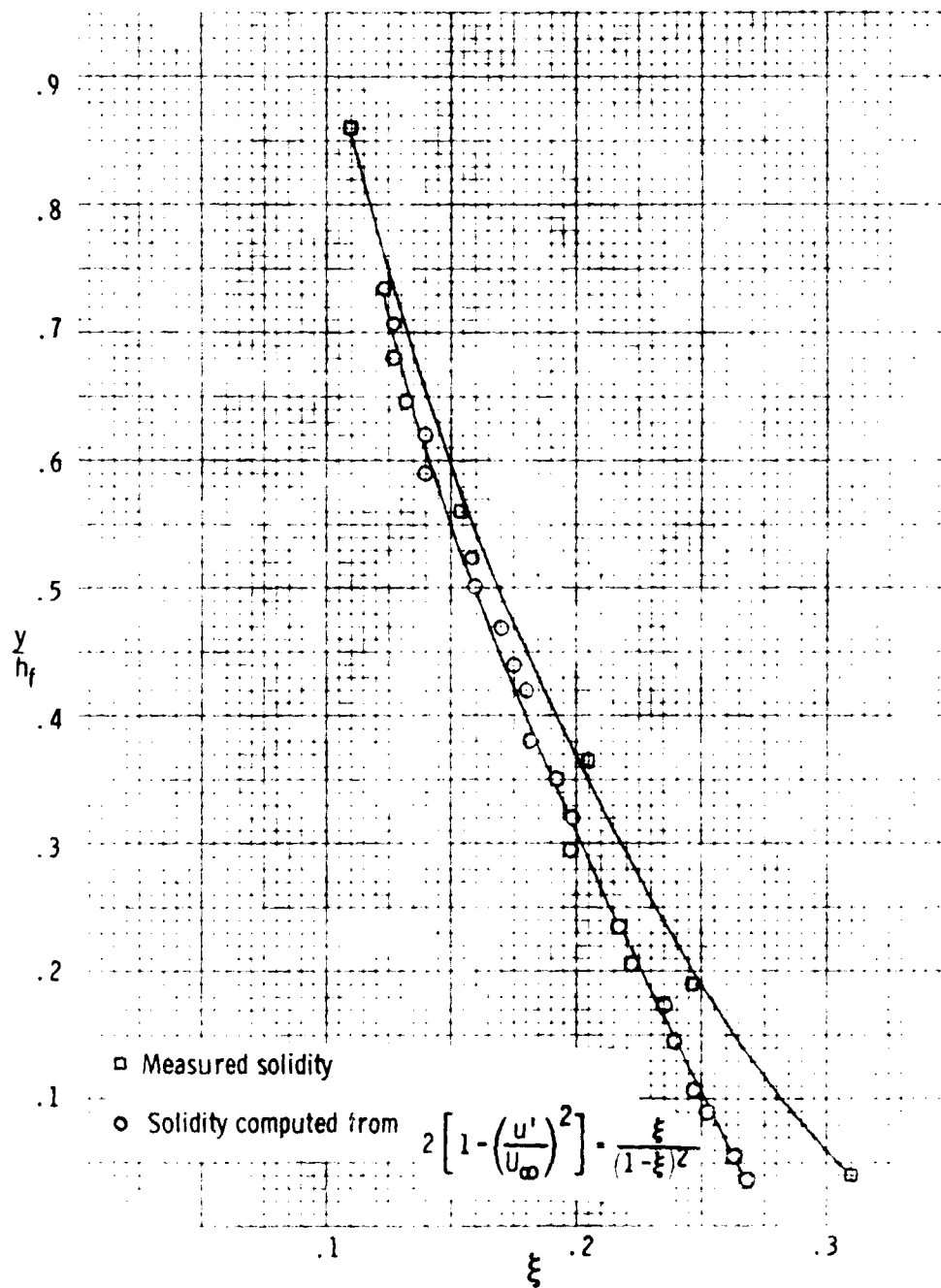
□ Measured solidity

○ Solidity computed from

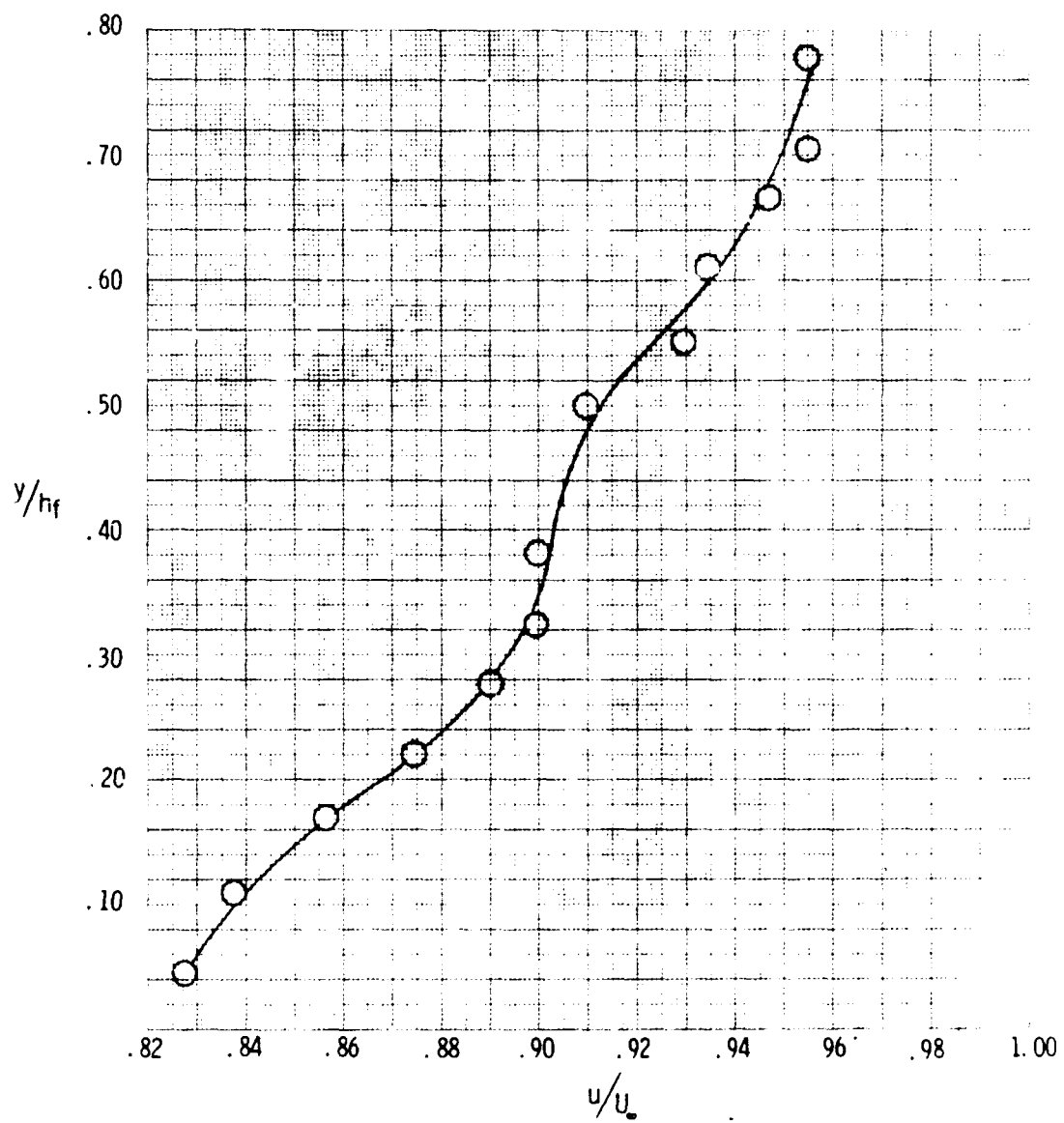Fig. 62- Computed solidity compared to actual solidity for parallel rod grid.

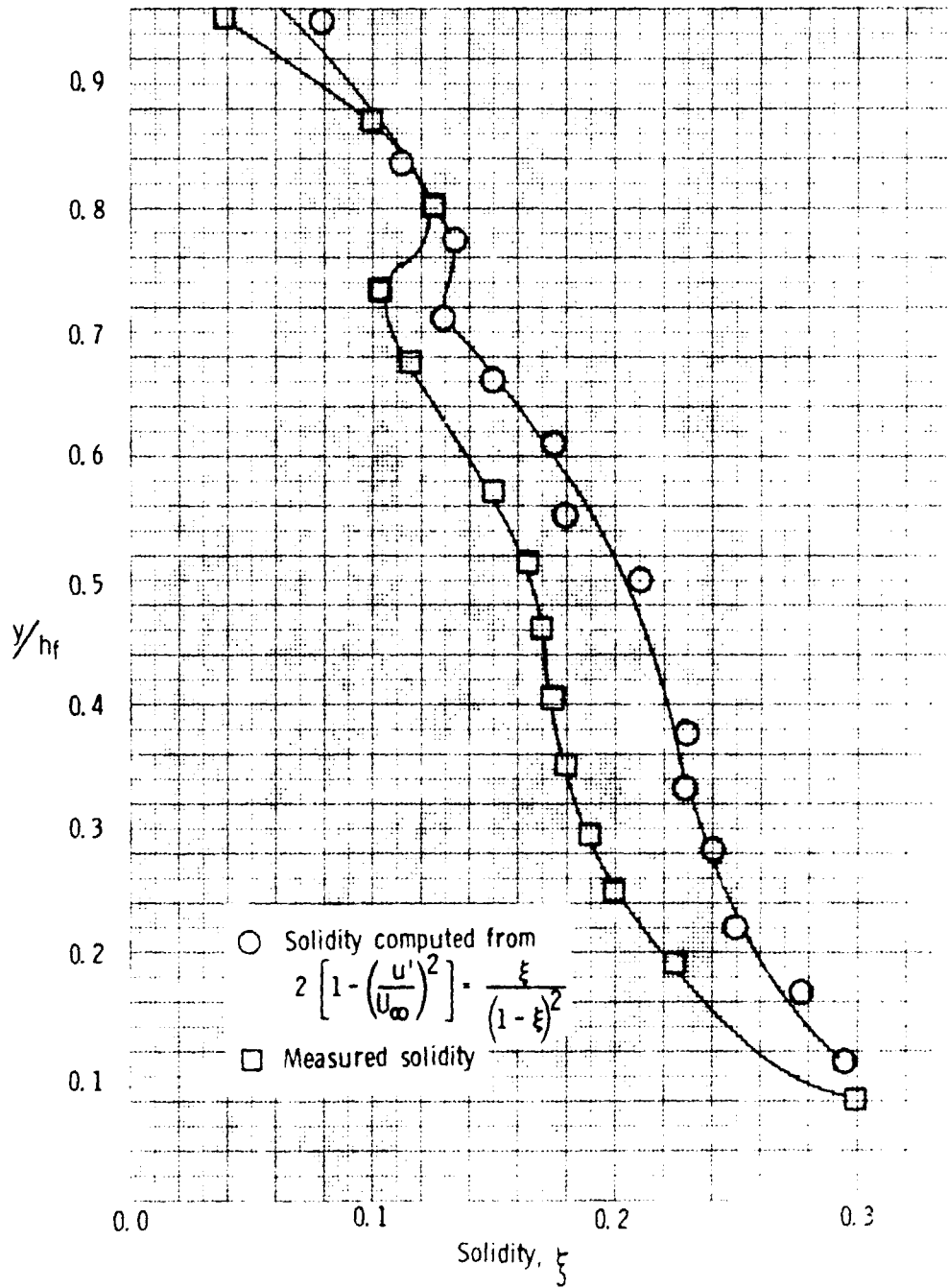Fig. 63- Velocity profile behind single element, variable solidity screen

Fig. 64- Computed solidity compared to actual solidity for single element, variable solidity screen.